Studies on Organic/inorganic Composites of Bio-based Polyamide Derivatives from 4-aminocinnamic Acid

Jakkapon PHANTHUWONGPAKDEE

Japan Advanced Institute of Science and Technology

Doctoral Dissertation

Studies on Organic/inorganic Composites of Bio-based Polyamide Derivatives from 4-aminocinnamic Acid

Jakkapon PHANTHUWONGPAKDEE

Supervisor: Professor Tatsuo Kaneko

Graduate School of Advanced Science and Technology
Japan Advanced Institute of Science and Technology
Materials Science

September 2020

Abstract

To expand the potential functions of high-performance bio-based polymers in the green society, organic/inorganic composites of these polymers were developed and tested for their suitable applications. The selected bio-based polymers in this study were biopolyamides (BPA) and biopolyimide (BPI). A multifunctional monomer, 4,4'-di(trimethylamino)-α-truxillic acid (Q-4ATA), was synthesized by the quaternarization of bio-based 4-aminocinnamic acid (4ACA) and was polymerized with various diamines to obtain a series of cationic BPA. All cationic BPA possessed high thermal properties, with 10% weight loss temperatures of 296 – 329 °C. One application of these cationic BPA bearing quaternary ammonium was the anion-exchange ability. They were employed to remove iodide (I^-) from the water. PA-R4 was highlighted as an entirely bio-based cationic polyamide as its precursors being Q-4ATA and the glucose diamine derivatives. It was calculated to have more than 95% use of renewable sources in the sustainability metric. With 120 min equilibrium time, more than 80% adsorption of 10 mg/L initial I^- concentration in 90 °C was confirmed. The ability of BPA to perform stable anion-exchange processes in various conditions has made them a new, sustainable, and promising system for anionic pollution remediation in water. For BPI, the flame retardant films having high optical transparency were developed from amino acid-based BPI salt with aluminum (BPI-COOAl) and copper ions (BPI-COOCu). The microscale combustion calorimetry analysis revealed that BPI-COOAl possessed high flame retardancy with 4.5 kJ/g total heat released and 427 s time to ignition. At the same time, high transparency of more than 80 % transmittance at a light wavelength of 450 nm and 64 MPa tensile strength were retained. The total heat released of 14.6 kJ/g and 47 MPa tensile strength were observed in BPI-COOCu. The char formation of Al_2O_3 and Cu_2O in their respective polymer complexes was deduced as main flame suppression mechanism. Comparing to the flame retardant films in the literature, the present films of BPI salts are advantageous in terms of flame retardancy and thermo-mechanical stability. Lastly, BPI complex containing the carboxylate europium (BPI-COOEu) was produced with europium ions. Under 330 nm ultraviolet excitation, BPI-COOEu yielded emission bands at 579, 592, 616, 650 and 692 nm which were associated with the $^5D_0 \rightarrow {}^7F_J$ (J = 0 – 4) transition of Eu^{3+}. The prominent band at 616 nm resulted in red emission that could be observed by naked eyes. The VOCs sensor application was tested, and the enhancements and quenchings in emission bands were detected after BPI-COOEu was left in contact with solvents.

Keywords: Polyamide; Polyimide; Ion-exchange; Flame Retardancy; Photoluminescent

Acknowledgements

I, the author of this dissertation, would like to express the deepest gratitude to *Prof. Tatsuo Kaneko* (JAIST main supervisor) for his supervision and words of encouragement throughout the course of this thesis completion. I strongly believe that the knowledge and wisdom that he has offered will become tremendous assets for my future endeavors.

For Sirindhorn International Institute of Technology (SIIT), I would like to express my gratefulness to *Prof. Sandhya Babel* (SIIT main supervisor) for her advices and support from Thailand. Indeed, her assistance has greatly contributed to the completion of this work.

I would also like to extend my appreciation to the other committee members of this dissertation defense; *Prof. Toshiaki Taniike* (JAIST second supervisor), *Prof. Kazuaki Matsumura* (JAIST minor research supervisor), and *Prof. Noriyoshi Matsumi*.

A special acknowledgement to the *dual degree doctoral program* arranged by the following institutions: JAIST (Japan), SIIT (Thailand), and National Science and Technology Development Agency (NSTDA, Thailand).

Lastly, I would like to thank my family and friends for their moral support and reassurance has made this PhD journey in JAIST less difficult.

September 2020

Jakkapon Phanthuwongpakdee

Contents

This dissertation was prepared according to the curriculum for the Collaborative Education Program organized by Japan Advanced Institute of Science and Technology and Sirindhorn International Institute of Technology.

CHAPTER 1

General introduction

1.1 Environmental problem and bio-based polymers

The world population growth and continuation of anthropogenic activities have led to numerous environmental issues. Some researches suggested that the human had welcomed the plastic age since the end of 1945, when the petrochemical-based polymers replaced the materials such copper, steel, and aluminium in many applications.[1] The overdependence on these petroleum-based plastics (polyester, polyethylene, polypropylene, and polystyrene) have been contributing to the natural resource depletion, waste accumulation, and global warming.[2,3] Consequently, the use of bio-based polymers, which are derived from renewable materials is essential as a part of solving the plastic problem.

One of the future trends for bio-based polymer lied within the polymer functional performance when compared to its conventional counterparts.[4] While, replacing gasoline and diesel by ethanol and biodiesel could be done easily, finding a substitution for the petrochemical polymer is not as simple.[5] Polyhydroxyalkanoate (PHA),[6] polylactides (PLA),[7] polybutylene succinate (PBS),[8] polyethylene furanoate (PEF),[9] and several other and first-generation bio-based polymers[10–12] exhibited low performance for super-engineering plastics and their associated applications. As a result, a bio-based polymer possessing considerable performance similar to that of conventional super-engineering plastics is desired. More time and efforts are required to degrade such durable bio-based polymer into oligomer or monomers. This provides several advantages like polymer recyclability, CO_2 stocking, and contribution to the deceleration of global warming.

1.2 Bio-based organic/inorganic composites and their applications

The organic/inorganic composites are considered as functional polymers. The functional polymers are the class of polymer (with heterogeneous backbone chain) possessing available reactive and polarizing functional groups. With these functional groups, the polymers often offer new or enhanced properties through the systems such as phase separation, reactivity and association.[13] The addition of inorganic materials has been proven to provide the polymer with novel or improved properties. With these properties, the functional polymers become more efficient materials for real-world applications. The information of some organic/inorganic composites prepared by bio-based polymers and their enhanced or new properties are tabulated in Table 1.1.

The organic/inorganic composites can be synthesized through the modification of polymer sidechain. For example, the chlorination of PHA was made possible via an addition or substitution reaction of PHA side chain by chlorine atom (Cl).[14,15] Fluorinated PLA and PHA were developed in the presence of fluorine gas.[16,17] PHA with fluorine atom (F) attached to its side chain could also be produced in vivo.[18] The mentioned PHA with halogens on its side chain showed improved thermal stability, while the fluorinated PLA was observed with enhanced water contact as well as antibacterial property.

The modified cationic polymers could also be considered as organic/inorganic composites due to its salt form being associated with hydroxide anion (OH^-) or anion halogen such as Cl^- and I^-. The natural polymer derived from shells of crustaceans, chitosan, contains amino groups on its side chain. These can be made cationic by quaternization[19] or grafting of gycidyltrimethylammonium chloride.[20] The cationic chitosan was used for drug delivery, antibiotics, and liquid separation.[19–22]

Another way to produce the organic/inorganic composites is to employ ionomer. The composites, usually in the form of complexes, were developed with the ionomer containing carboxylic acid side chain (carboxylate) ionically attached to the additional cationic metal. One well-known natural ionomer is the polysaccharide, alginic acid. In its salt form, alginate, the carboxyl group is ionically (and electrostatically) to cation(s). It can form coordination with multivalent metals, especially the egg-box model with divalent metal.[23] The coordination of alginate with multivalent metal cations (Al^{3+},Ba^{2+}, and Zn^{2+}) produced composites with flame retardant property.[24–26] Iron alginate was synthesized and utilized as a cationic adsorbent for removing anionic arsenic contaminants in the water.[27] The polymers could also be modified or mixed to contain carboxylic acid so that it can form desired complexes. PLA was blended with methacrylic acid to produce ethylene-methacrylic acid. The copolymer was brought to form composites with metal cations (Zn^{2+}, Li^{+}, Na^{+}, and Mg^{2+}), and the resulted composites exhibited improved mechanical strength.[28,29] PHA was grafted with N-acetyl-L-cysteine, and the polymer could form complexes with rare earth metal ions (Eu^{3+} and Tb^{3+}).[30] These composites exhibited photoluminescence properties under UV excitation. Apart from metal-carboxylate formation, metal complexes can also be formed by other bonding formations.[31,32]

Other widely acceptable composites preparation methodologies include direct mixing, extrusion, and solvent cast. The direct addition of aluminium bororate nanowhisker into PHA could enhance the mechanical strength while adding aluminium hypophosphite into PLA offered the polymer with flame retardancy.[33,34] The introduction of titanium dioxide (TiO_2) into PEF produce a photocatalytic composite.[30] The composite with enhanced osteogenic activity was obtained with the combination of PBS and calcium phosphate.[35] By adding zeolite during the synthesis of PBS, improved tensile strength and enzymatic degradation were observe.

Table 1.1 Organic/inorganic composites prepared from bio-based polymers and their properties

bio-based polymer	addition of inorganic substance	enhanced or new properties	ref.
PHA	addition reaction by Cl using excess chlorine gas produced by HCl and potassium permanganate	enhanced thermal properties (T_g increased from -50 °C in PHA to 58 °C in PHA with 21 wt% Cl)	14
PHA	substitution reaction by Cl using excess chlorine gas produced by HCl and potassium permanganate	enhanced thermal properties (T_g 10 °C and T_m 148 °C with 26.9 mol% Cl)	15
PLA	PLA film exposed in CF_4 gas in inductively coupled plasma reactor – substitution reaction by F	- enhanced water contact angel (increased from 54.2° in PLA to 80.3° in PLA with 25 wt% F) - enhanced antibacterial property (*E.coli* colonies reduced from 2213 in PLA to 294 in PLA with 25 wt% F)	16
PHA	fluorination with 5% F_2 in nitrogen	enhanced thermal stability (T_{d5} increased from ~ 200 °C in PHA to ~ 300 °C in fluorinated PHA)	17
alginate	forming metal carboxylate coordination with Zn^{2+} (in $ZnCl_2$ solution)	enhanced thermal stability and developed flame retardancy (T_{d5} 80 °C and *pHRR* 17.1 W/g)	26
alginate	forming metal carboxylate coordination with Zn^{2+} (in $ZnCl_2$ solution)	gained an ability to become cationic adsorbent used to remove AsO_2^- and AsO_4^{3-} in the water	27
PLA/EMMA co-polymer	forming metal carboxylate coordination with Zn^{2+}	enhanced mechanical properties (Torque strength ~ 15 Nm and Young's modulus $>10^3$ MPa in glassy region)	29

PHA grafted with *N*-acetyl-L-cysteine	forming metal carboxylate with Eu^{3+} and Tb^{3+}	gained fluorescent properties (with 320 nm, Eu-PHA and Tb-PHA exhibited strong $^5D_0 \rightarrow {}^7F_2$ and $^5D_4 \rightarrow {}^7F_5$ transition, respectively.)	30
PEF	spin-coated with silver nanowire and formed Ag-O coordination	gained in electrical properties (6.7% power conversion, 0.77 V open-circuit voltage and 15.40 mA/cm^2 short circuit current)	32
PHA	direct mixing in aluminium borate nanowires in chloroform at 50 °C with assisted ultrasound (solution casted into film)	enhanced mechanical strength (tensile strength increased from ~ 25 MPa in PHA to ~ 37.5 MPa in PHA with 0.4% Al_4)	33
PLA	direct mixing in aluminum hypophosphite and extruded at 175 °C	Enhanced flame retardancy (PHRR decreased from 361 W/g in PLA to 187 W/g in PLA with 30 wt% aluminum hypophosphite)	34
PEF	direct mixing with TiO_2, solvent evaporation and hot press to create film	gain photocatalytic property to degrade anti-inflammatory drug	30
PBS	PBS pallets mixed with calcium phosphide in an internal mixer at 160 °C, and the product was hydrolyzed with NaOH	enhanced osteogenic activity (maximum alkaline phosphatase strain in PBS increased from ~ 400 to ~ 800)	35
PBS	zeolite was added during the synthesis of PBS	- enhanced tensile strength (from 32.8 MPa in PBS to 38.1 in PBS with 1 wt% zeolite) - enhanced enzymatic degradation	36

T_g – glass transition temperature, T_m – melting temperature, *PHRR* – peak heat released rate, T_{d5} – temperature at 5% degradation

1.3 4-aminocinnamic acid and high-performance bio-based polymers

The exotic 4-aminocinnamic acid (4ACA) was previously created from the fermentation of sugar by *Escherichia coli*.[37] The synthesis route and structure of 4ACA is illustrated in Scheme 1.1. Through 254 nm UV irradiation of 4ACA, [2+2] photocycloaddition occurred, and a bio-based aromatic diamine, 4,4'-diaminotruxillic acid (4ATA) was produced. 4ATA became the monomer that led to the creations of high-performance bio-based polymers with excellent mechanical strength and thermal stability. The structure of 4ATA and its bio-based polymer derivatives are illustrated in Scheme 1.2. The biopolyimide (BPI) had a maximum temperature at 5% degradation of 410 °C and tensile strength of 98 MPa.[37] The biopolyamides (BPA) possessed a maximum temperature at 10% degradation (T_{d10}) of 370 °C and tensile strength of 407 MPa.[38] According to the literature, these values are comparable to those of the commercial counterparts. The characterizations of BPI and BPA have shown that they have the potential to be used in numerous other applications. For state of the art, the only example can be found in literature, which the modification of polyimide sidechain with indium tin oxide was performed, and an electrical property was observed in the resultant polymer.[39] Taking the functions of organic/inorganic composites into account, the expansion of applications for these bio-based polymers are still left to be explored.

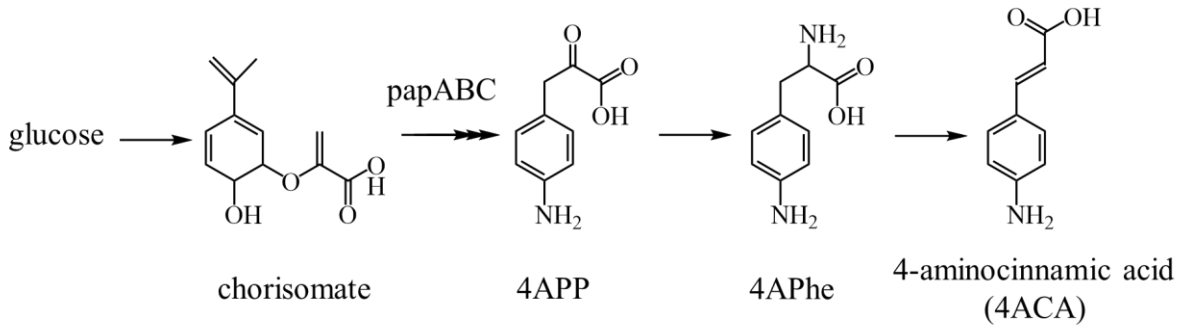

Scheme 1.1 Synthesis of 4-aminocinnamic acid (4ACA) by fermentation

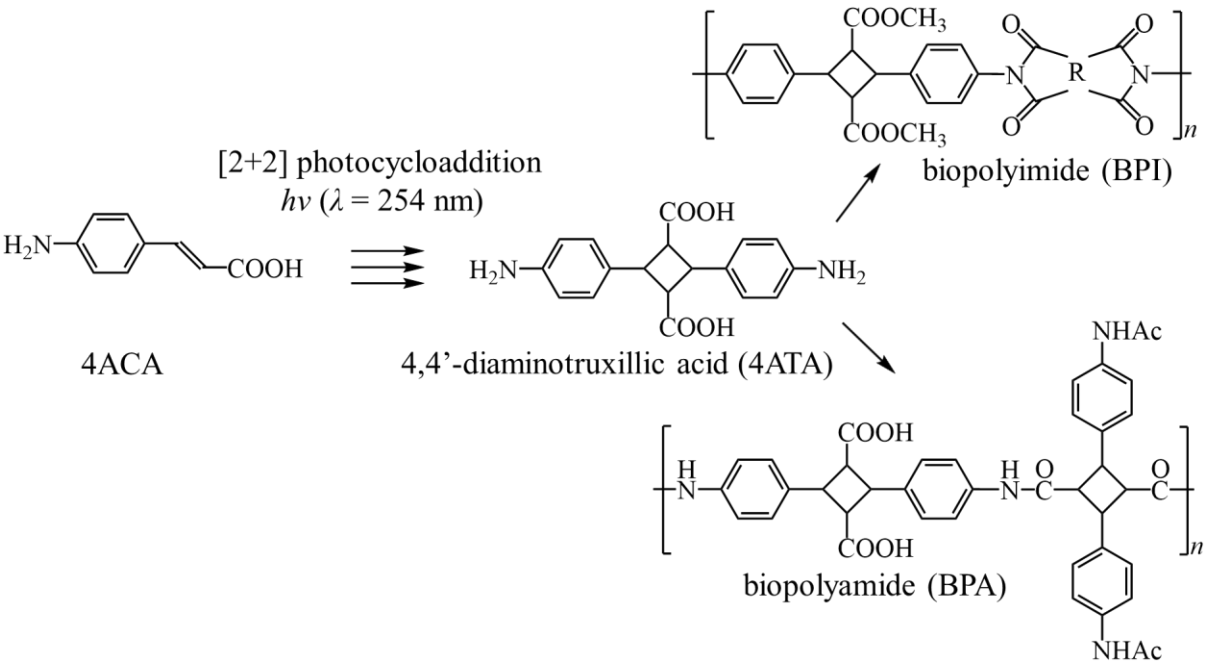

Scheme 1.2 Syntheses of high-performance bio-based polymers from 4ACA

1.4 Molecular design strategy for organic/inorganic polymers composites

Taking into account the structure of 4ATA the organic/inorganic composites can be developed from the monomer according to the desired functions. The molecular design of 4ATA is depicted in Figure 1.1. The benzenes provide the structure with performances related to thermal and mechanical properties. The cyclobutane is responsible for the rigidity. The carboxylic acid (COOH) offers an anionic property, while the ammonium (N_2H) is cationic in nature.

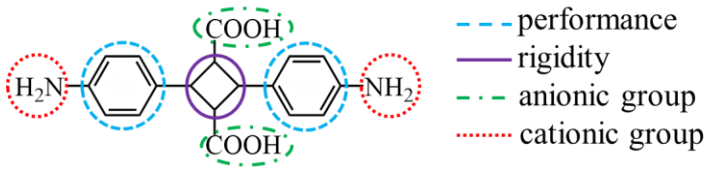

Figure 1.1. Molecular design of 4ATA

The applications of interest include anion scavenging, flame retardancy, and photoluminescent. The section summarized the planned design of organic/inorganic polymer composites for the mentioned functions.

1.4.1 Biopolyimide-metal complexation for flame retardancy and photoluminescence

The flame retardancy polymeric materials were used to increase the safety of infrastructure and transport. To create a bio-based flame retardant film, several other characteristics such as thermo-mechanical stability and high transparency are taken into account. The general development is still struggled to create such a flame retardant film that could maintain the other properties. The flame retardant additive might be responsible for hindering the other properties of the polymer. For instance, the thermal stability and transparency of PLA decreased as a higher combination of lithium, aluminium, layered double hydroxide (LDH) and 2-carboxyethyl phenyl-phosphinic acid (CEPPA) was added to the polymer.[40] At the same time, the total heat release (*THR*) of the PLA during the burn could be reduced to 9 kJ/g. In another case, the metal additive such as Ba^{2+}, Zn^{2+}, and Fe^{3+} could enhance the flame retardancy (V-0 rating of UL-94 standard and peak heat release rate (*PHRR*) of 12 W/g) of the natural polymer, alginate.[25,26,41] Nevertheless, the maximum tested thermal stability could only be improved to a small extent. The BPI created by 4ACA was observed with stable thermo-mechanical properties as well as high optical transparency. The monoamine can be employed to synthesize the bio-based flame retardant polymers while maintaining the other properties.

The photoluminescent materials are essential in the development of medical fields, electrical energy, and sensors. One strategy of obtaining a photoluminescent property is to include rare-earth metals into materials. Poly methyl methacrylate (PMMA) was incorporated with terbium and europium (Eu), which, under 254 nm excitation, the fluorescent emissions at

488, 546, 583, and 619 nm [$^5D_4 \rightarrow {}^7F_J$ (J = 6,5,4,3) transition] was identified.[42] In the mentioned study, the carbonyl groups were responsible for the interactions between PMMA and the rare earth metals. In another case, the ligand, 8-hydroxy-1,5-naphthyridine-2-carboxylic acid formed a complex with Eu in europium chloride solution.[42] Several bonds such as Eu−O (hydroxyl), Eu−O (carboxyl), and Eu−N were identified in its product.[42] Under 345 nm excitation, the product displayed emissions at 576, 589, 612, 646, and 689 nm, which are corresponding to $^5D_0$ to ^7F_J (J = 0 – 4) transitions of the Eu(III) ion.[42]

The syntheses of organic/inorganic composites containing flame retardancy and photoluminescence are similar. Scheme 1.3 illustrated the BPI-metal complex (PI-COOMt) synthesis. Firstly, BPI bearing carboxylic acid (PI-COOH) on its side chain could be produced. With the functional group, PI-COOH should be dissolved in a base like KOH to produce PI-COOK. Lastly, the composites could be developed in metal salt solution through the metal-carboxylate formation. To create flame retardant composites, metals that can offer such property will be chosen. For the luminescent function, a rare earth metal will be employed to produce the composite.

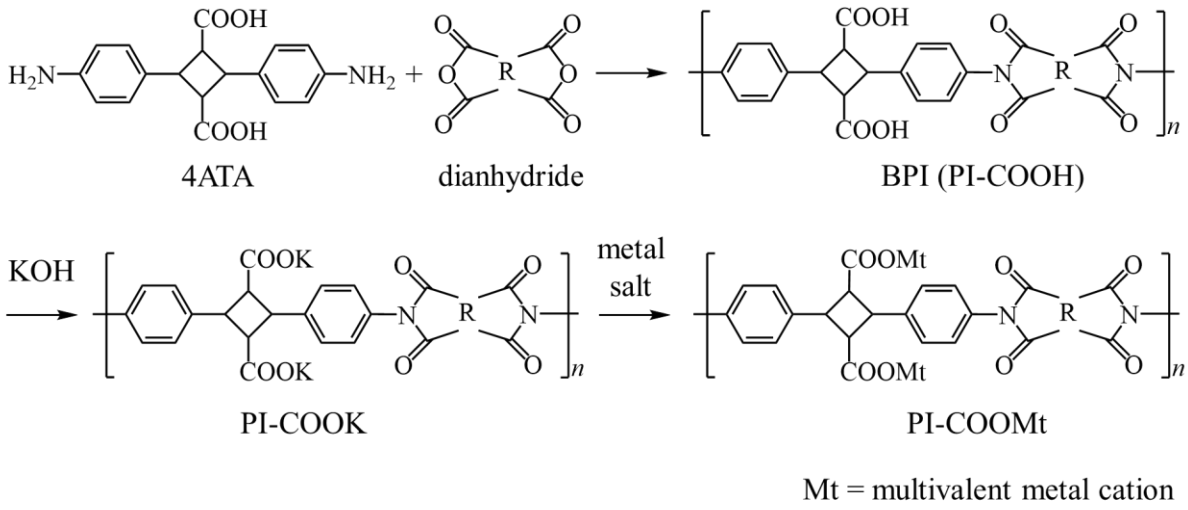

Scheme 1.3 Synthesis plan of BPI-metal complex (PI-COOMt) for the flame retardant and luminescent composites

1.4.2 Quaternization of monomer and cationic bio-based polyamide for anion scavenging

Removal of ionic pollution created by the growing industry is one of the essential environmental issues. The polymers have been modified to remove ionic pollutions in the water, by the mean of adsorption. One of the most common products is the ion-exchange resin, which is usually created by polystyrene or polyacrylic.[43–45] The removal of cationic pollution has been studied extensively, but the same cannot be applied to that of anionic species in the water.[46,47] This is a concern because anionic contaminant like I-131 (8-day half-life), in the form of iodide (I^-), has a high specific energy and can damage living cells and tissues.[48,49] A study showed a nearly 150 mg/g I^- adsorption capacity for the polystyrene-based resin.[50] However, the styrene is a product of non-renewable petroleum and was deemed as unsustainable. Also, polystyrene-based resin exhibited low thermal property (T_{d10} ~ 100 °C).[51] This limited its usage in some of the industries, where I^- was required to be removed in an extreme environment.[52]

The plan for cationic BPA synthesis toward anion scavenging application is illustrated in Scheme 1.4. The preparation of 4ATA could be done by [2+2] photocycloaddition, and the quaternary amine could be achieved by quaternization. The novel monomer would be polymerized with a series of diamine to produce cationic BPA bearing the side chain quaternary amine.

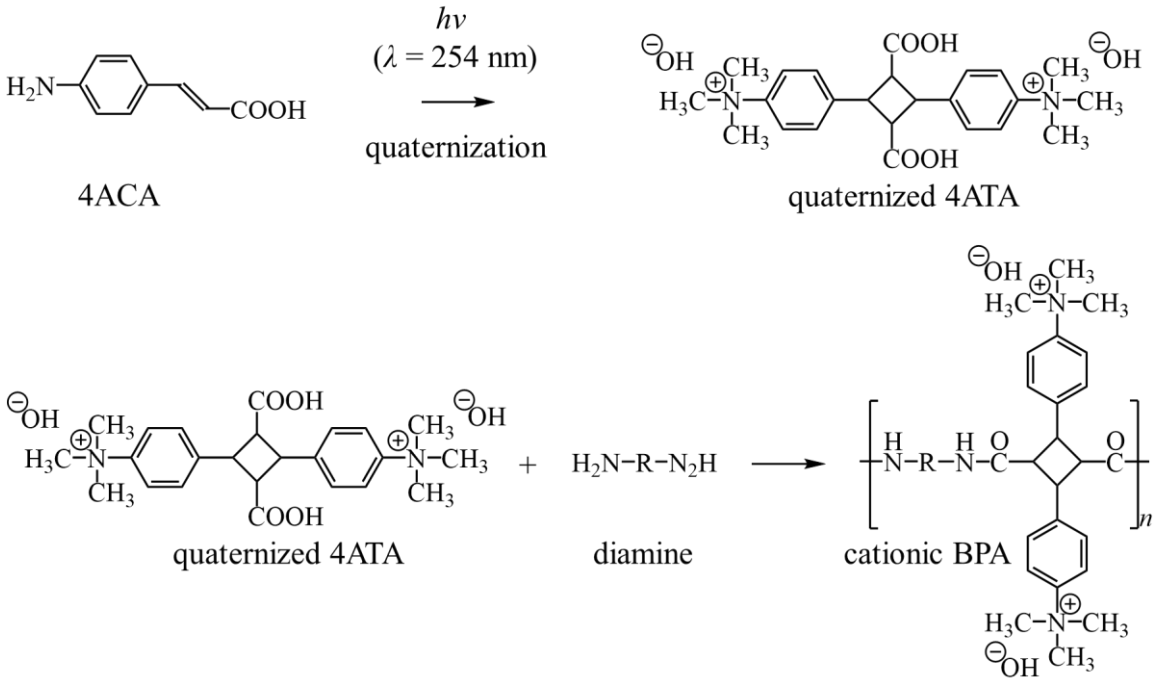

Scheme 1.4 Synthesis plan of cationic BPA for the scavenging of anion

1.5 General purpose

In this thesis, we would like to develop high-performance functional materials from a renewable source for a sustainable society. The main aim is about modifying 4ACA and its bio-based polymers derivatives to create organic/inorganic composites for desired functions. This takes into account the available functional groups on the existing BPA and BPI side chains, mainly COOH and NH groups. We expect that by making organic/inorganic polymer composite, novel properties of the polymer will be created. This would expand the bio-based polymer applications such as anion scavenging, flame retardancy, and photoluminescence. The objectives of this thesis are as follows:

- Develop a novel, monomer, quaternized 4ATA and its cationic BPA derivatives for anion scavenging in the water environment

- Develop BPI-metal complexes (BPI-COOMt) as novel flame retardant materials that can maintain or possess the properties such as thermal stability, mechanical strength and optical transparency
- Develop a BPI-rare earth metal complex as a novel luminescent material
- Characterize the developed organic/inorganic composites according to its specific function
- Test the efficiency of these materials in their respective application, and compare their important parameters with those of previous studies

CHAPTER 2

Cationic biopolyamides from quaternized 4-aminocinamic acid as inorganic anion exchanger

2.1 Introduction

The scavenging technologies for anionic pollutants such as iodine have not efficiently matured in term of performance and sustainability. Specifically, concentrated amounts of iodine-131 (I-131) or iodine-129 (I-129) found in a nuclear power plants and radioactive waste disposal sites, have been described as dangerous substances. Their release into the environment leads to strong radiation that can cause thyroid cancer and damage human organs.[49,53,54] Cesium iodide (CsI) is regarded as the source of soluble radioactive substance in the nuclear facility, while iodide (I^-) was found to be the iodine dominant species in the waste disposal sites.[55,56] For state-of-the-art, membrane separation and coagulation-flocculation-sedimentation systems are promising technologies. Nevertheless, the coagulation-flocculation-sedimentation systems require additives such as silver nitrate and poly aluminium chloride, and the results have shown low to moderate I^- removal efficiency.[57,58] The membrane separation technology yields a near-desalination-quality permeate, but the system produced a stream with concentrated contaminants, and it requires high electrical energy to operate.[59,60]

The adsorption has become an essential technology that improve the process of I^- removal in the water. Although the activated carbon was able to remove a high quantity of iodine compound (I_2), low I^- adsorption was observed for the adsorbent.[61,62] The efficiency could be improved with the inclusion of metal such as silver, iron and copper.[63–66] However, the metals can become contaminants and cause other environmental-related problems.[67,68] The conventional polystyrene-based cationic resin can remove I^- in groundwater and seawater

environments.[69,70] Despite an elevated I^- removal capacity of 148.23 mg/g for the silica-based poly(4-vinyl pyridine) resin, the petroleum-derived polymers are unsustainable due to their reliance on dwindling petroleum reserves.[50] Furthermore, polystyrene resins were found to possess low thermal stability [temperature at 10% degradation (T_{d10}) ~ 100 °C], which restricts the material applications at a high temperature.[51] The waste nuclear effluents are released or stored at high temperatures, and specifically in the waste container, where the radiation could cause the rise of temperature up to 120 °C.[52] Therefore, there is a demand of efficient systems to adsorb toxic ions evenly without an appreciable loss in efficiency and/or material degradation. The cationic nature of quaternary ammonium is mainly responsible for the anion exchange process but the stability problem of the functional group in the commercial anion-exchange resin has been addressed. At a high temperature, quaternary ammonium decomposes, resulting in lower resin ion-exchange capacity. Under heating, the Hoffman elimination occurs, and the quaternary ammonium is converted into the tertiary form with methyl alcohol as a byproduct.[71] Since OH^- in the salt form of the polymer triggered such degradation, it was proposed that by increasing the water molecules in the polymer complex, $OH^-(H_2O)_x$ clusters are formed and nucleophilic substitution is reduced.[72] As a result, there is a need to find a more sustainable, effective, highly thermally stable, alternative material that can remove anionic pollutions from water.

Recently a bio-based polymer has been developed from the monoamine, 4-aminocinnamic acid (4ACA), a compound obtained from the fermentation of glucose by genetically engineered *E. coli*.[37–39] The resultant biopolyamides (BPA) exhibited mechanical and thermal characteristics (T_{d10} and tensile strength up to 370 °C and 407 MPa, respectively) that are higher than conventional polyamide or cationic polystyrene and acrylamide polymers.[38,73,74] More importantly, the 4ACA-based biopolyamide showed degradation in

solution under ultraviolet (UV) irradiation. After 24 h of UV irradiation, with conc. hydrochloric acid (HCl), the starting monoamine can be retrieved.[38]

With the UV-degradation ability and high thermal stability, a modified form of the existing glucose-derived biopolyamide can be employed as the I^- removal agent for the application of radioactive iodine remediation in the water environment. In this research, we employed 4ACA to synthesize a quaternary diamine derivative. The biomonomer, 4,4'-di(trimethylamino)truxillic acid (Q-4ATA), was polymerized with various diamines to yield a series of BPA having cationic side chains. In addition, the synthesized BPA were tested for the I^- removal, and the efficiency was studied with variation in factors such as polymer dosage, time, solute concentration, pH and temperature.

2.2 Experimental

2.2.1 Materials

Diamine precursor, 4-aminocinnamic acid (compound 1), was produced by the fermentation of glucose, as described in a previous study.[38] A polymerization solvent, 1-methyl-2-pyrrolidinone (NMP, Tokyo Chemical Industries, Japan); condensation agent, triphenyl phosphate (TPP, Tokyo Chemical Industries, Japan); catalyst agent, pyridine (Py, Tokyo Chemical Industries, Japan); and iodomethane (CH_3I) stabilized with copper chip (Tokyo Chemical Industries, Japan); were used as received. *p*-Phenylenediamine and 4,4'-oxydianiline were purified by sublimation, and 4,4'-diaminodiphenyl sulfone was recrystallized with water after being received (Sigma-Aldrich, Japan). Citric acid, ammonium hydroxide, ammonium dihydrogen phosphate, tris[4-(phenylcarbonyloxy)phenyl]methyl bromide, mercuric chloride, and potassium peroxymonosulfate for the standard method of I^- quantification were used as received (Sigma-Aldrich, Japan). The common acids and bases such as hydrochloric acid (HCl), hydroiodic acid (HI), sodium hydroxide (NaOH), and

potassium hydroxide (KOH) were used as received (Kanto Chemical Co. Inc., Japan). The other reagents were salts from Tokyo Chemical Industries, Japan, which include potassium iodide (KI), sodium chloride (NaCl), sodium sulfate (Na_2SO_4), sodium hydrogen carbonate ($NaHCO_3$), and potassium bromide (KBr). DOWEX^{TM} 550, the commercial anion-exchange polystyrene-based resin, was used as received (DOW Chemical Thailand Ltd., Thailand).

2.2.2 Monomer synthesis

The synthetic route of quaternized 4,4'-diamino-α-truxillic acid (Q-4ATA) is illustrated in Scheme 2.1. A solution of 4ACA (4.0 g, 0.02 mol) in acetone (60 mL) was reacted with conc. hydrochloric acid solution. After stirring for 6 h, 4-aminocinnamic acid hydrochloride (compound 2) was produced (yield 85.9%). The obtained product was subjected to photo-dimerization for 24 h, under the irradiation of a 100-W high-pressure Hg-lamp (Omni Cure S1000, EXFO Photonic Solution Inc.). The reaction was monitored by proton nuclear magnetic resonance (^{1}H NMR, Bruker Biospin Inc., 400 MHz, DMSO-d_6). A complete [2+2] photocycloaddition in hexane yielded 4-aminocinnamic acid hydrochloride dimer (compound 3, yield 73.7%).

The obtained 4ATA was dissolved in water and purified by activated charcoal. After separation, NaOH was used to adjust the liquid phase to pH 3, where the white precipitate of 4,4' diamino-α-truxillic acid (4ATA, compound 4) was observed. The mixture was left agitated for 30 min before the separation. 1.0 g of dried compound 4 (3.07 mmol) in acetone (15 mL) was subjected to quaternization with CH_3I (30 mL) in the presence of 250 μM NaOH solution (10 mL). A complete quaternization was achieved after 24 h, yielding an orange solution. Conc. HI was added dropwise into the solution until the Q-4ATA (compound 5) precipitated (yield 96.9%). ESI-FT-ICR MS (9.4 T SolariX FT-ICR MS, Bruker Daltonics, USA) was used in positive mode to confirm the monomer mass components. Methanol was used as a solvent with

the sample prepared as 1 μmol/mL. The syringe and dry gas flow rates were set to 120 μL/h and 3 L/min, respectively, at a dry temperature of 200 °C. The capillary voltage was set to 4500 V, and the plate offset was -500 V. The structure of Q-4ATA was confirmed by ^{1}H and ^{13}C NMR; ^{1}H NMR (400 MHz, DMSO-d_6, δ, ppm): 3.62 (s, 18H), 3.92 (dd, 2H, J = 10.22, 7.38), 4.40 (dd, 2H, J = 10.24, 7.34), 7.63 (d, 4H, J = 9.04 Hz), 7.94 (d, 4H, J = 9.08 Hz), 12.37 (s, 2H); ^{13}C NMR (400 MHz, D_2O, δ, ppm): 40.6, 46.2, 56.8, 119.9, 129.3, 141, 145.5, 175.7

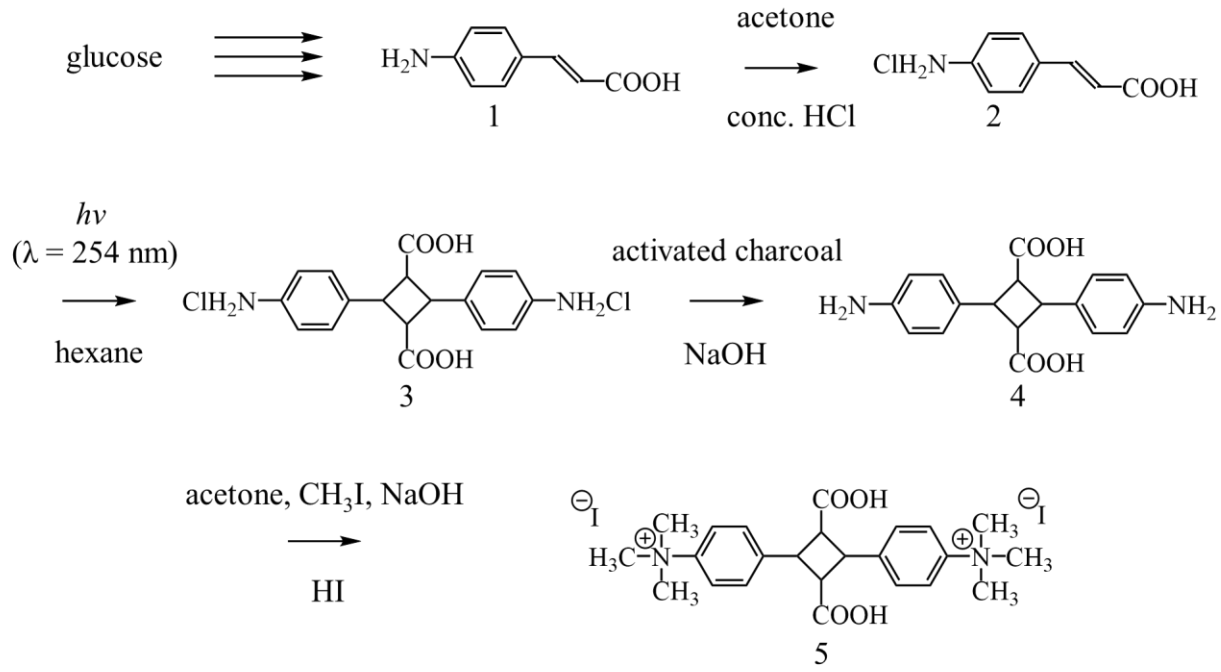

Scheme 2.1 Synthetic route of the quaternary derivative of 4-aminocinnamic acid (Q-4ATA)

2.2.3 Cationic biopolyamides syntheses

The preparation of cationic polyamides is depicted in Scheme 2.2. Under an inert atmosphere, an equimolar mixture of Q-4ATA (0.5 g, 1.20 mmol) and *p*-phenylenediamine (diamine R1, 0.13 g, 1.20 mmol) was set up to polymerize in a homogeneous solution of NMP (0.72 mL) in the presence of condensation reagents, TPP (0.41 mL, 1.48 μmol) and Py (0.36 mL, 4.49 mmol). The reaction was performed at 100 °C for 3 h to obtain a homogeneous, viscous solution. The resulting solution was re-precipitated in ethanol to obtain polyamide

fibrils, which were filtered and dried under vacuum at 60 °C for 12 h. The polymerizations of Q-4ATA with other diamines Scheme 2; 4,4'-oxydianiline (diamine R2), 4,4'-diaminodiphenyl sulfone (diamine R3) and 4,4′-diamino-α-truxillic acid dimethyl ester (diamine R4) were carried out by the procedure analogous to that with R1. R4 was chosen based on it being another derivative of the bio-based 4ACA, while R1, R2, and R3 were chosen as common aromatic diamines. The rigidity of these bridging diamines aromatic structures was also deemed favorable in term of molecular weight and thermal resistance for the polymerization of BPA.[75,76]

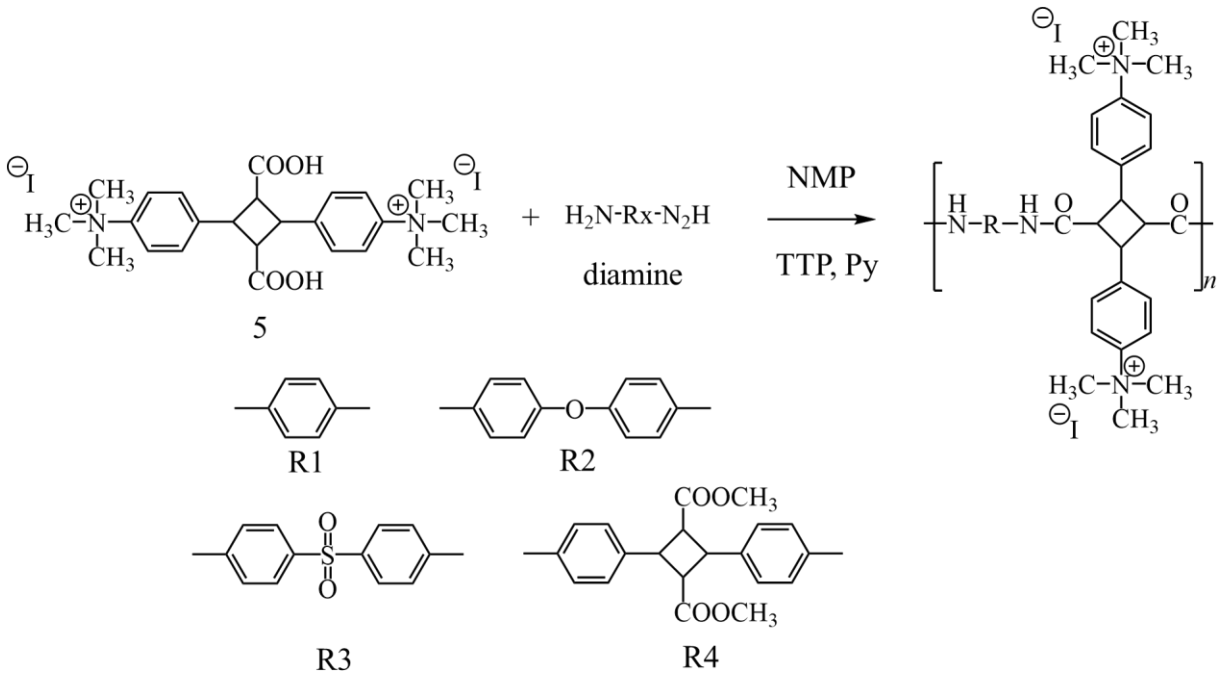

Scheme 2.2 Synthetic route of cationic BPA

2.2.4 Solubility tests

The solubility of monomers and polymers was tested in various solvents, such as hexane, toluene, dimethylacetamide (DMAc), ethyl acetate (EtOAc), acetone, dimethyl sulfoxide (DMSO), dimethylformamide (DMF), ethanol, methanol, and water. Solid sample (10 mg) was added to 0.5 mL of solvent. If the solute was not soluble, the mixture was heated,

and the solubility was checked under reflux conditions. Each solvent was heated to about 70% of its boiling point, to prevent complete evaporation.

2.2.5 Cationic biopolyamides characterization

Fourier transform infrared spectra (FT-IR) were recorded on a Perkin Elmer spectrometer using a diamond-attenuated total reflection (ATR) accessory between 4000 and 400 cm^{-1}.

A gel permeation chromatograph (GPC, concentration 5 g/L, DMF eluent, Shodex GPC-101, Showa Denko K. K., Tokyo, Japan) equipped with a reflective index detector (RI-2031 Plus, Jasco, Tokyo, Japan) and an ultraviolet detector (UV-2075 Plus, Jasco, Tokyo, Japan), was used to determine the number-average molecular weight (*Mn*), weight-average molecular weight (*Mw*), and the molecular weight distribution (PDI). The GPC was calibrated with polystyrene standards.

For the thermal characterizations, thermogravimetric analysis (TGA) and differential scanning calorimetry (DSC) were performed on STA 7200 (Hitachi, Tokyo, Japan) and X-DSC7000T (Hitachi, Tokyo, Japan), respectively. The moisture was eliminated at 150 °C for 6 h before TGA and DSC measurement. BPA were dried at 100 °C for at least 6 h before TGA and DSC analyses. TGA was measured under a nitrogen atmosphere in the temperature range of 25 – 800 °C, and the heating rate was set to 10 °C /min with a 10 min holding time. DSC was also set up with 10 °C /min heating rate. The TGA data of commercial polystyrene-based, DOWEX™ 550, from previous research was used for comparison.[51]

Since the BPA in this work were derived from the glucose-based monoamine, 4ACA, they were accessed for the percent use of renewable sources in their structures. The metric was previously proposed as one of the sustainability metrics for the life cycle assessment and green design in polymers.[77] In this case, Q-4ATA is also considered to be a renewable resource as

the added groups of CH_3 to create quaternized ammonium came from CH_3I, the product of iodine and methanol in the presence of phosphorus. All diamines presented in Scheme 2 were not considered as renewable resource except for R4, which was synthesized from 4ACA. The percent use of renewable sources was calculated from the theoretical atomic weight of the compounds in the BPA structures, and an example of the calculation is presented in Scheme 2.3.

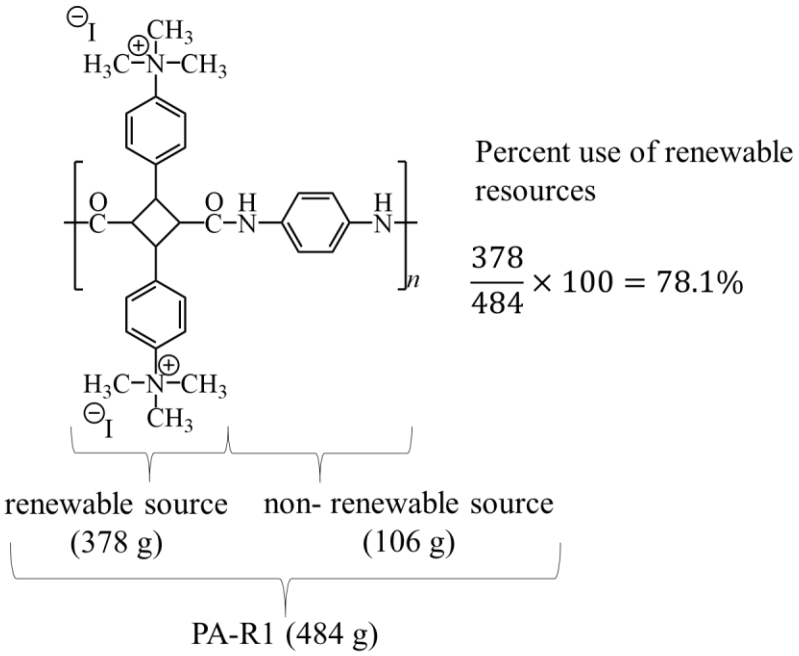

Scheme 2.3 Percent use of renewable resources calculation for PA-R1

2.2.6 Potassium hydroxide treatment treatment

KOH treatment was conducted to generate the hydroxide (OH^-) form of the quaternary ammonium in the cationic polymer for the target anion-exchange process. 1.0 g of BPA (initially in I^- form after the syntheses) were ground and submerged in 1 M KOH solution (30 mL) for 24 h. The solutions were filtered, and the obtained polymer was washed thoroughly in DI water. Before the KOH treatment, right after the treatment, and after being washed with DI water, scanning electron microscopy coupled with energy-dispersive X-ray spectroscopy

(SEM-EDX, JEOL, Japan) was used to analyze the polymer morphology and its elemental composition. The confirmation of anion-exchange by EDX was adopted from the literature.[78] The molecular weight of the treated BPA was checked, with the GPC analysis, for the possibility of hydrolysis of the amide backbone.

2.2.7 Iodide removal in water

KI was used as the I^- source. The standard method of Leuco Crystal Violet was used for the supernatant I^- quantification.[79] The ultraviolet–visible (UV–Vis) optical absorption spectra were recorded on a Perkin-Elmer, Lambda 25 UV/Vis spectrophotometer at room temperature at 592 nm.

The I^- removal at different BPA dosages (0.01, 0.1, 1, 2, 5, and 10 g/L) was tested to determine a suitable amount of BPA for the kinetic test. I^- concentration of 10 mg/L was selected, according to the concentration of radioactive iodine I-131 in a pressurized nuclear reactor.[80] The experiment was conducted with 120 min of contact time in a water bath, maintaining room temperature. The removal percentage (%) was determined by Equation 2-1:

$$I^- \text{ removal } (\%) = \frac{C_i - C_e}{C_i} \times 100 \quad (2\text{-}1)$$

where, C_i is the initial I^- concentration (mg/L), and C_e is the final concentration after the removal test (mg/L).

The kinetic test was performed using the synthesized cationic BPA to remove I^- from a solution and to determine the equilibrium time of the anion-exchange process. The range of contact time was 0 – 180 min, and the polymer dosage was determined previously. The experiment was conducted with a 10 mg/L initial I^- concentration, at room temperature. The exponential decrement in the sorbate concentration with time exemplifies the linear form of the

pseudo-first and pseudo-second-order reactions represented by Equations 2-2 and 2-3, respectively. For the mentioned equations, k_1 and k_2 are the pseudo-first and pseudo-second-order reaction constants, respectively. q_t represents the adsorbed solute per weight of adsorbent at a given time, t. q_e is the adsorbed solute per weight of adsorbent at equilibrium.

$$\log(q_e - q_t) = logq_e - \frac{k_1}{2.303}t$$

(2-2)

$$\frac{t}{q_t} = \frac{1}{k_2 q_e^2} + \frac{t}{q_e}$$

(2-3)

The batch concentration experiment was conducted to determine the adsorption isotherms. The optimum set of conditions (equilibrium time and dosage) for each respective biopolyamide was used, according to the results from the previous section. The adsorption with an I^- initial concentration of 5 – 1000 mg/g was conducted at room temperature. The results were fitted with linear (Equation 2-4), Langmuir (Equation 2-5), and Freundlich (Equation 2-6) isotherms.

$$K_D = \frac{q}{C_e}$$

(2-4)

$$\frac{1}{q} = \frac{1}{q_{max}} + \frac{1}{K_L\, C_e\, q_{max}}$$

(2-5)

$$Logq = \frac{1}{n} LogC_e + Log\ K_F$$

(2-6)

where, q is the of adsorption or amount of the solute mass adsorbed per unit mass of the adsorbent. K_D, K_L, and K_F are the adsorption coefficients of the linear, Langmuir, and Freundlich isotherms, respectively. The value of q_{max} is the predicted sorption capacity, corresponding to the total number of surface sites, obtained from the Langmuir model. n is the exponent related to the sorption intensity and sorption free energy, obtained from the Freundlich model.

The I^- exchange tests were also conducted at various temperatures (10, 20, 40, 60, 80 and 90 °C) and pH (2, 5, 7, 10, and 12). HCl and NaOH solution were employed for the pH adjustment in the I^- solution, and DOWEX^{TM} 550 was used as a reference. To access the selectivity of PA-R4 for removing I^-, the adsorption experiment was conducted in the presence of other anions. NaCl, Na_2SO_4, $NaHCO_3$, and KBr were used as the sources of chloride (Cl^-), sulfate (SO_4^{2-}), bicarbonate (HCO_3^-), and bromide (Br^-), respectively. The competitive species and their added concentration (1000 times that of I^- molar concentration) were selected based on the seawater composition.[81] Additionally, I^- adsorption by PA-R4 was also tested with tap water and filtered seawater (collected from Chon Buri province, Thailand). For the effects of temperature variation, pH variation and selectivity test, the 10 mg/L initial I^- solution was used with 120 min contact time and pre-determined BPA dosages.

The reusability of the PA-R4 was investigated using I^- adsorption-KOH regeneration cycle. The dosage of 5 g/L was employed in the adsorption of 10 mg/L I^- until the equilibrium was achieved. After separation, the used PA-R4 was submerged in 1 M KOH solution for 6 h (about 3 times that of I^- adsorption time) while maintaining the same polymer dosage. The regenerated PA-R4 was washed with DI water and employed for the next cycle of I^- adsorption-

KOH regeneration. For each cycle, the final I^- concentration was quantified, and adsorption efficiency was determined.

2.3 Results and discussion

2.3.1 Quaternized synthesis

4ATA was quantitatively synthesized by the photonic dimerization of a microbially-derived molecule, 4ACA, which was thoroughly dried about 60 °C *in vacuo*, for a yield of over 99 mol%. The microbial products contained a small amount of water, but the water and a trace amount of inorganic salts in the cultivation media can induce *E-Z* isomerization of 4ACA, which disturbed the aimed-for reaction. The successive recrystallization of 4ATA over charcoal was significant for quaternization, and polymerization required the accurate one-to-one molar balance of diacid and diamine monomers. The yield of each step was more than 95%. Q-4ATA as a final product appears as yellow crystals, as shown in Figure 2.1.

The formation of Q-4ATA was spectroscopically confirmed by ^{1}H NMR (400 MHz, DMSO- d_6), ^{13}C NMR (400 MHz, D_2O) and ESI FT-ICR MS as shown in Figure 1. The ^{1}H NMR spectra in Figure 2.2 show a strong singlet signal at δ 3.62 ppm (s, 18H), which corresponded to the CH_3 protons at the quaternary ammonium, together with double-doublet signals at δ 3.92 and 4.40 ppm, characteristics of cyclobutane ring. Proton signals assigned to benzene rings are shown in a lower magnetic field at δ 7.63 and 7.94 ppm, and there is a broad carboxylate signal at δ 12.37 ppm.

^{13}C NMR spectra in Figure 2.3 shows signals at δ 40.6 and 46.2 ppm, depicting the 4 carbon atoms of the cyclobutene ring. A strong peak at δ 56.8 ppm corresponded to the 3 carbon atoms of each quaternary ammonium group. The signals at δ 119.9, 129.3, 141.1, and 145.5 ppm exhibited the formation of the benzene rings, while the signal at δ 175.7 ppm signified the existence of carboxylic acid groups. The ratio of integral values of all the signals is consistent

with the calculated ratio of Q-4ATA protons and carbons. The ESI-FT-ICR-MS spectrogram of Q-4ATA (Figure 2.4) depicted an adjusted peak of M^{2+} that is equal to 206.11735, which was found to be similar to the calculated m/z of 206.11756.

Figure 2.1 Q-4ATA crystals

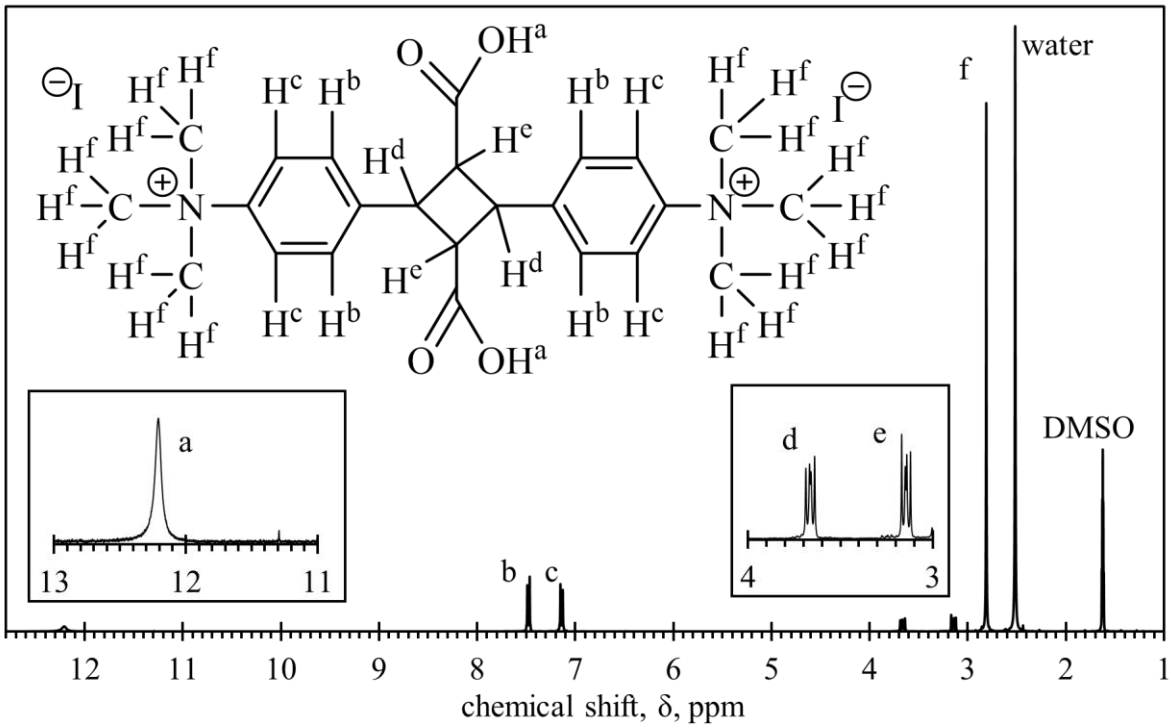

Figure 2.2 ^{1}H NMR spectrum of Q-4ATA

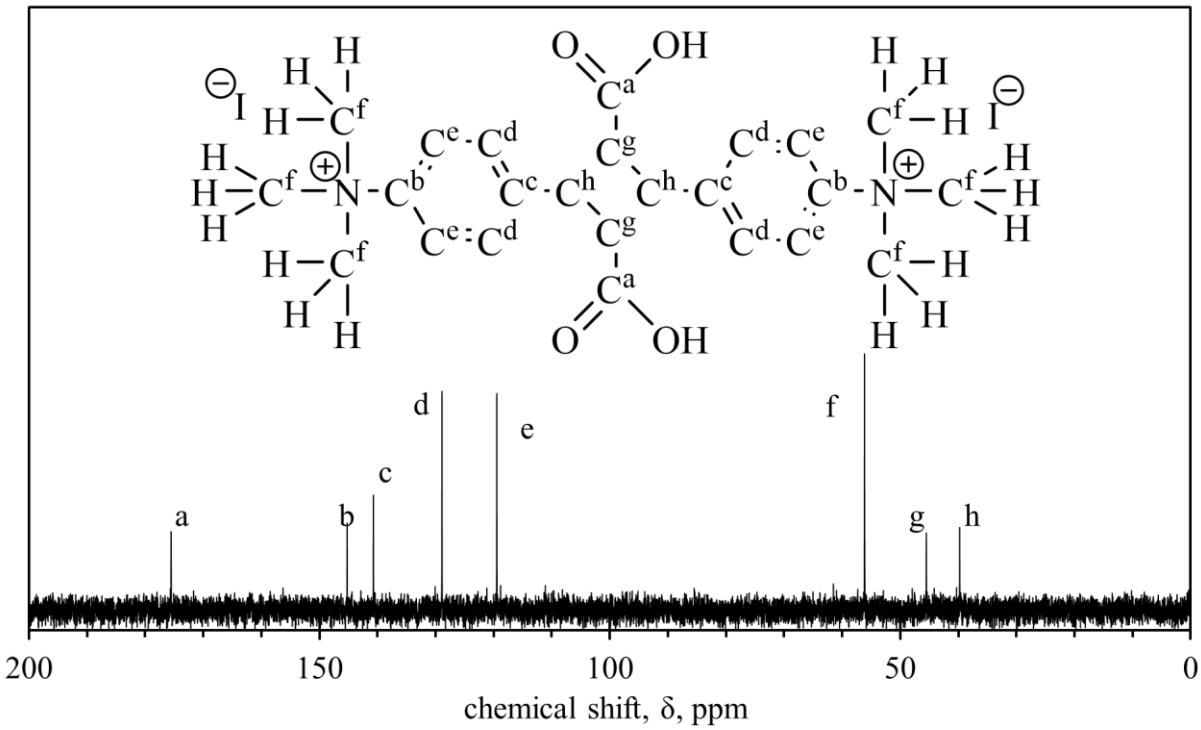

Figure 2.3 ^{13}C NMR of Q-4ATA

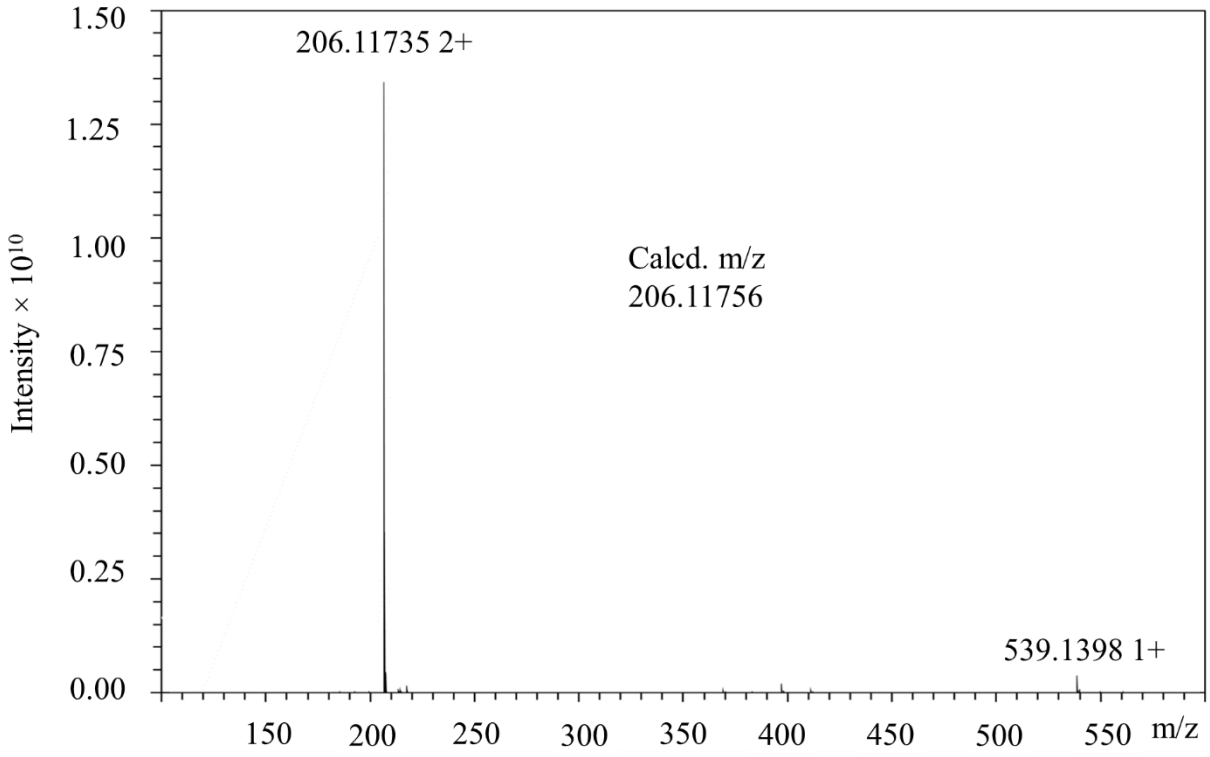

Figure 2.4 Mass spectrum of Q-4ATA

2.3.2 Cationic biopolyamides

The Q-4ATA shows appreciable reactivity, to obtain various BPA with most of the diamine yielding greater than 90%. The images for the synthesized BPA are shown in Figure 2.5, where PA-R2 was obtained as a white precipitate, and the other BPA were yellow.

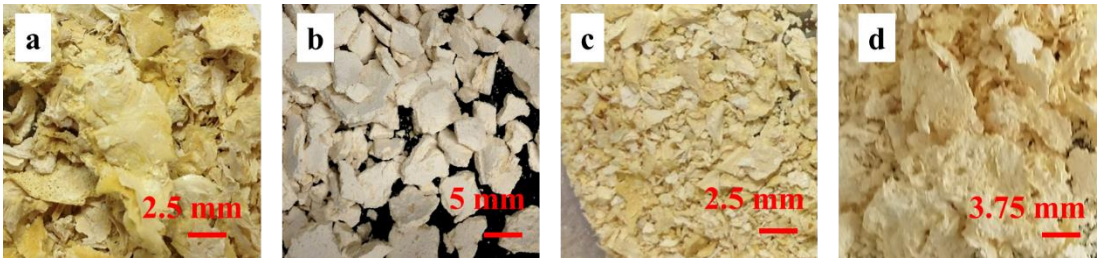

Figure 2.5 Images of cationic BPA in fibril form. (a) PA-R1, (b) PA-R2, (c) PA-R3, (d) PA-R4

The formation of BPA was confirmed by FT-IR/ATR spectra (Figure 2.6), showing characteristic amide I and amide II bands at ranges of 1600-1700 cm^{-1} and 1600-1500 cm^{-1}, respectively. PA-R2 showed C-O-C stretching of the ether group at about 1215 cm^{-1}. Distinct peaks were observed at 1150 and 1310 cm^{-1} in PA-R3, which correspond to the S=O stretching of the sulfone group. C=O stretching was observed at 1730 cm^{-1} in PA-R4, which corresponded to the carboxylate ester group. ^{1}H NMR results of the BPA are shown in the Figure 2.7. While the BPA still maintained the quaternary amines (δ 2.5 - 3 ppm), the main chain signals for amides and cyclobutene also appeared around δ 9.8 - 10.1 and 3.7 - 4.3 ppm, respectively. The aromatics were observed with the signal range δ 6.5 - 7.3 ppm.

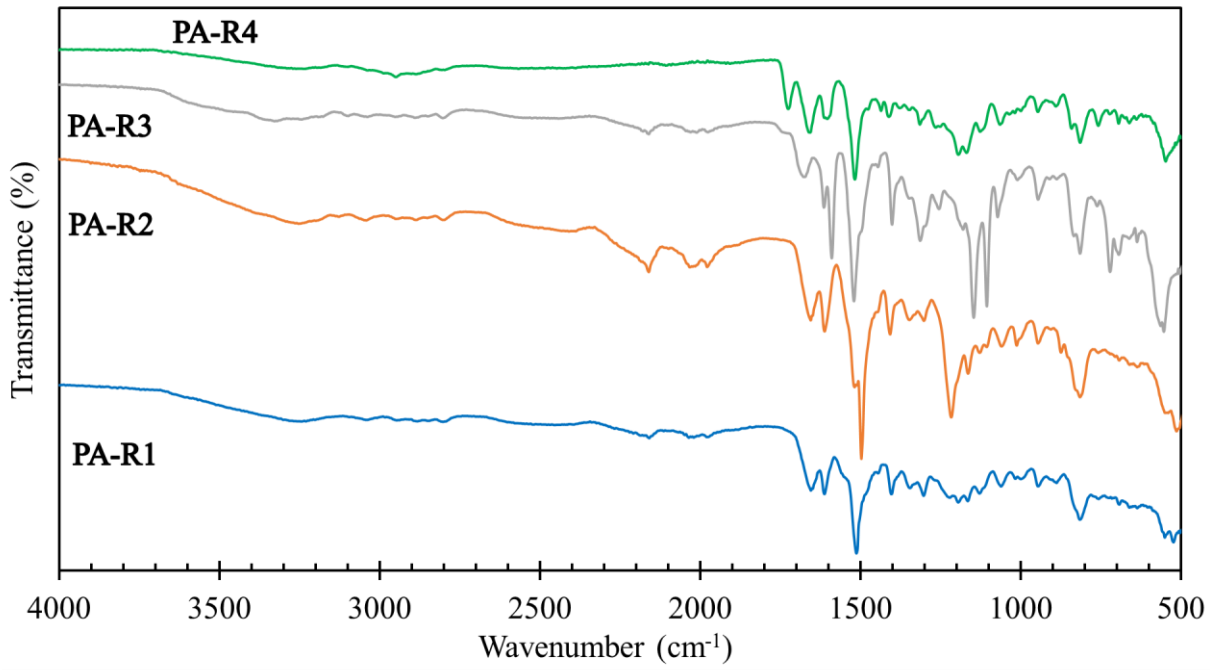

Figure 2.6 FTIR spectra of cationic BPA

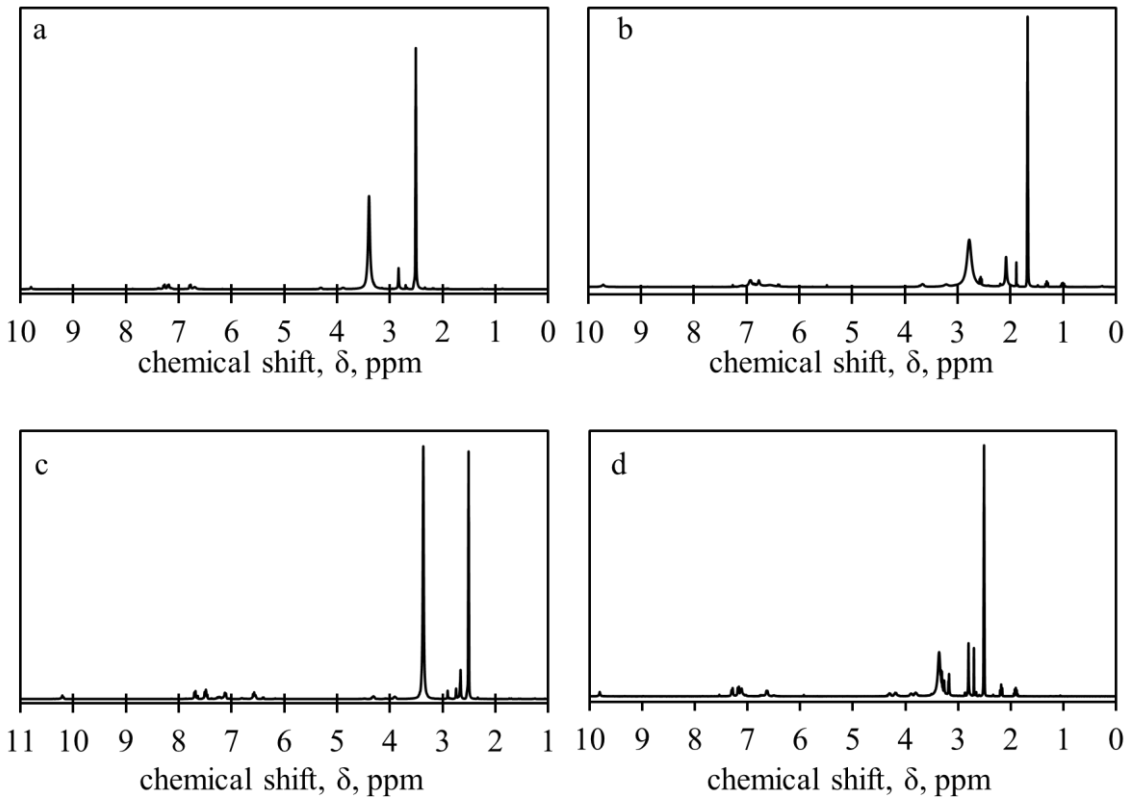

Figure 2.7 ^{1}H NMR results of the cationic BPA. (a) PA-R1, (b) PA-R2, (c) PA-R3, (d) PA-R4

The weight average molecular weight (*Mw*) of the BPA were confirmed with GPC, which was found to be in the magnitude 10^4 g/mol (Table 2.1). Due to the high reactivity of the monomers, PA-R4 acquired the highest *Mw*, while low solubility of R3 in NMP led to low *Mw* for PA-R3. All the PDI values were about 2 and deemed acceptable for the condensation polymerization experiment.[82]

Table 2.1 Thermal properties, molecular characteristics of cationic BPA and percent use of renewable sources

cationic BPA	GPC			TGA			DSC	percent use of renewable sources (%)[a]
	Mw (x 10^4)	*Mn* (x 10^5)	PDI	T_{d1} (°C)	T_{d5} (°C)	T_{d10} (°C)	T_g (°C)	
PA-R1	1.74	0.705	2.47	245	271	296	162	78.1
PA-R2	1.21	0.469	2.58	185	280	303	ND	65.6
PA-R3	0.419	0.177	2.37	199	269	297	ND	60.6
PA-R4	4.33	1.87	2.31	272	300	329	ND	> 95
DOWEX™ 550	n/a	n/a	n/a	~60	~70	~100	n/a	n/a

[a]calculated by the equation inset of Scheme 2.3

Mw – weight-average molecular weight, *Mn* – number-average molecular weight, PDI – molecular weight distribution, T_{d1} – temperature at 1% degradation, T_{d5} – temperature at 5% degradation, T_{d10} – temperature at 10% degradation, T_g – glass temperature, ND – not detected, n/a – not available

2.3.3 Thermal analyses

The bridging amines (R1 – R4) and their rigid structure contributed to the thermal properties of the polymer (as explained in the Experimental section). BPA in this research

exhibited moderately high resistance against thermal decomposition. The plots of TGA curves are shown in Figure 2.8. All types of cationic BPA exhibit temperature at 1% degradation (T_{d1}), temperature at 5% degradation (T_{d5}), and T_{d10} in ranges of 185 – 272, 269 – 300, and 296 – 329 °C, respectively (Table 2.1). PA-R4 possessed the highest heat resistance with T_{d10} of 329 °C, and this may result from the cyclobutane of R4, which help to increase the rigidity of the polymer structure. In contrast, according to the literature, the commercial polystyrene resin for water treatment had a T_{d10} of approximately 100 °C [51], which was less than that of the presented BPA. The glass transition temperature (T_g) for PA-R1 was detected by DSC to be 162 °C, while those of the others remained undetected, presumably because their values were above the thermal degradation onset Table 2.1. The DSC curves are available in Figure 2.9.

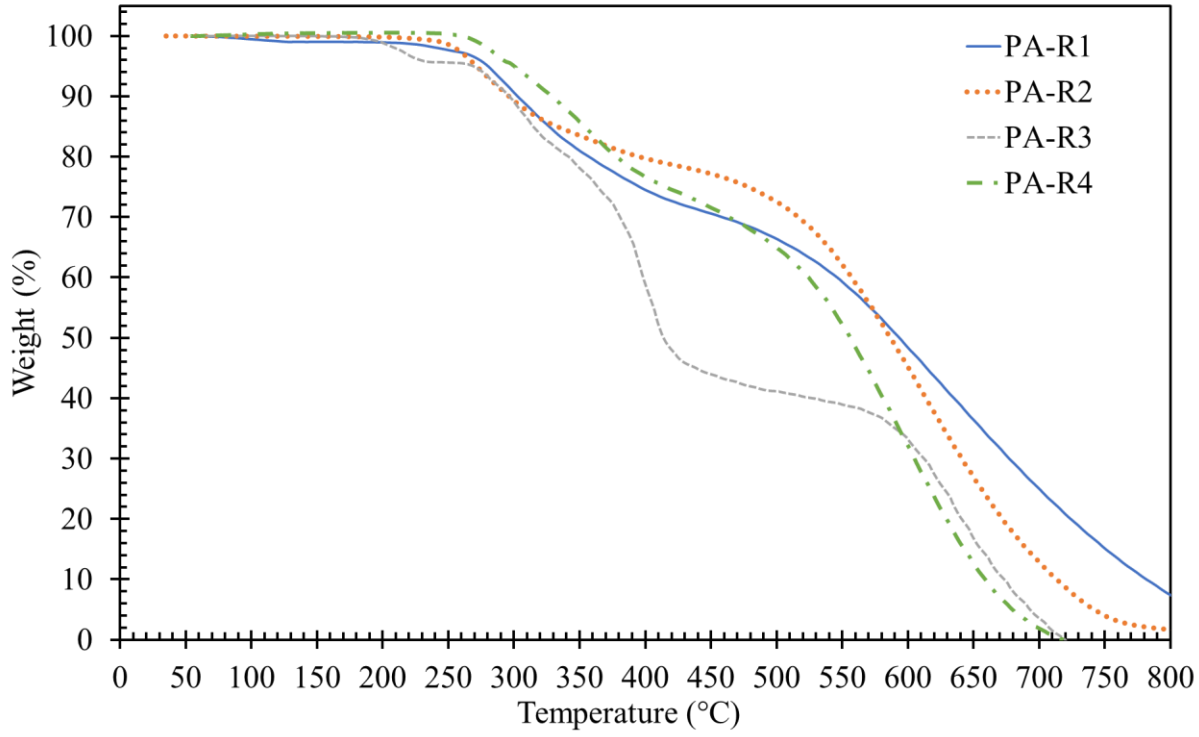

Figure 2.8 TGA curves of cationic BPA measured under nitrogen condition

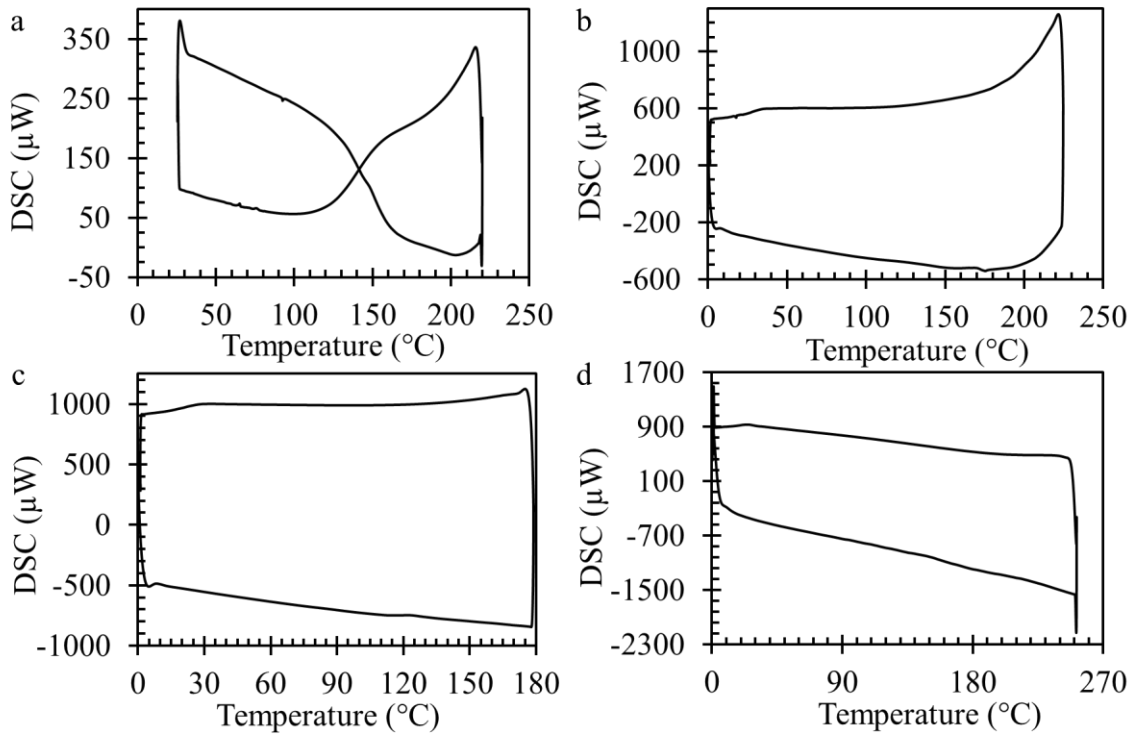

Figure 2.9 DSC curves of cationic BPA measured under nitrogen condition. (a) PA-R1, (b) PA-R2, (c) PA-R3, (d) PA-R4

2.3.4 Sustainability metric – use of renewable resource

As one of the sustainability metrics, the percent use of renewable resource was calculated for all the BPA (Table 2.1). More than 99% was calculated for PA-R4 as it is solely regarded as a fully bio-based polyamides. Both of its precursors (Q-4ATA and diamine R4) were synthesized from the glucose-derived 4ACA. The other cationic BPA consist of more than 50% of renewable resources in its structure.

2.3.5 Solubility

The solubility of Q-4ATA and BPA is summarized in Table 2.2, where the relative polarity was taken from the literature.[83] The monomer and BPA were readily soluble in a strong polar aprotic solvent such as DMAc, DMF, and DMSO. The relative polarity of the monomer was assumed to be similar to that of methanol as it rapidly dissolved in the solvent. In ethanol,

a small difference in the relative polarity between the monomer and solvent requires heat, for complete dissolution. As an ionic salt, the monomer was expected to be soluble in water. However, due to the relative polarity difference, heat is again required for the monomer to be soluble in water.

Table 2.2 Solubility of Q-4ATA and cationic BPA

sample	solvent (relative polarity[a])									
	hexane (0.009)	toluene (0.099)	EtOAc (0.228)	acetone (0.355)	DMAc (0.377)	DMF (0.386)	DMSO (0.444)	ethanol (0.654)	methanol (0.762)	water (1)
Q-4ATA	-	-	-	-	++	++	++	+	++	+
PA-R1	-	-	-	-	++	++	++	-	-	-
PA-R2	-	-	-	-	++	++	++	-	-	-
PA-R3	-	-	-	-	++	++	++	-	-	-
PA-R4	-	-	-	-	++	++	++	-	-	-

[a] Empirical parameters stated in a previous study[83]

- insoluble, + partially soluble (soluble upon heating), ++ soluble

2.3.6 Anion-exchange ability – potassium hydroxide treatment

To evaluate the I^- removal from the water by the cationic bio-polyamide groups, I^- initially attached to the synthesized BPA was exchanged with hydroxide ion (OH^-) (Figure 2.10a). Before the anion exchange process, PA-R4 was found to have a clustered morphology with 5.8% of iodine element (I), observed in the elemental analysis (Figure 2.10b). After the KOH treatment, I was undetectable, while the potassium element (K) was present over the polymer surface with 11.6% (Figure 2.10b,c). Subsequent washing with DI water spread out the fibrils to show a uniform polymer surface morphology, and the reduction of I to 0.03% verified the replacement of I^- by OH^- (Figure 2.10b,c). The full elemental composition can be found in the

Appendix. The molecular weight of the KOH-treated BPA in Table 2.3 shows that the amide bonds did not go through hydrolysis during the KOH treatment as the BPA retain the values of *Mw* and *Mn*.

a

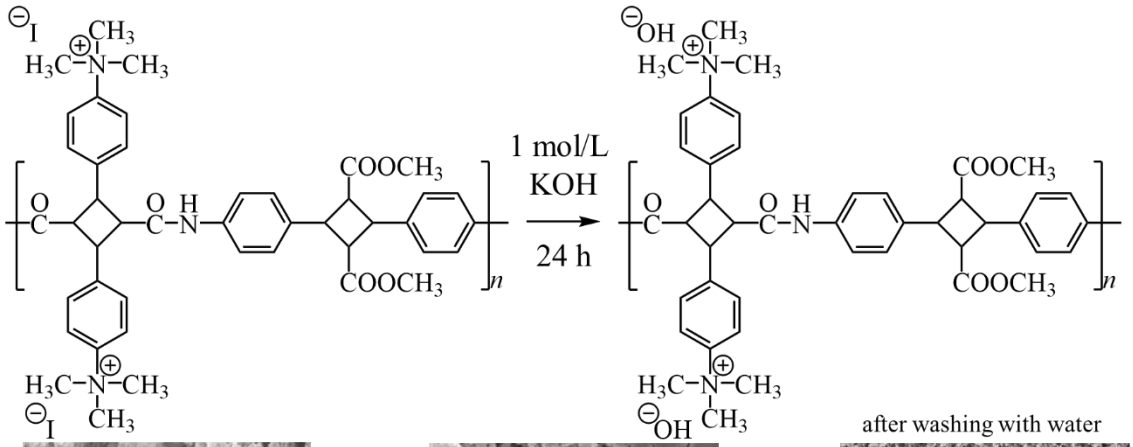

b

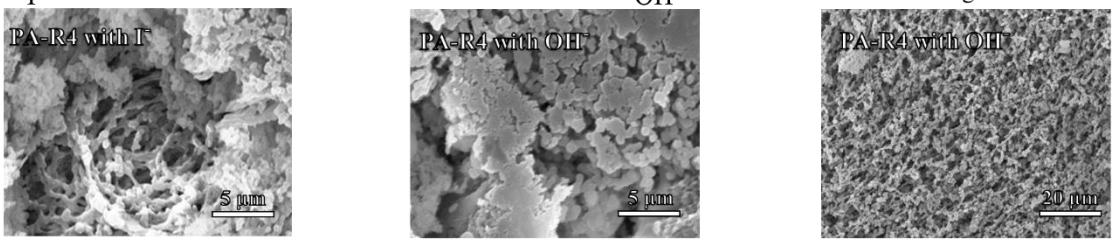

c

EDX (%)				
	K	0.00	11.6	0.36
	I	5.8	0.00	0.03

Figure 2.10 (a) Scheme for KOH treatment of cationic BPA (PA-R4), (b) PA-R4 surface morphology before and after treatment, (c) elemental composition of PA-R4 by EDX for tracking the anion exchange process

Table 2.3 Molecular weight characteristics of cationic BPA after the KOH treatment

cationic BPA	GPC		
	M_w (x 10^4)	M_n (x 10^5)	PDI
PA-R1	1.78	0.71	2.52
PA-R2	1.15	0.45	2.57
PA-R3	0.36	0.17	2.17
PA-R4	4.15	1.68	2.47

Mw – weight-average molecular weight, *Mn* – number-average molecular weight, PDI – molecular weight distribution

2.3.7 Iodide removal

The I^- removal efficiency with a variation of BPA dosages is shown in Figure 2.11. An increase in the cationic BPA dosage leads to greater I^- adsorption within 2 h of contact time. At 2 g/L, all BPA can remove up to 50% of the 10 mg/L I^- in water. At 5 g/L, PA-R1, PA-R2, and PA-R4 tend to remove 92 – 95%, while PA-R3 can remove 80% of the same I^- concentration. At a 10 g/L dosage, all BPA could remove 10 mg/L I^- from the solution except PA-R3, which adsorbed about 95% of the initial concentration. Considering the limiting BPA concentration, in the kinetic experiment, a 10 g/L dosage was selected for PA-R3, and 5 g/L was used for the other BPA.

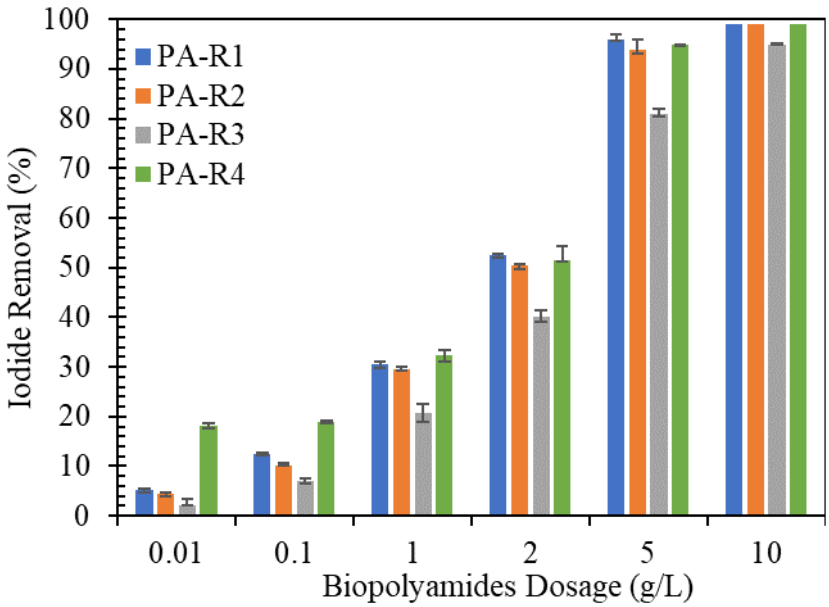

Figure 2.11 Dosage variation of cationic biopolyamide in removing 10 mg/L I^- for 120 min under room temperature

The I^- adsorption performance with a 3-hour contact period of the BPA is presented in Figure 2.12a. The equilibrium time of contact was determined to be approximately 120 min.

PA-R1, PA-R2, and PA-R4 showed a similar I^- removal pattern, with nearly 100% at equilibrium. PA-R3 I^- adsorption efficiency reached the equilibrium within the same duration but with a lower efficiency (almost 80%). At the optimum time, 0.8 mg/g adsorption capacity was observed for PA-R3, while the other types of cation polyamides removed up to 2 mg/g (Figure 2.12b). The lower efficiency of PA-R3, compared to that of other BPA, may be due to its lower *Mw*. The molecular weight may affect the physical adsorption of I^-, such that at a low concentration, a higher molecular weight polymer allows for more coiling of polymer chains, leading to entrapment of more I^-.[84]

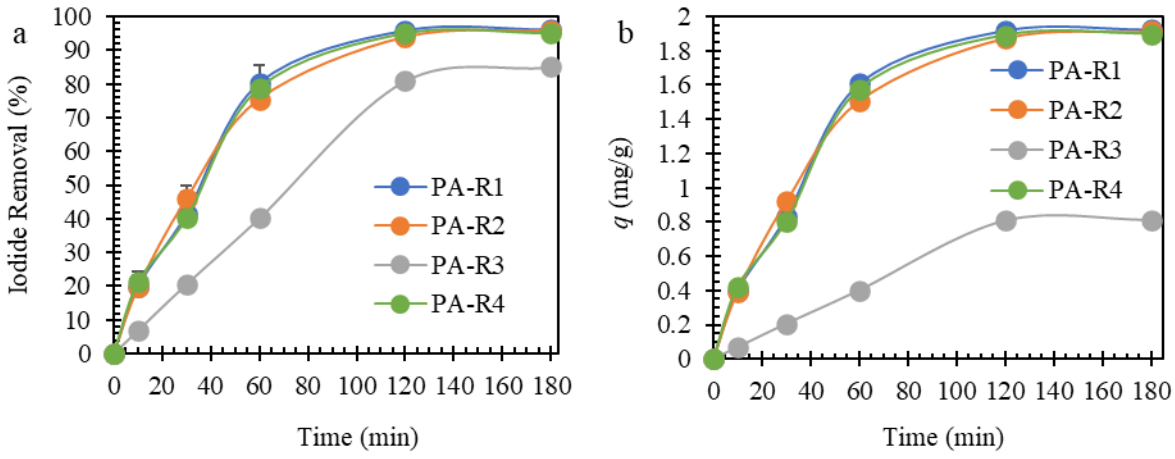

Figure 2.12 I^- removal of cationic BPA over time using optimum dosage under room temperature. (a) percent removal efficiency calculated by Equation 1, (b) adsorption capacity

The numerical values for linear fits of pseudo-order-reaction rates are tabulated in Table 2.4. The actual fitting of the first- and second-order can be found in Figure 2.13a and Figure 2.13b, respectively. It was observed that the logarithmic plot for the I^- removal of PA-R3 was almost linear (R^2 = 0.994) with time, and therefore, followed the pseudo-first-order reaction. The linear first-order kinetics depicted the anion-exchange reaction that was proportional to only the amount of I^-, and not the amount of adsorbent.[85] In contrast, PA-R1, PA-R2, and PA-R4 fitted both order reactions, inferring that their adsorption mechanisms are influenced by the amount of both the solute and the polymer.[85] A combination of chemisorption and

physisorption for the I^- adsorption by the bio-based cationic polymer could be deduced from the results of the pseudo reaction order fitting.

Table 2.4 Derived parameters of the linear fitting pseudo-order reactions and isotherms for the I^- removal by cationic BPA

catio-nic BPA	pseudo-first-order reaction[a]			pseudo-second-order reaction[b]			Langmuir isotherm[c]			Freundlich isotherm[d]		
	k_1 (L/min)	Q_e (mg/g)	R^2	k_2 (g/mg/min)	Q_e (mg/g)	R^2	K_L (L/g)	q_{max} (mg/g)	R^2	K_F (L/g)	n	R^2
PA-R1	0.046	1.64	0.952	7.60×10^{-3}	2.57	0.971	n/a	n/a	n/a	n/a	n/a	n/a
PA-R2	0.033	1.42	0.987	0.051	2.50	0.988	n/a	n/a	n/a	n/a	n/a	n/a
PA-R3	0.012	0.92	0.994	7.36×10^{-6}	30.6	0.565	n/a	n/a	n/a	n/a	n/a	n/a
PA-R4	0.046	1.57	0.958	8.10×10^{-3}	2.51	0.972	0.078	32.3	0.998	0.032	0.2	0.977

[a]parameters calculated by Equation 2, [b]parameters calculated by Equation 3, [c]parameters calculated by Equation 5, [d]parameters calculated by Equation 6

n/a – not available

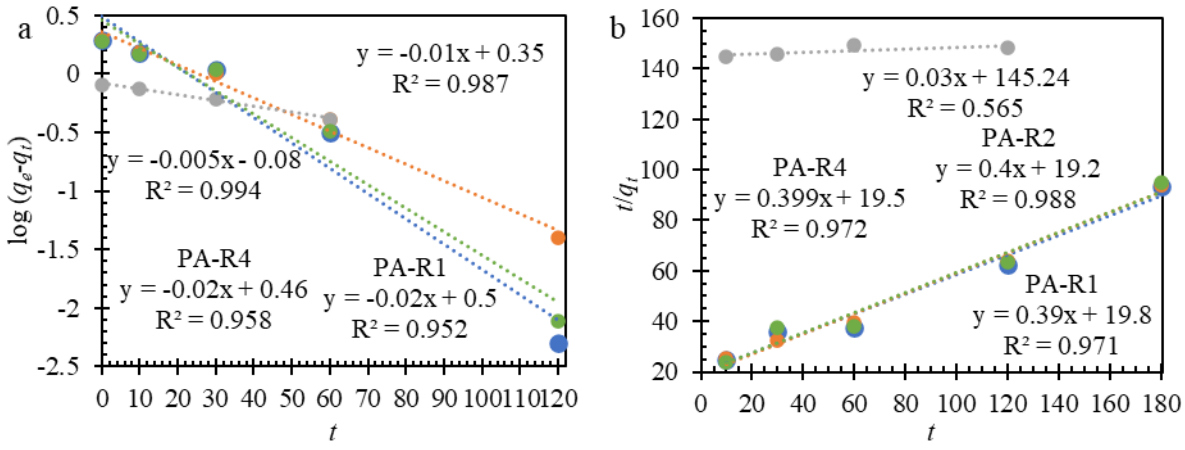

Figure 2.13 Linear fits of pseudo-order-reaction for the I^- removal by cationic biopolyamide. (a) first-order, (b) second-order

PA-R4 was further tested for the batch experiment due to its performance, and the maximum *q* obtained from the experiment is about 30 mg/g (Figure 2.14a). The fit of linear isotherm is depicted in Figure 2.14b, where the distribution coefficient (K_D) is calculated to be 7.58 L/g. The value was similar to that of various types of polystyrene-based resin.[70] The fittings of Langmuir and Freundlich isotherms are shown in Figure 2.14c and Figure 2.14d, respectively. The q_{max} value of 32.3 mg/g yielded by the Langmuir model (Table 2.4) is found to be similar to that of the mentioned experimental maximum *q* (Figure 2.14a). In comparison with other bio-based adsorbents from the literature, which were observed to remove I^- in similar experimental conditions, the performance of the presented cationic BPA is deemed acceptable. The reported values of q_{max} for copper-modified activated carbon and TiO_2-Fe_2O_3-PVA alginate beads were 1.91 and 20 mg/g, respectively.[65,86] PA-R4 was best represented by the Langmuir isotherm with an R^2 of 0.998 (Table 2.4 and Figure 2.14c), which inferred that there was a conformity of ion-exchange reactions in all sites of the cationic polyamide.[87] With an R^2 of 0.977 (Table 2.4 and Figure 2.14d), the Freundlich model too, can used to predict the behavior of PA-R4. The model yielded 0.2 for *n*, which means the free adsorption energy is constant throughout different I^- concentrations.[87]

The PA-R4 results for the 10 mg/g I^- adsorption efficiency at various temperatures are shown in Figure 2.15a. At 20 °C, DOWEX™ 550 was found to be superior for I^- adsorption, as it has 100% I^- removal capacity, while PA-R4 I^- adsorption was up to 98%. An increase in the temperature led to a significant loss in the I^- adsorption efficiency for the conventional resin. In contrast, the BPA maintained their anion-exchange efficiency throughout the measured temperature range, and the performance began to fall after 80 °C. From 40 °C, except for PA-R3, the I^- removal efficiency of BPA started to surpass that of DOWEX™ 550. The lower efficiency of the commercial-grade resin was may be attributed to the low thermal stability of the polystyrene resin (Table 1.1). Moreover, the water absorption characteristics of

the BPA may increase the OH^- $(H_2O)_x$ clusters in the complex, subsequently preventing the degradation of quaternary ammonium to further facilitate the uniform adsorption of the dissolved impurities at a higher temperature.[72,88] This phenomenon was less observed in a polystyrene-based material like Dowex™ 550, as reported during water immersion tests.[89]

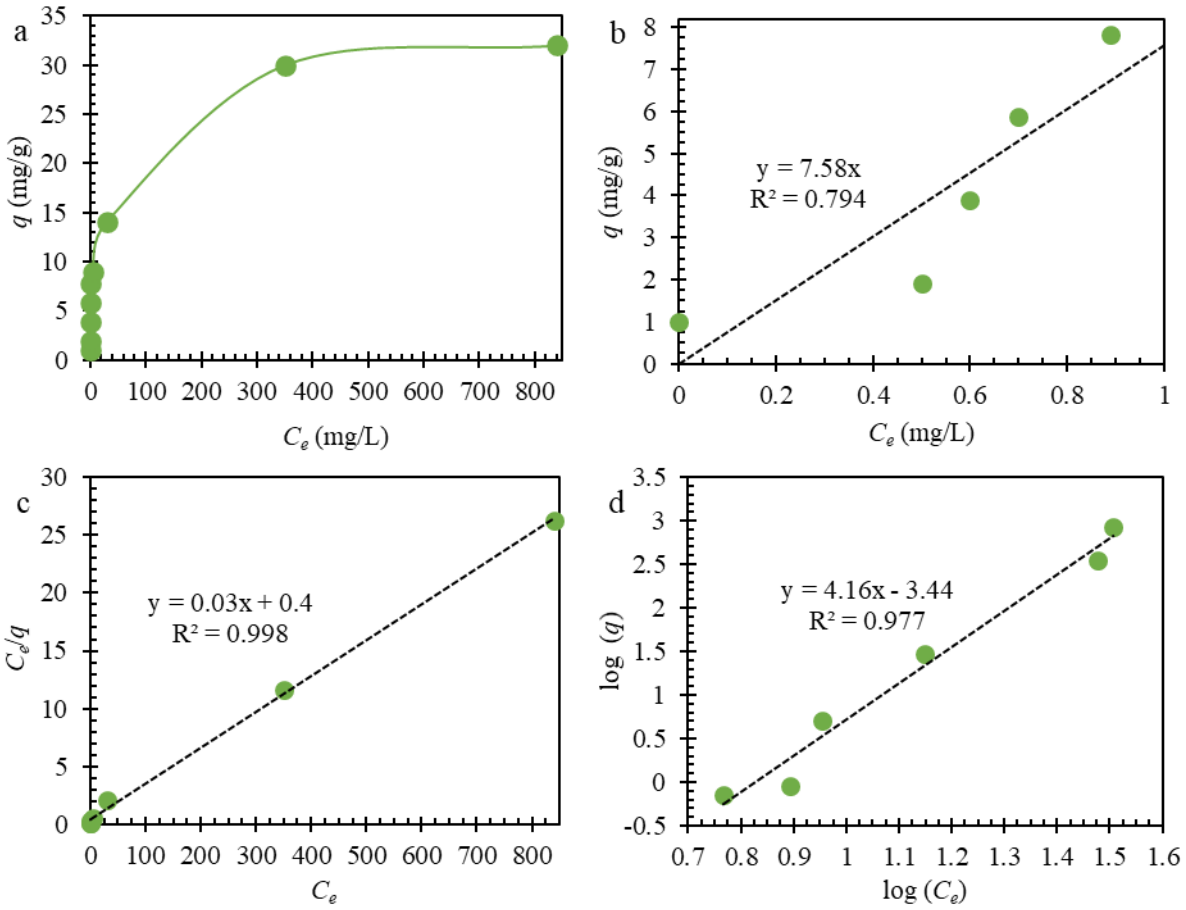

Figure 2.14 PA-R4 isotherm fits. (a) adsorption capacity over final I^- concentration, (b) linear isotherm, (c) Langmuir isotherm, (d) Freundlich isotherm

All the cationic polymers exhibited the same trend of I^- removal efficiency in various pH condition (Figure 2.15b). The highest removal was observed at pH 2 and remained stable until about pH 7, where the decrease in I^- removal occurred. The acidic condition promoted the sorption of I^- by positive charges in the sorbents, while under high pH condition, the presence of OH^- would create a competition for iodine anions.[90] While the performance of PA-R1 and PA-R2 was drastically affected from the pH increase, especially from pH 10 onwards,

PA-R4 and the commercial-grade resin were perceived to be stable with more than 80% I^- removal at pH 12.

The selectivity of PA-R4 for I^- was briefly accessed (Figure 2.15c). In the presence of other anions, PA-R4 could maintained the I^- removal efficiency above 70%. The adsorption efficiency was most affected by SO_4^{2-}. The efficiency of almost 100% was observed in the tap water, while about 50% could be achieved in the seawater where numerous competitive anions existed in high concentration.

Figure 2.15d depicted the reusability of the PA-R4 for 5 cycles. The I^- adsorption efficiency was maintained above 90% in the second cycle. The fifth cycle of regeneration and I^- adsorption yielded an efficiency of less than 50%.

All in all, our research has produced a series of cationic BPA with high thermal properties and ability to remove I^- from the water with a performance comparable to that of conventional polystyrene resin and metal-inclusive adsorbents. The reusable PA-R4 is not only considered to be fully bio-based, but its anion-exchange processes in the water were observed to be stable throughout different temperature and pH. It also has a fair selectivity toward I^- and is reusable after KOH regeneration.

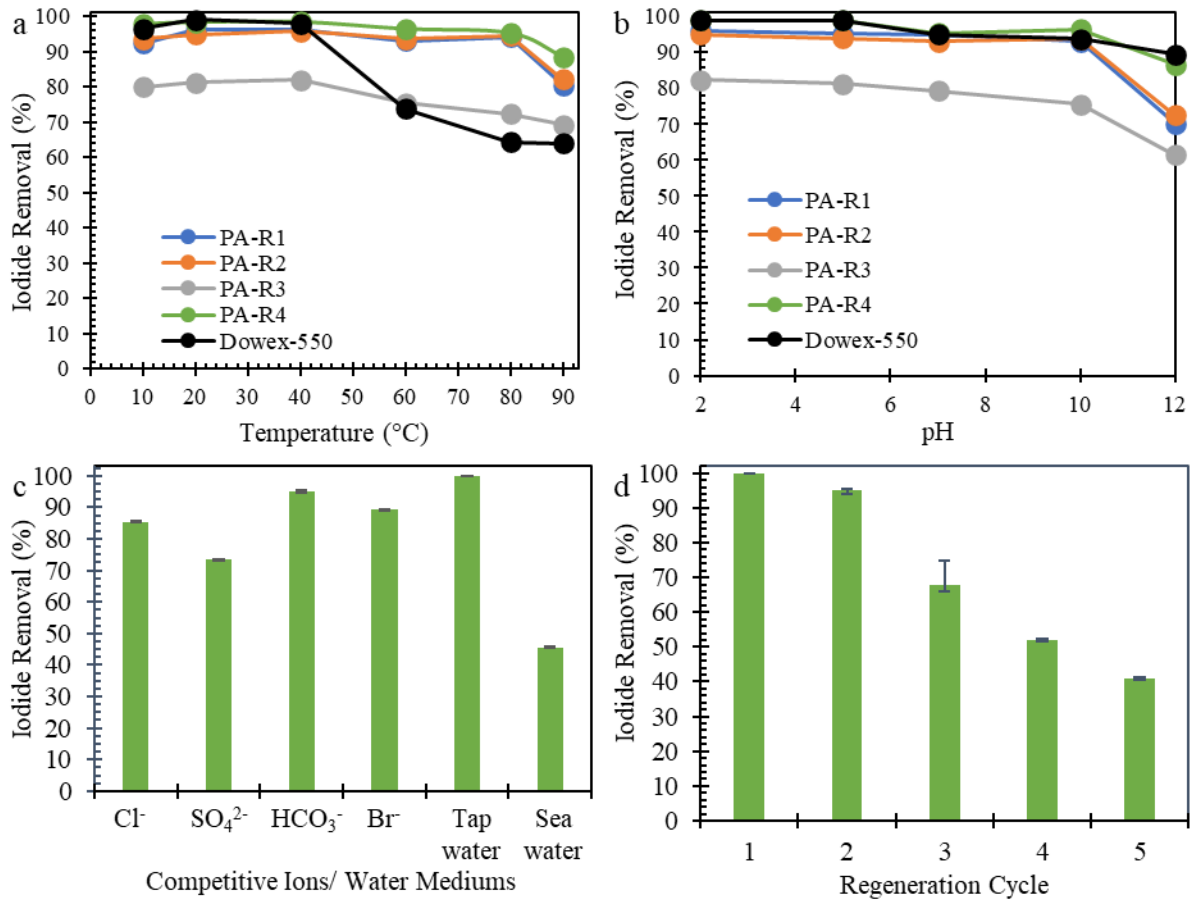

Figure 2.15 I^- removal performance of BPA in different background conditions and regeneration cycles. (a) temperature variation [20 – 90 °C], (b) pH variation [2 – 12], (c) selectivity of PA-R4 for removal of I^-, (d) performance of regenerated PA-R4 for 5 cycles. The experiment was performed with 5 g/L BPA, 10 mg/L I^-, and 120 min of contact time. The regeneration by 1 M KOH took 6 h. The conventional cationic resin, DOWEX^{TM} 550, was used for comparison in the temperature and pH variation experiment

2.4 Conclusions

A multifunctional molecule (Q-4ATA) was synthesized from the bio-derived exotic amino-acid, 4ACA. The cationic monomer functionality was utilized to prepare a series of BPA that was employed for removing I^- from aqueous solution. All BPA consist of more than 50% renewable source (sustainability metric) in its structure with PA-R4 having more than 99%. The I^- removal of the fully biobased PA-R4, from the experiment, q, and the Langmuir equation fitting, q_{max}, were calculated to be the maximum of the series at 30.0 and 32.3 mg/g, respectively. With high thermal stability, the BPA surpassed the commercial polystyrene resin, DOWEX^{TM} 550, for I^- adsorption performance at higher temperatures. The high solubility of the BPA in aprotic solvents provides for easy processing despite a high glass transition temperature. This research opens new horizons in bio-based synthetic polymers for the removal of toxic ions from solutions. The successful I^- removal indicates the importance of the continue examination of cationic BPA to remove other anionic contaminants such as IO_3^-, F^-, NO_3^{2-} and AsO_4^{3-}. Further development in removing toxic ions demands the fusion of industrial biotechnology and synthetic chemistry for creating more functional and advanced polymers.

CHAPTER 3

Anionic biopolyimide metal hybrids for flame retardant and thermostable transparent films

3.1 Introduction

Polymer transparent films are an essential material for wrapping, coating, and separating materials in display devices, windows of buildings, and vehicles. Flame retardancy is an important property that improves the safety of film utilization. For the state of the art, we still struggle to develop a flame retardant film that can balance properties such as thermal degradation and mechanical strength. The hyperbranched polyphosphonate acrylate exhibited high transparency at 450 nm (T_{450nm} ~80%) and an acceptable decomposition temperature of 5% weight loss (T_{d5} 286 °C), but the film failed the Underwriters Laboratories vertical burning standard test (UL-94V).[91] The mix of poly(vinyl alcohol), ethylene glycol, and magnesium hydroxide yielded a highly flame retardant (*THR* 3.7 kJ/g) and optical (T_{500nm} >90%) film, with a T_{d5} value of less than 250 °C.[92]

In the making of flame retardant polymer films, additives are required. These additives act (physically or chemically) to interfere with heat transmission, thermal degradation, pyrolysis, and ignition. Adding them can, however, affect other properties and undermine the performance of the films. The added combination of lithium, aluminum, layered double hydroxide, and 2-carboxyethyl phenyl-phosphinic acid helped to reduce the total heat release (THR) of polylactide (PLA) from 12 to 9 kJ/g.[40] However, the thermal stability and transparency of the PLA film also decreased.[40] Layer-by-layer assembly was employed to introduce the natural flame retardant additive montmorillonite (MMT) into polymers such as poly(allylamine) and polyethylenimine.[93,94] In both cases, high mechanical strength and flame

retardancy could be achieved, but the films yielded low thermal stability of about 250 °C for the temperature at 5% weight loss (T_{d5}). An increasing amount of MMT also lessened the film transparency.[95]

Metal ions and metal hydroxides were used to improve the flame retardancy of materials.[96,97] While the direct mixing of metal flame retardants is conventional, the research on flame retardancy of a metal-carboxylated film is still limited.[98,99] The formation of metal carboxylate has been studied extensively for the alginate in the process of removing heavy metals from water.[100–102] The exchange of Na in the sodium alginate and multivalent cationic metal ion produced an egg-box model for the metal-alginate. This led to opportunities to study metal-alginates for further applications, especially the ones related to flame retardancy. Metal alginate films (made from Ba^{2+}, Zn^{2+}, Fe^{3+}) exhibited excellent flame retardancy with a limited oxygen index (LOI) of up to 52%, extinguished second burning time of less than 10 s (V-0 rating for UL-94 standard), and 12 W/g peak heat release rate (*pHRR*).[25,26,41] However, their thermal degradation stability (maximum 188 °C T_{d5}) became a notable setback, while the mechanical and optical properties were not reported.

Polyimide (PI) has been known for its mechanical strength and thermal stability. Without an additive, an engineered PI could demonstrate flame retardancy to a certain degree due to the abundance of structural aromatic rings.[103] The addition of graphene, MMT, and phosphorus elevated the flame retardancy of PI with a maximum of 55% LOI and V-0 UL-94 rating.[104–106] While the values associated with the thermo-mechanical properties remained high (548 – 573 °C T_{d10} and 133.5 – 146.3 MPa tensile strength), a mixture of PI and boron phosphate produced a film with transparency (T_{600nm}) of 41.9 – 58.9%.[106]

Amino acid 4-aminocinnamic acid (4ACA) was obtained from sugar fermentation.[37] Its bio-based PI derivatives (BPI) could be cast into a series of flexible films with high-

performance characteristics (T_{d10} and tensile strength of up to 410 ºC and 98 MPa, respectively), comparable to those of the commercial PI.[37] Due to the availability of the carboxylic acid side chain, BPI with potassium ion (K^+) attached to the carboxylate (COO^-) was previously developed.[39] This brought about the opportunity to create BPI-metal films by a metal-scavenging technique. The metal carboxylate complexation can happen through the exchange of K^+ and multivalent metal ions. The latter may act as a flame retardant additive for the BPI-metal film.

In the present study, high-performance BPI was employed to create a flame-retardant BPI-metal film, preserving or enhancing the thermo-mechanical properties and optical transparency. The films were synthesized with a complexation technique with Al^{3+} and Cu^{2+}. The kinetic and thermodynamic properties were studied for the prepared complexes. The films were characterized for thermal stability, mechanical properties, optical transparency, and flame retardancy to determine the overall performance.

3.2 Experimental

3.2.1 Materials

4-aminocinnamic acid (4ACA, Compound 1 in Scheme 1) was prepared from glucose according to the literature.[37] N, N-dimethylacetamide (DMAc, Kanto Chemical Co., Japan) was left in 4 Å molecular sieves under a nitrogen atmosphere for 24 h before being used for polymerization. 1,2,3,4-tetracarboxycyclobutane dianhydride (CBDA, Tokyo Chemical Industries, Japan), hydrochloric acid (HCl, Kanto Chemical Co., Japan), sodium hydroxide (NaOH, Kanto Chemical Co., Japan), potassium hydroxide (KOH, Kanto Chemical Co., Japan), copper (II) chloride dihydrate ($CuCl_2 \cdot 2H_2O$, Ajax Finechem, Australia), and aluminum sulfate-18-hydrate ($Al_2(SO_4)_3 \cdot 18H2O$, Sigma-Aldrich, USA), were used as received.

3.2.2 Monomer and polymer syntheses

The monomer and polymer syntheses are depicted in Scheme 3.1. A mixture of 4 g ACA in 11 ml conc. HCl and 60 ml acetone was stirred for 6 h. The product, 4-aminocinnamic acid hydrochloride (compound 2, yield 86%), was photodimerized under the irradiation of a 100-W high-pressure Hg-lamp with a 250 − 450 nm band-pass filter and an intensity of 2.7 mW/cm^3 (Omni Cure S1000, EXFO Photonic Solution Inc.). A complete photocycloaddition (observed with ^1H NMR) produced 4,4'-diamino-truxillic acid dihydrochloride dimer (compound 3, yield 75%). Thereafter, the compound was dissolved in water, heated at 70 °C, and purified with activated carbon. The pH of the solution was adjusted to 3 with 1 M NaOH. A white precipitate of 4,4'-diamino-truxillic acid (4ATA, compound 4, yield 74.9%) was obtained. 4ATA was dried in a vacuum oven for 6 h at 60 °C.

The polymerization was conducted with an equimolar mixture of 4ATA and CBDA, left stirred in 2.5 ml dry DMAc under nitrogen. CBDA was chosen as it was observed to produce a highly transparent product under the polycondensation reaction, and it was developed from maleic acid, which could be bio-based.[107,108] The formation of poly(amic acid) was completed within 24 h. The viscous solution was cast onto a glass substrate and heat-annealed for imidization at 150, 200, and 250°C (1 h interval) under an inert atmosphere. The resulting BPI-COOH was dissolved in KOH solution with a 1:1 molar ratio of COOH: K. A solution was produced and dropped slowly into ethanol where a white fibril of BPI-COOK was formed. After the separation, the fibril was dried in a vacuum oven for 6 h at 60°C.

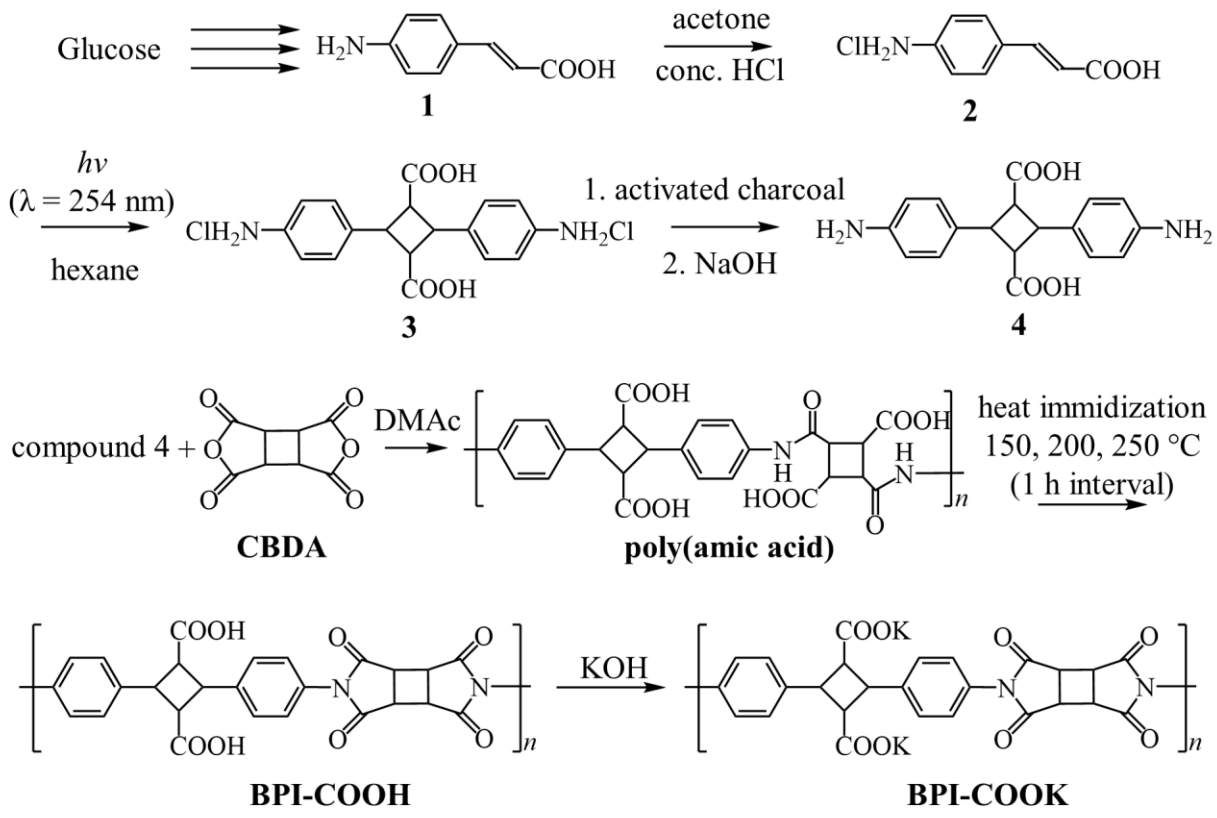

Scheme 3.1 Monomer and polyimide syntheses

3.2.3 Complexation kinetics and thermodynamic

The syntheses of BPI-metal films are shown in Scheme 3.2. The BPI-COOK fibril was dissolved in water to produce a viscous 50 g/L solution. The solution was cast onto a glass substrate and dried at 40 °C on a hot plate. The resulting film had a thickness of 0.13 ± 1 mm. A BPI-COOK film sample was cut to have dimensions of 200 × 500 mm. The metal solutions were prepared with $Al_2(SO_4)_3 \cdot 18H_2O$ and $CuCl_2 \cdot 2H_2O$. The complexation equilibrium time was determined by the kinetic experiment of BPI-COOK film submersion in 1 mol/L metal ion (Al^{3+} and Cu^{2+}) solution for 0 – 120 min. The metal ion concentration left in the solution after the complexation was quantified. Equation 3-1 is used to determine the metal removal (%).

$$\text{Metal removal (\%)} = \frac{C_i - C_e}{C_i} \times 100$$

(3-1)

where, C_i is the initial metal ion concentration (mol/L), and C_e is the metal ion concentration left in the solution after complexation (mol/L). The equilibrium time was taken from a plot of metal removal over time, where the metal removal is stable.

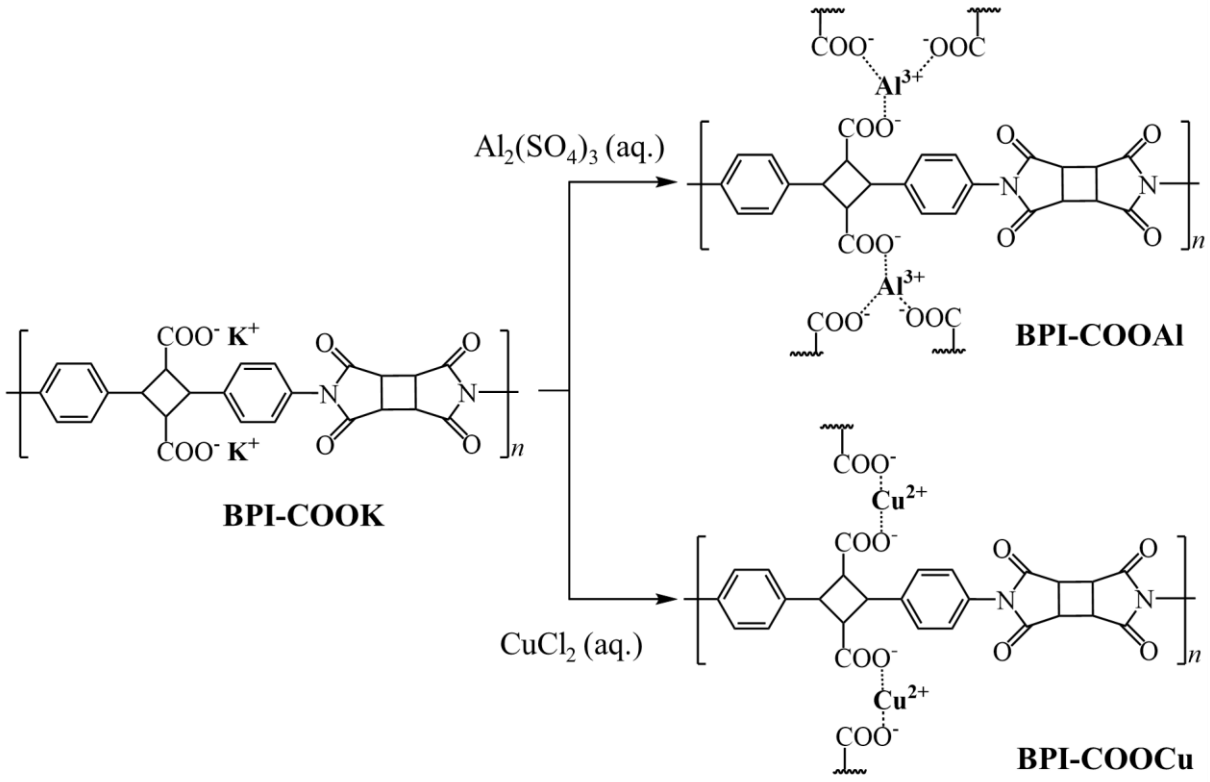

Scheme 3.2 BPI-COOAl and BPI-COOCu syntheses

An equilibrium time of 30 min (refer to Results & discussion section) was used to observe the metal complexation in different metal ion concentrations. A BPI-COOK film sample was submerged into 10 ml of 0.5, 1, 2, 4, and 6 mol/L metal ion solutions. BPI-COOAl and BPI-COOCu were obtained. Depending on the concentration, the film was dissolved in the metal solution, and/or a precipitate was formed. The separation of the solution and precipitate was done by a filter paper (Whatman™ 11 μm pore). If the film of BPI-COOAl and BPI-COOCu formed without precipitation, they were removed from the solution directly. The complexes were washed with DI water, dried in an oven, and used for further characterization.

The metal ions were quantified using inductively coupled plasma atomic emission spectroscopy (ICP-OES, Avio 200, PerkinElmer). The ICP-OES was set up as follows: 1.50 mL/ min peristaltic pump and auto-autosampler flow rate (with autosampler washed between every sample), 20 s flush time, and 30 s normal time.

The thermodynamic properties for the metal complexation were measured under a temperature-controlled environment of 298.15 – 338.15 K (25 – 65 °C), using a closed incubator (NB205-V, N-BIOTEK). The thermodynamics values were determined for the complexation with the metal solution with Al^{3+} and Cu^{2+} concentrations of 0.05 – 6 mol/L. The amount of metal bound to a unit of BPI, q (mol/g), and the metal concentration in the final solution, C_e (mol/L), were obtained. These were used for the linear fit of the Langmuir model (Equation 3-2) as recommended from the literature.[109]

$$\frac{1}{q} = \frac{1}{q_{max}} + \frac{1}{K_L\, C_e\, q_{max}}$$

(3-2)

where q_{max} is the saturation binding capacity (mol/g), and K_L (L/g) is the binding constant. The thermodynamic parameters were obtained from the linear plot of Equation 3-3 and the calculation of Equation 3-4.

$$\ln K_L = -\frac{\Delta H}{RT} + \frac{\Delta S}{R}$$

(3-3)

$$\Delta G = \Delta H - T\Delta S$$

(3-4)

where ΔH and ΔS are the change in enthalpy (kJ/K/mol) and entropy (kJ/mol), respectively. T is the temperature (K), and R is the gas constant (8.314 J/mol/K). ΔG is the change in free energy (kJ/mol).

3.2.4 Characterizations

To analyze the changes in the functional groups after metal complexation, reflection infrared spectra were obtained using an attenuated total reflection mode Fourier-transform infrared spectroscope (ATR-FTIR, Nicolet iS50 FTIR Spectrometer, Thermo Scientific) from 400 to 4000 cm^{-1}. BPI-COOAl and BPI-COOCu from the complexation using 0.5, 1, and 2 mol/L metal ion were analyzed. BPI-COOH and BPI-COOK were also analyzed for comparison.

The study of the metal oxidation state and the local structure in the BPI-metal complex were done using X-ray absorption spectroscopy (XAS) at Beamline 5.2 (BL5.2), Synchrotron Light Research Institute (Public Organization), Nakhon Ratchasima, Thailand. The electron energy was 1.2 GeV. Due to the unavailability of the energy for Al in the facility, only BPI-COOCu was subjected to this analysis. The resulted complexes of BPI-COOCu from 0.5, 1, and 2 mol/L Cu^{2+} were analyzed. XAS spectra were recorded by setting Cu as the probe element (K-edge at 3609 eV). The Silicon (110) double crystals were utilized as a monochromator with the transmission mode applied for the X-ray absorption near edge structure (XANES) and extended X-ray absorption fine structure (EXAFS). For EXAFS, the structure of $CuH_2(CO_2)_2$ was used as the fitting reference. The probable structure of BPI-COOCu was illustrated using ChemDraw Professional 16.0 (PerkinElmer).

To minimize the metal waste, 1 mol/L metal ion solutions were used to create BPI-metal films for further characterization unless stated otherwise (refer to the Results &

discussion section for more information on the minimum metal ion concentration of film complexation).

The tensile measurements were carried out for BPI-metal at room temperature with the elongation of 0.5 mm/min on a tensiometer (Instron 3365, Instron).

The thermogravimetric analysis was performed on STA 7200 (TGA, Hitachi). The sample weight was 6.00 ± 0.3 mg. To eliminate the excess moisture, the sample was left to dry in a vacuum oven at 150 °C for 6 h. The pre-heated period in the TGA chamber was set at 100 °C for 30 min. TGA was measured under a nitrogen atmosphere at 25 – 800 °C. The heating rate was set to 10 °C /min with a 10 min holding time.

The optical transparency was measured by an ultraviolet-visible (UV-vis) spectrophotometer (Lambda 25 UV/vis, Perkin-Elmer) at room temperature for 200 – 800 nm.

The comparative burning characteristics of the polymers were measured using the 20-mm vertical combustion test (UL-94V, IEC60695-11-10B method, ASTM D3801 standard, Dainihon Jyushi Kenkyujyo Corporation). A test piece with dimensions of 125 × 13 mm was mounted vertically on a clamp. It was burned by a 20-mm indirect flame for 10 s with cotton placed under the sample. The dripping and the cotton ignition were observed for each sample. A test piece was burned twice, and each time, the burning time was recorded. t_1 and t_2 are defined as the recorded time after 10 s of the first and second burning, respectively. t_3 is the glowing time after the second burning. There were 5 repetitions performed, giving a kind of BPI, and the longest t_1 and t_2 were taken into consideration. A UL-94V rating was assigned to the polymer. V-0 was the rating for a polymer with a t_2 of less than 10 s, and no dripping observed. V-1 was given to a polymer with a t_2 of less than 60 s, and no dripping observed. V-2 was assigned to a polymer with a t_2 of less than 60 s, and dripping was observed. The rating

was assigned as “fail” if the flame reached the top of the sample piece or t_2 was more than 60 s.

Due to the laboratory-scale production of the films, cone calorimetry was unsuitable for this study. Instead, microscale combustion calorimetry (MCC, FMVSS302 instrument set, Dainihon Jyushi Kenkyujyo Corporation) was performed with 0.8 ± 0.02 mg of the sample. The set-up temperature range was 75 – 800 °C with a 0.8 °C/sec heating rate. Nitrogen and oxygen flows were adjusted to approximately 80% and 20%, respectively. The gas temperature was controlled at 19 – 21 °C. BPI-COOK and BPI-COOH were used as references.

The char residues of BPI-COOAl and BPI-COOCu were analyzed for polymer flame retardant characteristics and mechanisms. The films were burned in an open-air oven at 800 °C. The sample weight was 0.1 ± 0.01 g. The char residues were analyzed at room temperature using a Raman spectrometer (NRS-4100, Jasco) equipped with a green laser (532.248 nm). The topography of the char residues was studied by a scanning electron microscope (SEM, JEOL JSM-7800F, JEOL) with 15 kV of accelerating voltage. The SEM was equipped with an energy-dispersive X-ray spectroscope (EDX), which was used to perform elemental composition on the same set of samples. BPI-COOAl and BPI-COOCu films and their respective char residues were analyzed by X-ray photoelectron spectroscopy (XPS, Shimadzu Kratos AXIS-ULTRA DLD instrument, Kratos) equipped with monochromatic Al-Kα radiation. The change in the metal oxidation before and after burning was used for comparison.

3.3 Results and discussion

3.3.1 Metal complexation and thermodynamic

The metal removal (calculated by Equation 3-1) over time (min) is exhibited in Figure 3.1a. Both complexation systems had an equilibrium at about 30 min, where the metal removal became stable. With 1 mol/L initial metal ion concentration, BPI can bind more with Cu^{2+}

(more than 90% Cu^{2+} removal) than Al^{3+} (more than 80% Al^{3+} removal). *q*, the amount of metal (bound to a unit of BPI (g/mol) was used to plot against C_i, initial metal ion concentration (mol/L), and the graph is depicted in Figure 3.1b. For both complexation systems, while *q* started to stabilize at 2 mol/L C_i, BPI-COOAl and BPI-COOCu films could be obtained at a C_i of 1 mol/L. With a C_i of less than 1 mol/L, the metal ions were not concentrated enough, and the submerged BPI-COOK film was observed to scatter in the metal solution, forming precipitates. As a result, 1 mol/L was used as the minimum metal ion concentration for BPI-metal complexation. The actual images of BPI-COOAl and BPI-COOCu made from 1 mol/L C_i are shown in Figure 3.1c. The thickness of the films was 0.143 ± 0.015 mm.

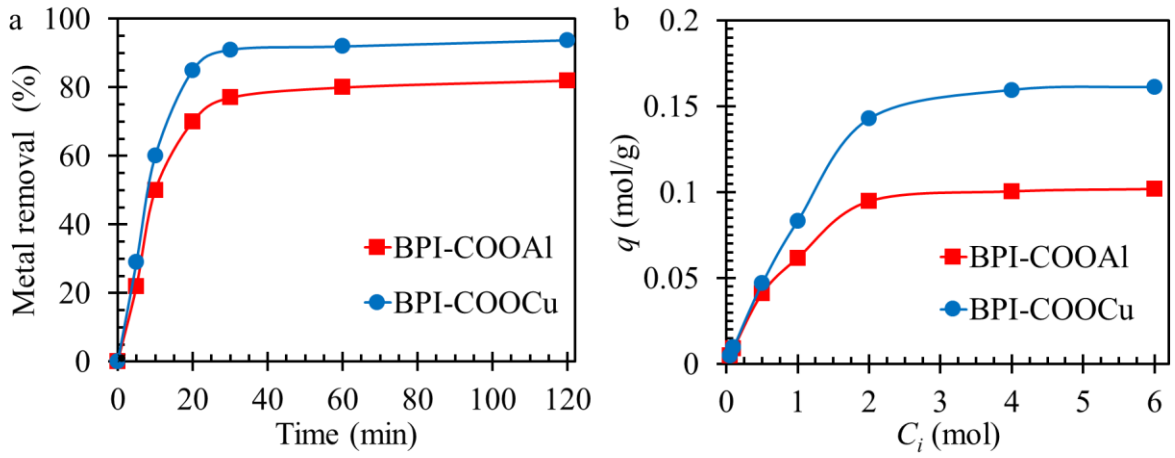

Figure 3.1 Kinetic study of metal complexation. (a) metal removal (%) calculated by Equation 1 over time for 0 – 120 min of BPI-COOK submerged in 1 mol/L Al^{3+} and Cu^{2+} solution, (b) batch experiment of BPI-COOK submerged in 0.5 – 6 mol/L Al^{3+} and Cu^{2+} solution for 30 min. *q* is the amount of metal bound to a unit of BPI (mol/g), and C_i is the initial metal ion concentration (mol/L).

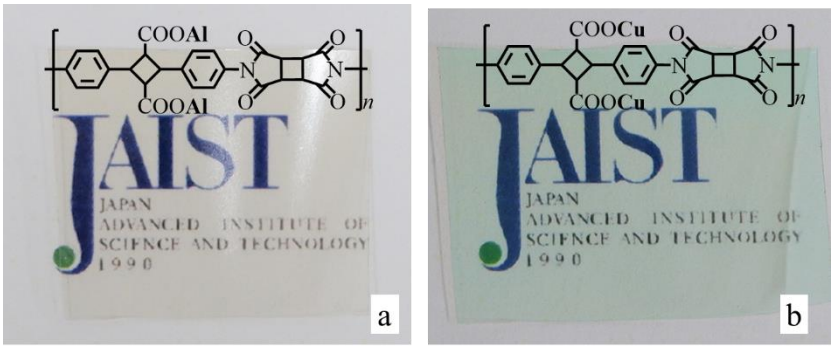

Figure 3.2 BPI films made from 1 mol/L metal ion. (a) BPI-COOAl, (b) BPI-COOCu

The graphs of q (mol/g) vs. C_e (mol/L) for 25 – 65 °C and the linear fitting of the Langmuir isotherm (Equation 3-2) are found in Figure 3.3. The capacity of metal complexation decreased as the temperature increased (Figure 3.3a-b), and the R^2 values for the Langmuir isotherm fittings are 0.999 (Figure 3.3c-d). This reflected the exothermic reaction, which corresponded to the negative values of ΔH and ΔS (Table 3.1). The parameters of thermodynamics (calculated by Equation 2-4) are displayed in Table 3.1.

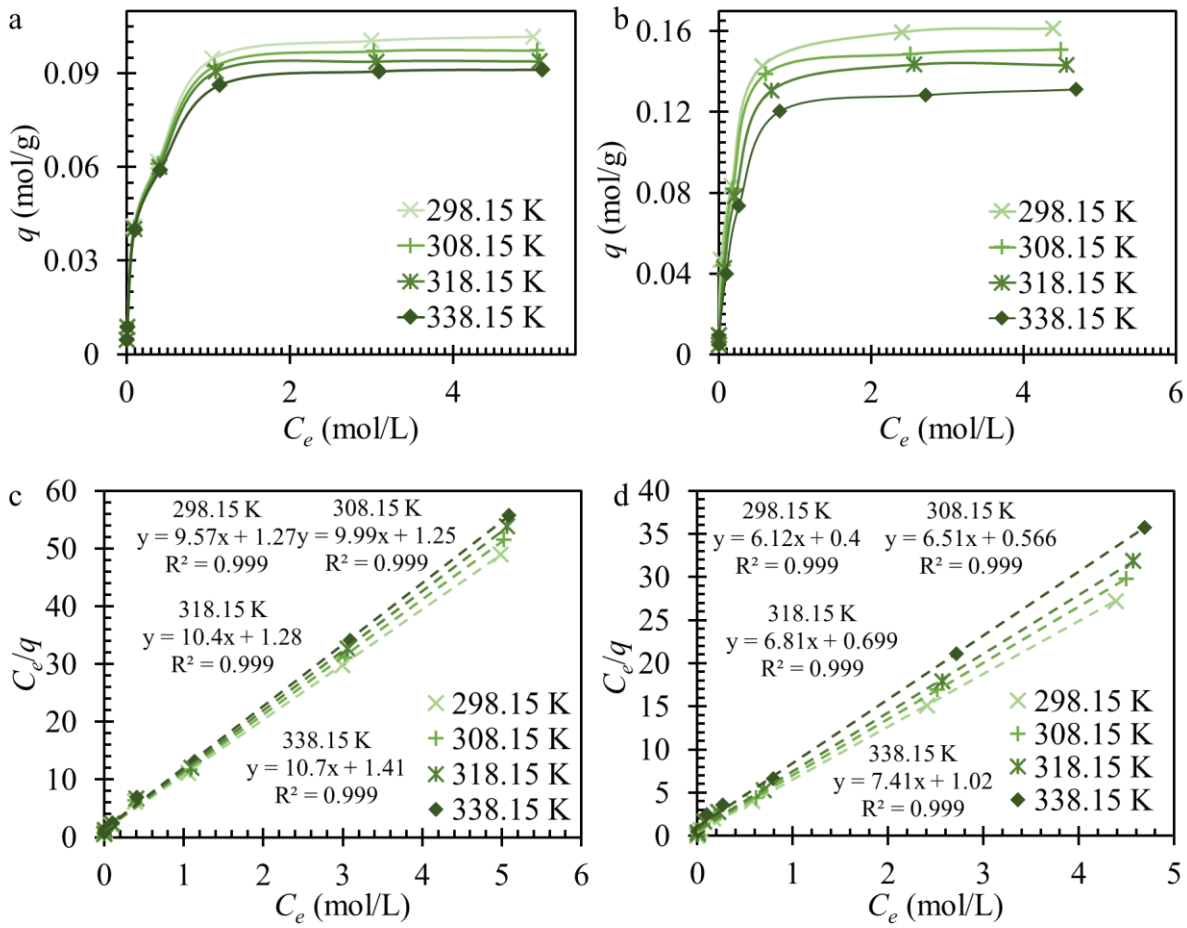

Figure 3.3 Graphs for thermodynamic parameters. (a) q (mol/g) over C_e for BPI-COOAl, (b) q over C_e for BPI-COOCu, (c) Langmuir linear fittings of BPI-COOAl, (d) Langmuir linear fittings of BPI-COOCu. q is the amount of metal bound to a unit of BPI (mol/g), and C_e is the final metal ion concentration (mol/L)

Table 3.1. Thermodynamic parameters of BPI-metal complexation conducted by submerging BPI-COOK into 1 mol/L of Al^{3+} and Cu^{2+} solution under various temperature

sample	T (K)[a]	K_L[b] (L/g)	ΔH[c] (kJ/mol)	ΔS[c] (kJ/K/mol)	ΔG[d] (K/mol)
BPI-COOAl	298.15	7.55	-9.02	-0.0136	-4.97
	308.15	6.50			-4.83
	318.15	5.80			-4.70
	338.15	4.89			-4.43
BPI-COOCu	298.15	15.3	-15.2	-0.0288	-6.66
	308.15	11.5			-6.37
	318.15	9.73			-6.08
	338.15	7.26			-5.51

[a]metal ion solution temperature controlled by closed incubator, [b]calculated by Equation 3-2, [c]calculated by Equation 3-3, [d]calculated by Equation 3-4.

The ATR-FTIR spectra, focusing on the fingerprint region of BPI-COOAl and BPI-COOCu, are shown in Figure 3.4. The full spectra can be found in the appendix. BPI-COOH and BPI-COOK were used for comparison. A high-intensity band of carboxylic acid stretch (1690 – 1750 cm^{-1}) could be observed in BPI-COOH. In contrast, the deprotonated carboxylic acid stretches (1540 – 1650 cm^{-1} and 1300 – 1420 cm^{-1}) appeared in the spectra of BPI-COOK, BPI-COOAl, and BPI-COOCu. Such alteration could be explained by metal-carboxylate coordination. The same phenomenon was reported when the alginic acid formed metal-alginate in a metal solution.[23] The increase in Cu^{2+} led to a higher intensity of the deprotonated carboxylic acid stretches of BPI-COOCu, while the opposite occurred in the system of Al^{3+} and BPI-COOAl. A band corresponding to C-N aromatic amine at about 1300 cm^{-1} appeared in all kinds of polyimides, but a weaker intensity could be observed in BPI-COOAl and BPI-COOCu. The bands at 1050 and 550 cm^{-1} correspond to sulfur from the added $Al_2(SO_4)_3$ (Figure 3.4a).

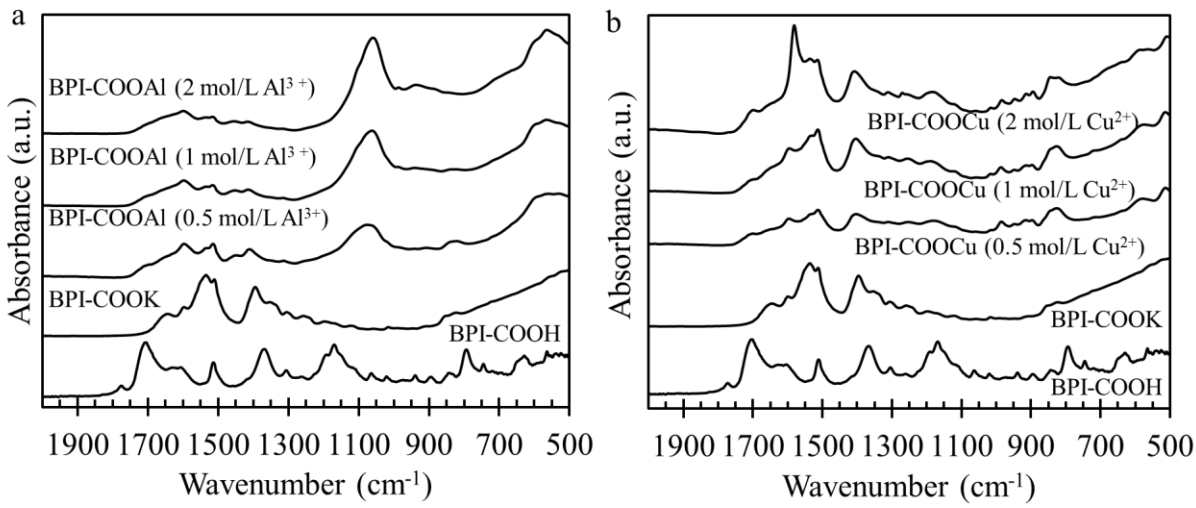

Figure 3.4 FTIR spectra in the fingerprint region of BPI-metal complex made from various metal ion concentrations with the spectra of BPI-COOH and BPI-COOK as references. (a) BPI-COOAl, (b) BPI-COOCu

XANES data of the Cu K-edge can be found in Figure 3.5a. The characteristic absorption edge was observed at about 8995.52 – 8996.63 eV, with no pre-edge peaks. This coincides with the previously reported XANES results of Cu^{2+} in $Cu(OH)_2$.[110] The graph of transformed K-space/R-space Figure 3.5b, while the EXAFS fits data for Cu K-edge is displayed in Table 3.2. The fitting of all samples yielded values of R-factor (fractional misfit) below 0.02. The local structure focused on Cu atom with radial distances taken from the fit of BPI-COOCu (Table 3.2) is illustrated in Figure 3.6. The distance between the single-bonded O atoms of carboxyl groups and the Cu atom is 1.94 Å. With respect to the Cu atom, the carboxyl C atom and double-bonded O atom are located at 2.85 and 4.26 Å, respectively. The local structure displayed monodentate metal-carboxylate formation. This was also the case for Cu^{2+} and α-L-guluronate anions of alginates.[111] For both complexes, Al^{3+} and Cu^{2+} attract the surrounding water molecules to achieve a stable geometry since the BPI has no other available hydroxyl groups (except on the carboxylate).[112,113]

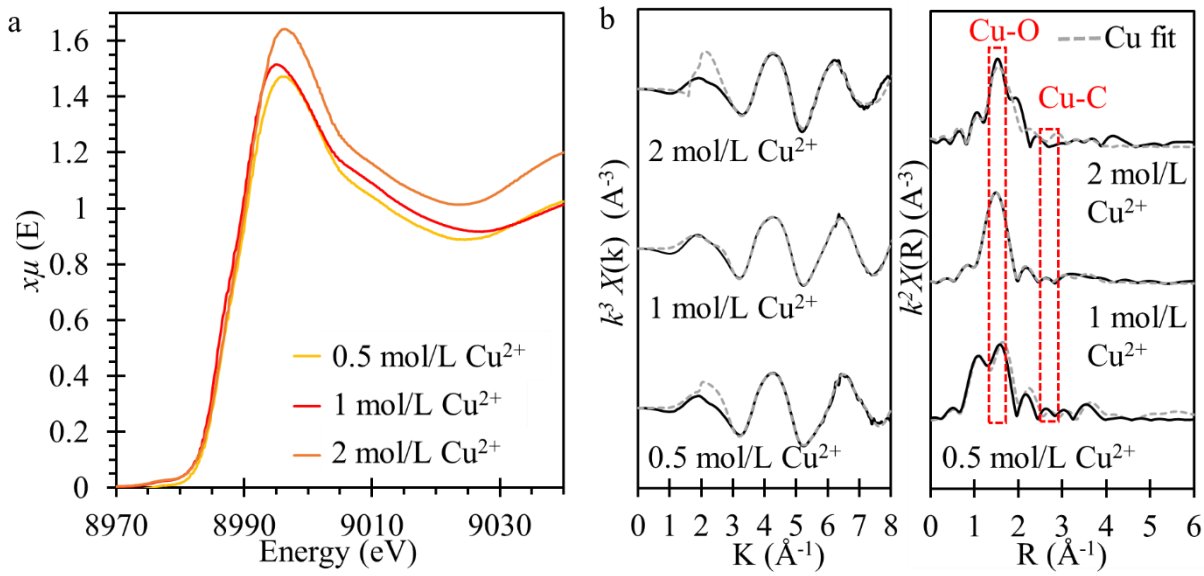

Figure 3.5 XAS of BPI-COOCu at Cu k-edge. (a) XANES, (b) EXAFS K-space and R-space

Table 3.2 BPI-COOCu EXAFS fit with the model structure of $CuH_2(CO_2)_2$

Sample	Path	*N*	S_0^2	e^0	R (Å)	σ^2 (Å^2)	R-factor[a]
BPI-COOCu (0.5 mol/ L Cu^{2+})	Cu-O(1)	6	0.901	2.932	1.930	0.01188	0.006
	Cu-C(1)	4	0.901	2.932	2.826	0.01873	
	Cu-O(1)-C(1)	8	0.901	2.932	3.008	0.01919	
	Cu-O(2)	4	0.901	2.932	4.259	0.00478	
BPI-COOCu (1 mol/ L Cu^{2+})	Cu-O(1)	4	0.968	3.338	1.943	0.00644	0.002
	Cu-C(1)	4	0.968	3.338	2.854	0.04017	
	Cu-O(1)-C(1)	8	0.968	3.338	3.055	0.01912	
	Cu-O(2)	4	0.968	3.338	4.045	0.01203	
BPI-COOCu (2 mol/ L Cu^{2+})	Cu-O(1)	6	0.944	9.767	2.014	0.01275	0.010
	Cu-C(1)	4	0.944	9.767	3.167	0.00656	
	Cu-O(1)-C(1)	8	0.944	9.767	3.291	0.01101	
	Cu-O(2)	4	0.944	9.767	4.314	0.01704	

[a]fractional misfit

N – coordination number, S_0^2 – amplitude reduction term, e^0 – energy shift (where k = 0), R – near-neighbor distance, σ^2 – mean-square disorder in R

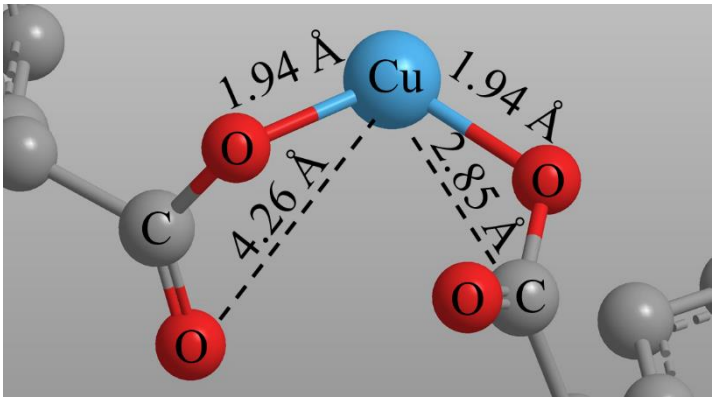

Figure 3.6 Local structure at Cu atom of BPI-COOCu made from 1 mol/L Cu^{2+} initial concentration

3.3.2 Thermo-mechanical properties, optical transparency, flame retardancy

The actual stress-strain curves of BPI-metal complexes are shown in Figure 3.7, while the TGA weight loss graphs are displayed in Figure 3.8. The UV-vis spectra of transmittance are shown in Figure 3.9. Heat release rate (HRR) results from the MCC tests are plotted against time and temperature, which are all displayed in Figure 3.10. The essential parameters of mechanical properties, TGA, and optical transparency are tabulated in Table 3.3, while those related to flame retardancy can be found in Table 3.4. For comparison, these tables also contain the information from the selected studies that examined flame retardancy of the functional polymer film with MCC tests.

BPI-COOAl and BPI-COOCu exhibited a tensile strength of 64 and 47 MPa, respectively (Figure 3.7 and Table 3.3). BPI-COOAl showed an improvement in tensile strength compared to that of BPI-COOK (47 MPa) in this study and BPI (46 MPa) in a previous study.[39] The enhanced tensile strength in BPI-COOAl may arise from the electrostatic interactions between Al^{3+} and COO^{-}. However, the value of elongation for BPI-COOAl (11%) and BPI-COOCu (8.8%) decreased, compared to that of BPI-COOK (14%) (Table 3.3). This suggested the lessened elasticity and elevated stiffness in BPI-metal complexes, which is also

indicated by Young's modulus values. The tensile strengths of BPI-COOAl and BPI-COOCu were acceptable, compared to the flame retardant polymer film from the literature in Table 3.3 and elsewhere.[114,115] Nevertheless, the mechanical properties can still be improved to match the other flame retardant films with a tensile strength above 100 MPa.[106,116]

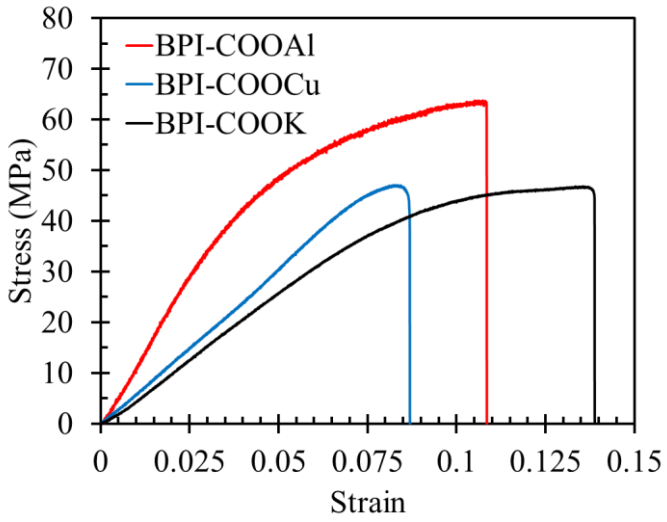

Figure 3.7 Stress-strain curve of BPI-COOAl and BPI-COOCu films with BPI-COOK as a reference

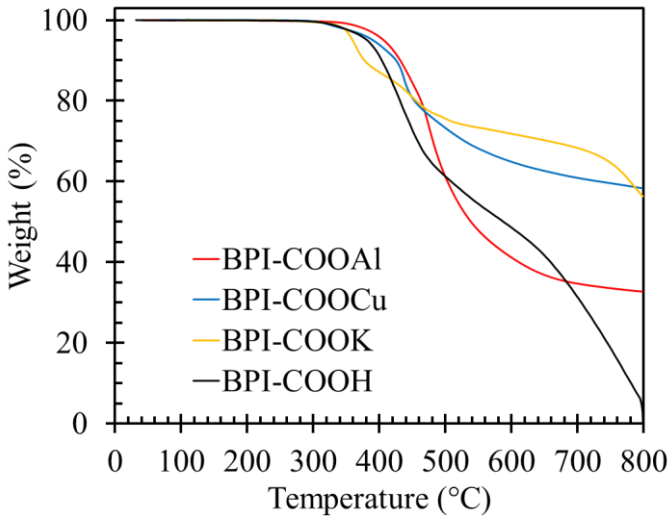

Figure 3.8 TGA weight loss graphs of BPI-COOAl and BPI-COOCu with BPI-COOH and BPI-COOK as references

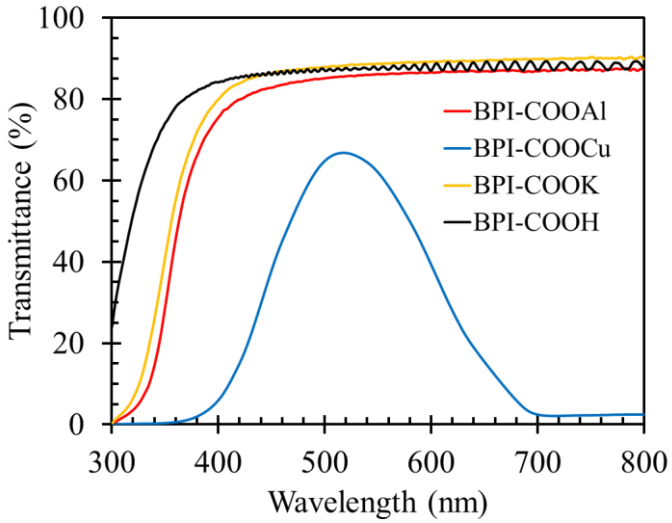

Figure 3.9 UV-vis spectra for film transmittance of BPI-COOAl and BPI-COOCu with BPI-COOH and BPI-COOK as references

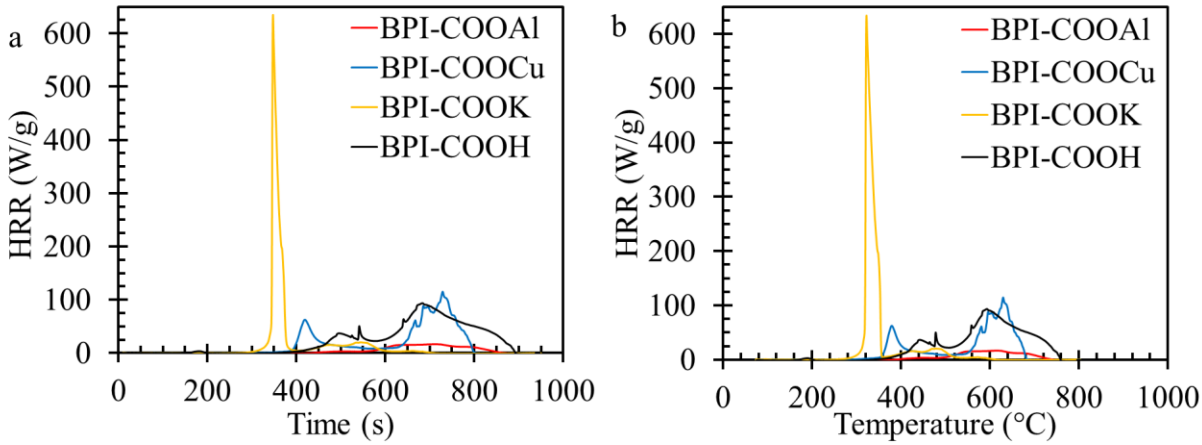

Figure 3.10 MCC curves of BPI-metal complexes. (a) HRR over time, (b) HRR over temperature

In term of thermal stability, BPI-COOAl and BPI-COOCu were presented with higher temperature of 5% (T_{d5}) and 10% decomposition weight loss (T_{d10}) than those of their precursors (Table 3.3). The values are acceptable when compared to those of other flame retardant films in Table 3.3 and elsewhere, which T_{d5} or T_{d10} not exceeding 400 °C.[93,98,114] Nevertheless, other film flame retardant functional polymer, that possessed T_{d5} or T_{d10} well exceeding 400 °C also existed.[104,106]

The characterization of transparency showed 75% transmittance at 400 nm (T_{400}) and 83% transmittance at 450 nm (T_{450}) for BPI-COOAl, which were lower by a small extent than the values of BPI-COOK and BPI-COOH (Table 3.3). BPI-COOCu yielded 6% and 38% for T_{400} and T_{450}, respectively. This occurred due to the absorption of light by the colored Cu^{2+} complex (Figure 3.2). However, the transmittance spectrum of BPI-COOCu (Figure 3.9) displayed the characteristics of a green filter with 68% transmittance at 518 nm.[117]

According to Table 3.4, BPI-COOAl and BPI-COOCu were rated V-0 for the UL-94V test, while BPI-COOK was rated V-1 because its t_2 was higher than 10 s. BPI-COOH failed the UL-94V test as the flame reached the top of the film in its initial burning (Table 3.4). The UL-94V test showed that metal complexation for BPI films could prevent the spreading of flames. In the video provided in the supporting material, a polypropylene film was used as a control in the UL-94V test, and dripping was apparent when it was burned. In contrary, BPI-COOAl, BPI-COOCu, and BPI-COOK did not experience dripping during the test. The cotton did not catch fire in all cases.

The value of time to ignition (*TTI*) shows that BPI-COOAl could suppress fire until coming to ignition at 427 s (Table 3.4). The MCC test comparison of various flame retardant polymer films in Table 3.4 shows that BPI-COOAl exhibited the lowest *THR* and heat release capacity (*HRC*) at 4.5 kJ/g and 23 J/g·K, respectively. The film had 18.9 kJ/g *pHRR* at a temperature (T_p) of 615 °C (Table 3.4). These values demonstrated the ability of BPI-COOAl to suppress heat effectively at high temperatures during a fire. For BPI-COOCu, its *THR* of 15 kJ/g was less than that of BPI-COOH (21 kJ/g). However, BPI-COOCu (116 W/g) also possessed a higher *pHRR* than that of BPI-COOH (95.8 W/g). The values of *TTI* inferred that BPI-COOCu ignited at 278 s, which was earlier than BPI-COOH (354 s).

During the thermal degradation of a material, the heat spread, and amount of volatile materials control the formation of graphitized char. As a result, the phenomenon can be used to assess flame retardancy. From the Raman shift, the intensity of the D peak (disordered char of A_{1g} vibration mode) at 1380 cm^{-1} over the intensity of the G peak (E_{2g} vibration of the aromatic layers in graphite crystalline) at 1600 cm^{-1} (I_D/I_G) is assumed to be inversely proportional to the in-plane microcrystalline size and in-plane phonon correlation length of the char layer.[118–120] The Raman shift in Figure 3.11 shows that BPI-COOAl, BPI-COOCu, and BPI-COOK char have I_D/I_G values of 1.71, 1.55, and 1.14, respectively. This infers that BPI-COOAl char residues possessed a smaller size of carbonaceous microstructures than those in the other films. The small microcrystalline size was related to the shielding effect of heat transfer, leading to more efficient flame retardancy.[99,121] This is also reflected in the SEM images, where the small carbonaceous size of BPI-COOAl char residue resulted in visibly homogenous and smooth surface morphology (Figure 3.12). BPI-COOCu has a loosely compacted structure while holes can be observed on the surface of BPI-COOK (Figure 3.12). The chemical composition of the char residues from the EDX analysis is tabulated in Table 3.5. Cu and Al still exist in their respective char residues.

Table 3.3 Comparison of thermo-mechanical properties and optical transparency of various bio-based flame retardant films

sample	mechanical properties[a]			TGA[b]				optical transparency[e]		ref.
	tensile strength (MPa)	moduli (GPa)	elongation (%)	T_{d1} (°C)[c]	T_{d5} (°C)[c]	T_{d10} (°C)[c]	char yield (%)[d]	T_{400} (%)[f]	T_{450} (%)[f]	
BPI-COOAl	63.7	0.573	11.0	355	407	431	32.7	75	83	this work
BPI-COOCu	47.1	0.607	8.81	321	390	425	58.3	6	38	
BPI-COOK	46.8	0.372	13.8	327	360	378	56.3	80	86	
BPI-COOH	n/a			325	381	403	0	84	86	
PVC/ZnO coated with poly(amide-imide) (C-PPN 2)	41.7	1.49	3.60	n/a	213	244	18.3	n/a		122
PVA/ $Mg(OH)_2$ (PVA/NMH-10phr)	n/a			n/a	217	n/a	34.2	97[g]	97[g]	92
PVA/graphene/ chitosan (PVA/CS/RGO-0.8%)	6.45	n/a	76.5	n/a				n/a		123

PLA/Ni/Al/ layered double hydroxides	n/a	n/a	250 [g]	300 [g]	n/a	65 [h]		40
epoxy acrylate resin/ hyperbranched polyphosphonate acrylate (EA/HPA-3)	n/a	n/a	286	n/a	n/a	80 [g]	85 [g]	91
alginate/ $Zn(Cl)_2$	n/a	n/a	80	n/a	n/a	n/a		26
soybean oil/ PE/ DOPO-HQ (E30-P6)	n/a	n/a	341	n/a	3.3	n/a		124

[a]parameters obtained from tensiometer at room temperature, [b]thermogravimetric analysis scanned at a heating rate of 10 °C/min under nitrogen atmosphere, [c]1%, 5% and 10% weight loss temperatures, [d]char residue left at the end of TGA, [e]measured by UV-vis spectrometer, [f]transmittance measured by ultraviolet-visible spectrometer, [g]value estimated from the figure in the literature, [h]ASTM D 1003 standard

T_{d1} – temperature at 1% degradation, T_{d5} – temperature at 5% degradation, T_{d10} – temperature at 10% degradation, T_{400} – transmittance at 400 nm, T_{450} – transmittance at 450 nm, n/a – not available

Table 3.4 Comparison of flame retardancy tests of various bio-based films

sample	UL-94V[a]						MCC[b]					ref.
	rating	t_1 (s)	t_2 (s)	t_3 (s)	dripping	igniting cotton	*TTI* (s)	*pHRR* (W/g)	*THR* (kJ/g)	*HRC* (J/g·K)	T_p (°C)	
BPI-COOAl	V-0	1	0	25	no	no	427	18.9	4.5	23	615	this work
BPI-COOCu	V-0	0	0	60	no	no	278	116	14.6	144	632	
BPI-COOK	V-1	7	14	2	no	no	251	634	13.3	791	321	
BPI-COOH				fail			354	95.8	21.3	121	593	
PVC/ZnO coated with poly(amide-imide) (C-PPN 2)				n/a			n/a	86.9	6.1	105.2	n/a	[122]
PVA/ $Mg(OH)_2$ (PVA/NMH-10phr)				n/a			n/a	332	7.3	198	264	[92]
PVA/graphene/ chitosan (PVA/CS/RGO-0.8%)				n/a			n/a	85	12	n/a	250	[123]

PLA/Ni/Al/ layered double hydroxides				n/a			n/a	400	9.7	n/a	n/a	[40]
epoxy acrylate resin/ hyperbranched polyphosphonate acrylate (EA/HPA-3)				fail			n/a	167	13.7	166	n/a	[91]
alginate/ $Zn(Cl)_2$	V-0	n/a	n/a	n/a	no	no	n/a	17.1	n/a	n/a	423	[26]
soybean oil/ PE/ DOPO-HQ (E30-P6)	VTM-2[c]		2[c]		yes	yes	n/a	175	16.5	162	415	[124]

[a]IEC60695-11-10B method, ASTM D3801 standard vertical combustion test (refer to the Experimental section for the parameters definition), [b]microscale combustion calorimetry, [c]GB/T 15903−1995 standard

TTI – time to ignition, *PHRR* – peak heat release rate, *THR* – total heat released, *HRC* – heat released capacity, T_p – temperature at *pHRR*, n/a – not available

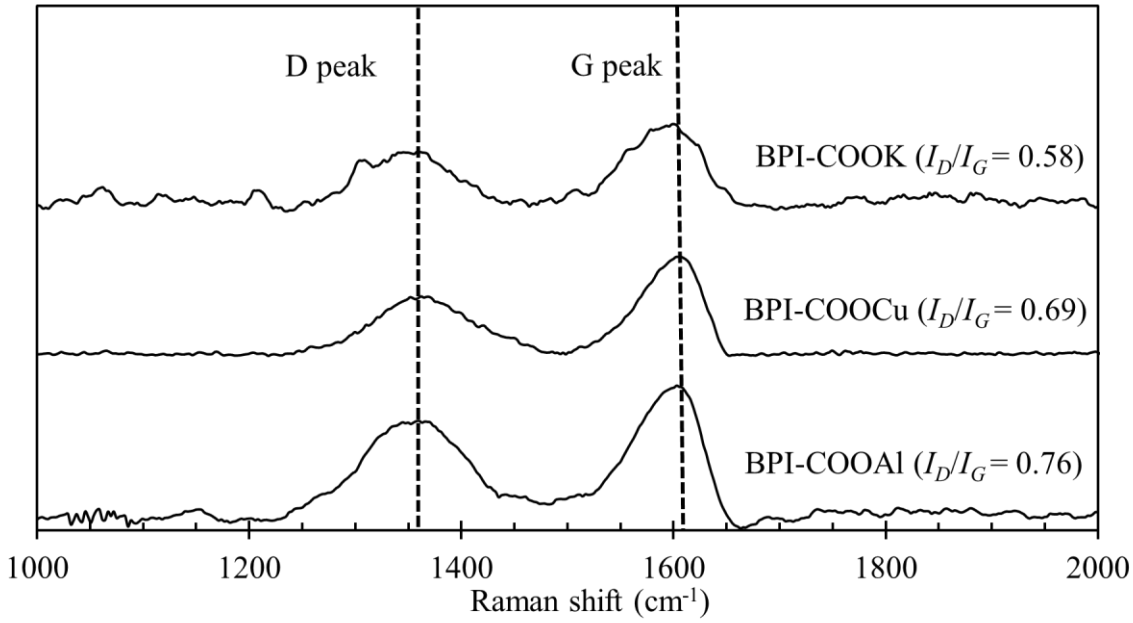

Figure 3.11 Raman spectra of BPI-COOAl and BPI-COOCu char residues were burned in an open-air oven at 800 °C with that of BPI-COOK as a reference. Characteristic intensity of disordered char (D peak at 1380 cm^{-1}) and graphite crystalline (G peak at 1600 cm^{-1}) with their fraction (I_D/I_G) inversely proportional to microcrystalline size

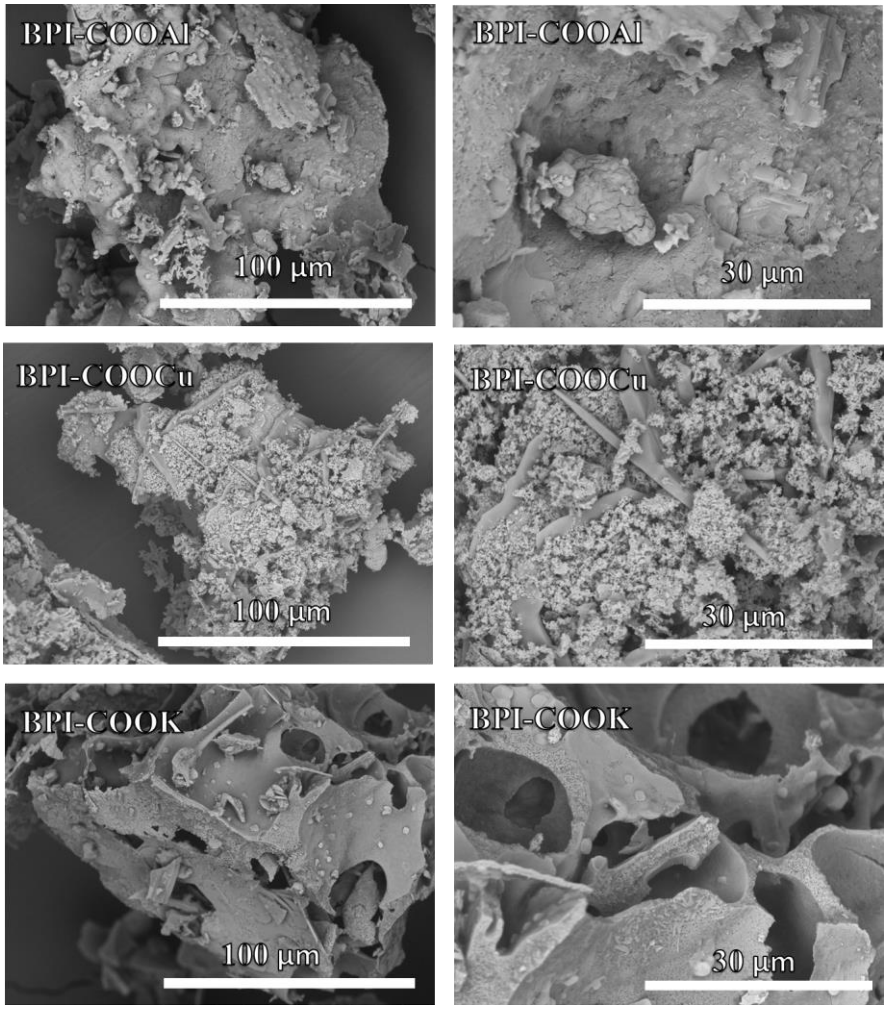

Figure 3.12 SEM images magnified at 100 and 30 μm of BPI-COOAl and BPI-COOCu char residues with that of PI-COOK as a reference

Table 3.5 Elemental composition of of BPI-COOAl and BPI-COOCu char residues with that of BPI-COOK as a reference

char residues	elemental composition (%)							
	C	O	N	Cl	K	Cu	Al	Total
BPI-COOAl	62.9	20.9	ND	2.2	13.4	ND	0.6	100
BPI-COOCu	37.4	33.9	ND	0.7	14.0	14.0	ND	100
BPI-COOK	35.2	64.8	ND	ND	ND	ND	ND	100

3.3.3 Mechanism of flame retardancy

The fitting of Al2p XPS spectra for BPI-COOAl in Figure 3.13 was adopted from the literature.[125] The results showed $Al(OH)_3$ from Al^{3+} of aluminum carboxylate (~74 eV) as the main species in BPI-COOAl. The BPI-COOAl char residue contained $Al(OH)_3$ and Al-O from Al_2O_3 (~73.7 eV). The latter was formed according to Equation 3-5 with the O_2 from the atmosphere. H may also come from the atmosphere or the degradation of cyclobutene and benzene rings in the BPI structure.

$$2Al + \frac{5}{2}O_2 + 4H \xrightarrow{\Delta} Al_2O_3 + 2H_2O \quad (3\text{-}5)$$

The mechanism in Figure 3.13 shows that an Al_2O_3 char layer formed and prevented the spreading of heat. Moreover, the water molecules released during the reaction suppressed smoke, prevented access to O_2, and provided further support for flame retardancy.

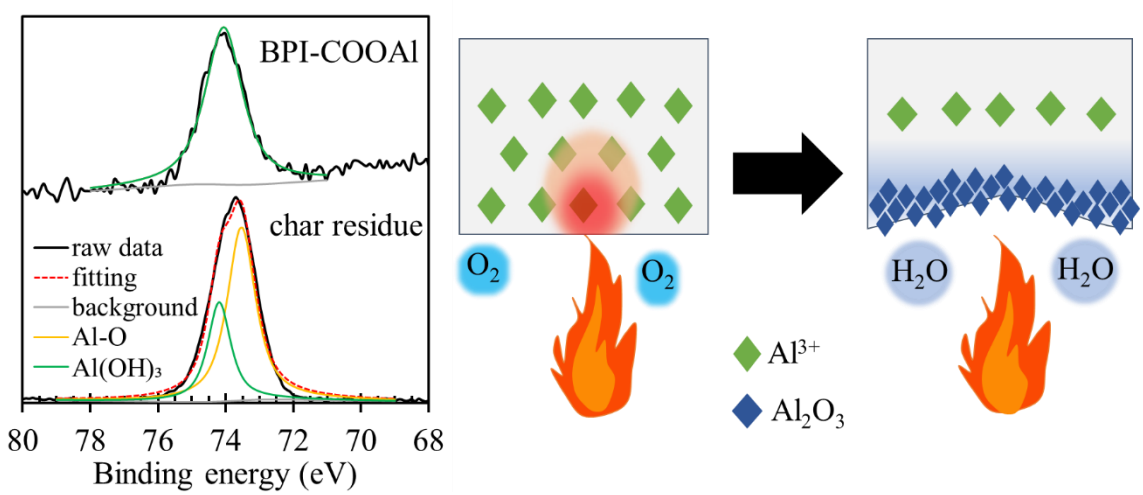

Figure 3.13 Proposed flame retardant mechanism of BPI-COOAl. (a) Al2p XPS spectra, (b) flame retardant mechanism diagram

XPS spectra of BPI-COOCu, focusing on the Cu2p3 region, is displayed in Figure 4c. The results show that CuO from the carboxylation of Cu^{2+} is the main species of BPI-COOCu. Cu_2O was observed in the film char residue. This suggests that the Cu_2O char layer is an intumescent material during burning (Figure 3.14). The accumulation of the char layer can also be explained by Equation 3-6.

$$4CuO \xrightarrow{\Delta} 2Cu_2O + O_2$$

(3-6)

In the formation of Cu_2O at high temperatures, a previous study revealed that about 10% oxygen (O_2) was created in the process.[126] Cu_2O could act as an intumescent material that prevented the transfer of heat, but the addition of O_2 promoted fire. This resulted in a lower flame retardancy of BPI-COOCu as compared to BPI-COOAl. The phenomenon may be responsible for the high value of t_3 in the UL-94V standard test (Table 3-4).

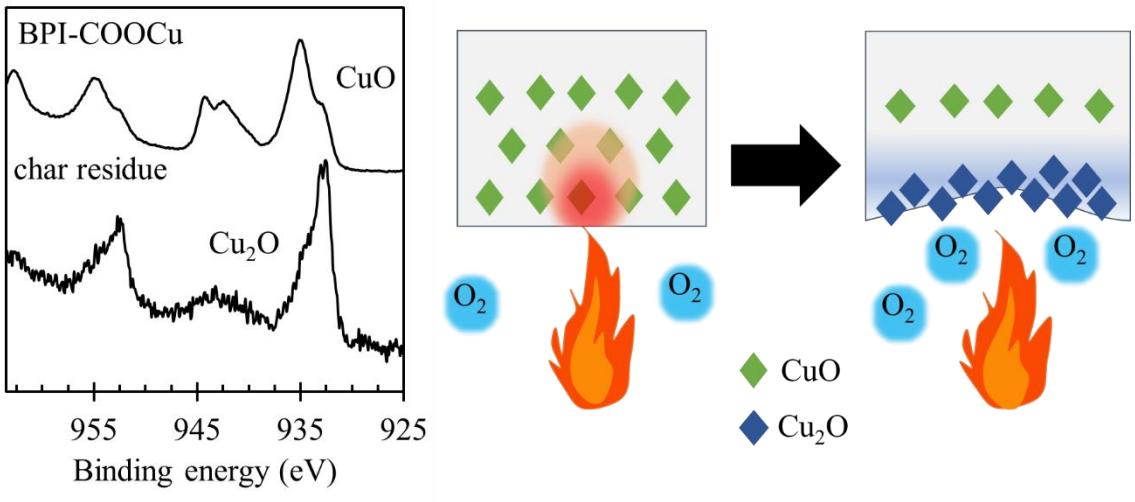

Figure 3.14 Proposed flame retardant mechanism of BPI-COOCu. (a) Cu2p3 XPS spectra (b) flame retardant mechanism diagram

3.4 Conclusion

The carboxylic acid side-chain group of BPI-COOH was modified by neutralization with KOH to form a potassium salt, BPI-COOK. Complexation by an exchange of K^+ into targeted multivalent metal ions (Al^{3+} and Cu^{2+}) was determined to be an exothermic reaction. Films of BPI-COOCu and BPI-COOAl salts were obtained. When compared to the values of the polymer films in the literature, BPI-COOCu and BPI-COOAl were suitable as flame retardant materials. Both films were rated V-0 for the UL-94V test. The *THR* value (4.5 W/g) of BPI-COOAl was lower than those of BPI-COOH, BPI-COOK, or other polymer films reported in the literature. BPI-COOAl had a T_{d10} of 431 °C and a tensile strength of 64 MPa, exhibiting an improvement of thermo-mechanical properties by metal substitution, as compared to BPI-COOK. The T_{450} transparency value (83%) of BPI-COOAl was preserved after the metal substitution. A probable mechanism of flame retardancy was proposed. The Cu_2O and Al_2O_3 char layer, formed during the material degradation, functioned as an intumescent material to suppress the transfer of heat and promoted flame retardancy. Further study should consider the minimization of metal concentration and incorporation of environmental-friendly additives into the molecular design to create a high-performance film. In addition, the metal-scavenging BPI could also be employed for removing toxic metal ions from a water environment. The development of thermo-mechanically and transparent biopolyimide films with enhanced flame retardancy serves as a new opportunity to create more efficient materials for electronic displays and light-weight films, for a sustainable society.

CHAPTER 4

Biopolyimide and europium ions composites as photoluminescent sensor for volatile organic compounds detection

4.1 Introduction

Activities in the household and industry have been causing the excessive amount of volatile organic compounds (VOCs) in indoor environments. These VOCs are known to be responsible for many diseases.[127–129] As a result, the ongoing researches aim to solve VOCs-related problems include the technologies that remove as well as monitor a certain amount of the compounds.[130–132] For a better living and health risk reduction, it is essential that the VOCs are well-monitored and kept within the minimal level.

VOCs monitor could be done by employing materials that could act as sensors. The sensor mechanism relied on the chemical reactions or change in the physical structure of these materials after interacting with target VOCs. The change can be detected by the systems such as electrochemical,[133,134] surface acoustic wave,[135] and colorimetric.[136,137] One of the most studied systems is the metal oxide semiconductor, which the nanoscale metal oxides (SnO_2, In_2O_3, ZnO, TiO_2, and others and their combinations) were coupled with semiconductor systems to detect several species of VOCs.[138,139]

The photoluminescence has been used for VOCs detections. Photoluminescence is a process which an electron of the molecules went into electronic excited state by adsorbing photon. When the electron returns to lower energy states, the photon is emitted making the molecules glow. The technique offers advantages in metallic impurities avoidance due to the electrical contacts between material structures and real-time information based on the change

in the photoluminescence spectra.[139] After contacting VOCs, the centers of material may experience intensity quenching (decrease) or enhancement (increase).

Rare earth metal cations such as europium (Eu^{3+}) and terbium (Tb^{3+}) are two of the best candidates for photoluminescent due to their suitable transition energy gap [ΔE = 12300 ($^5D_0 \rightarrow {}^7F_6$) and 14800 ($^5D_0 \rightarrow {}^7F_0$), respectively].[140] However, the cations themselves possess a weak *f-f* transitions due to the shielding of the 4f orbitals by the filled $5s^2$ and $5p^6$ sub-shells.[141] As a result, the cations are chelated by the chromophore-containing group (NH and CO) which can transfer energy to the cations. Many studies concentrated on lanthanide-based metal-organic frameworks (Ln-MOF) as the materials for photoluminescence VOCs detections. The inclusion of Eu^{3+} into bpy-UiO frame work [$Zr_6(\mu_3\text{-}O)_4(OH)_4$(2,2-bipyridine-5,5-dicarboxylic acid)$_{12}$] displayed emission bands at 590, 613, 653, and 701 nm (355 nm excitation) which quenched or enhanced in the presence of benzene, toluene, o-xylene, m-xylene, p-xylene, ethylbenzene, chlorobenzene, and benzonitrile.[142] Ln-MOF of 4-carboxy-1-(4-carboxybenzyl)pyridinium chloride containing Tb^{3+} were used to monitor many VOCs with acetone detection resulted in quenching at the luminescent centers (489, 544, 582, and 619 nm).[143] The quenching of acetone by the mentioned Ln-MOF was recycled for 5 cycles through methanol washing. The double system framework of hexa-(4-carboxyl-phenoxy)-cyclotriphosphazene containing Eu^{3+} and Tb^{3+} had its emission intensity bands quenched after sensing styrene gas (from ~ 1000 to almost 0 a.u. in 240 s).[142] Ln-MOF and its photoluminescent ability have also been studied for pH, temperature, and ions sensing.[144] Beside Ln-MOF, a complex of alginate and Eu^{3+} was used for VOCs sensing, which its emission bands (594, 617, 650 and 698 nm) were affected by different solvents.[145]

The monomer created from sugar fermentation, 4-aminocinnamic acid (4ACA), was developed, and its derivative bio-based polymers exhibited excellent thermo-mechanical properties.[37,38] The modification of bio-based polyimide (BPI) would resulted in carboxylic

acid on its side chain. The polymer becomes a potential photoluminescence green material for VOCs sensor if complexified with rare earth metal cations.

In this study, we created an organic/inorganic complex (BPI-COOEu) with the modification of BPI-COOH derived from 4ACA. Eu ion (Eu^{3+}) was chosen in this study due to its transition energy gap mentioned above. It emitted orange-red light and had one of the longest fluorescent lifetimes (9.67 ms) among the lanthanide ions (Gd ion exhibited the longest lifetime but was considered unsuitable due to its UV emission). The BPI-COOH was neutralized with KOH to form BPI-COOK. The complexation forming BPI-COOEu was achieved with an ion-exchange between K^+ and Eu^{3+}. BPI-COOEu, in the form of film, was characterized for its photoluminescent property. It was also briefly tested for VOCs sensing ability, in which the luminescent centers were quenched or enhanced, depending on the types of VOCs.

4.2 Experimental

4.2.1 Materials

4-aminocinnamic acid (4ACA) was prepared from bacterial fermentation of sugar according to the methods presented previously. N, N-dimethylacetamide (DMAc, Kanto Chemical Co., Japan) was left in 4 Å molecular sieves under nitrogen atmosphere for 24 h before being used for polymerization. 1,2,3,4-tetracarboxycyclobutane dianhydride (CBDA, Tokyo Chemical Industries, Japan), hydrochloric acid (HCl, Kanto Chemical Co., Japan), sodium hydroxide (NaOH, Kanto Chemical Co., Japan), potassium hydroxide (KOH, Kanto Chemical Co., Japan), europium chloride ($EuCl_3$, Kanto Chemical Co., Japan) were used as received. The solvents used as VOCs were obtained from Kanto Chemical Co., Japan, and these include acetone, ethanol, ethyl acetate, hexane, and methanol.

4.2.2 Monomer and polymer syntheses

4,4'-diamino-truxillic acid (4ATA), BPI-COOH, and BPI-COOK was synthesized according to the experimental section of CHAPTER 3 (p 45). BPI-COOK was obtained in fibril form and was kept in a closed environment for further use.

4.2.3 Biopolyimide-europium complexation

Scheme 4.1 illustrates the synthesis of BPI-COOEu from BPI-COOK. A solution of 50 g/L BPI-COOK was produced from dissolving BPI-COOK in DI water. BPI-COOK film was made by the method of solution casting on a glass substrate. After drying at 40 °C on a hot plate, the film of thickness 0.13 ± 1 mm was obtained. A BPI-COOK film sample was cut to have a dimension of 100 x 300 mm before being submerged into a metal solution prepared with $EuCl_3$.

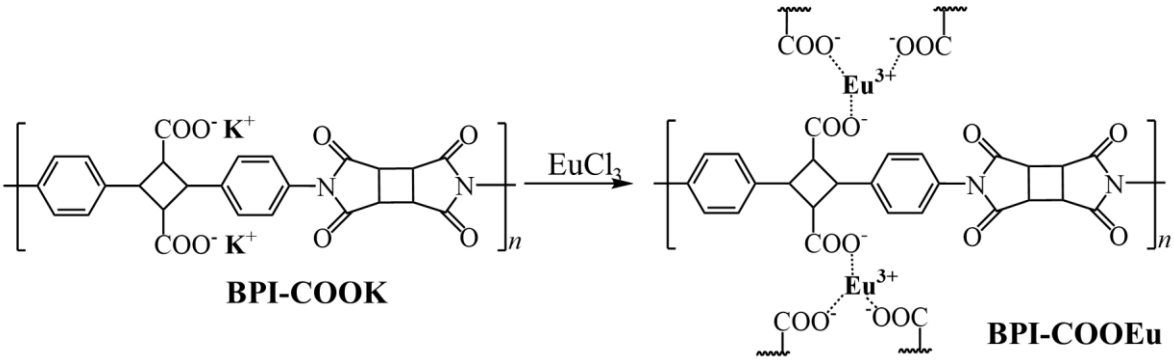

Scheme 4.1 Synthesis of BPI-COOEu

The complexation equilibrium time was determined by the kinetic experiment of BPI-COOK film submersion in 1 mol/L Eu^{3+} solution for 0 – 120 min. The metal ion concentration left in the solution after the complexation was quantified with an inductively coupled plasma atomic emission spectroscopy (ICP-OES, Avio 200, PerkinElmer). The set-up of ICP-OES was as follows: 1.50 mL/ min peristaltic pump and auto-autosampler flow rate (with autosampler

washed between every sample), 20 sec flush time, and 30 sec normal time. To determine the amount of Eu^{3+} left in the solution, Equation 4-1 was used.

$$Eu^{3+}\ \text{Removal}\ (\%) = \frac{C_i - C_e}{C_i} \times 100 \quad (4\text{-}1)$$

where, C_i is the initial Eu^{3+} concentration (mol/L), while C_e is the concentration left in the solution after complexation (mol/L). The equilibrium time was taken from a plot of Eu^{3+} removal (%) over time, where the former is stable.

The equilibrium time was determined to be 30 min (refer to Results & discussion section). It was used to observe the metal complexation in different Eu^{3+} concentrations as BPI-COOK film sample was submerged into 10 ml of 0.5, 1, 2, 4, and 6 mol/L Eu^{3+} solutions. After 30 min, BPI-COOEu was obtained.

4.2.4 Characterizations for photoluminescent properties

For the purpose of measuring the photoluminescent at low intensity, BPI-COOEu in particles form was prepared using 0.1 mol/L Eu^{3+}. The particles were washed with DI water and dried at 60 °C for at least 6 h under vacuum. PI-COOEu particles were first viewed under a xenon lamp equipped with 320 nm bandpass filter (Asahi Spectra MAX-303, Japan). After that, the particles were confirmed for its photoluminescent properties with the spectrofluorometer (FP-8600, JASCO, Japan) of excitation range 300 – 350 nm. At 330 nm excitation, $EuCl_3$ solution (0.1 mol/L), BPI-COOH, and BPI-COOK were also measured for control.

The PI-COOEu films were created from 1 mol/L Eu^{3+} (refer to Results & discussion section for more information on the minimum metal ion concentration of film complexation). The PI-COOEu film was first viewed under a xenon lamp equipped with 320 nm bandpass

filter. The film was exposed to the solvents for 10 min. The set-up for solvent exposure is shown in Figure 4.1. The film was clipped and inserted through a small rectangular hole into a 5 cc.-vial. After the desired time, the film was removed and rechecked for the emission spectrum. The excitation of 320 nm was used to check the quenching and enhancement after solvent contact. This is because the 330 nm excitation resulted in the emission intensity of BPI-COOEu higher than 10000, above the detection limit of the spectrofluorometer.

The circularity and sensing sensitivity of BPI-COOEu were tested. Acetone was chosen for these tests due to its strong quenching effects of the film (refer to results and discussion for more information). After an acetone contact, the film was washed thoroughly with DI water. Then, the test was carried out again for acetone quenching. The circularity was conducted for 5 cycles. For the acetone sensing sensitivity, BPI-COOEu film was tested for its quenching ability at various acetone concentrations (0.05%, 0.5%, 1%, 10%, and 100%).

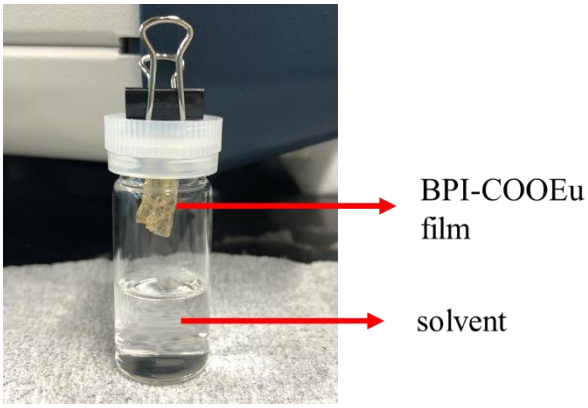

Figure 4.1 Set-up for film exposure to VOC vapor with 3 ml solvent in 5 cc. vial (room temperature)

4.3 Results and discussion

4.3.1 Biopolyimide-europium complexation kinetic study

According to Figure 4.2a, there is a steady increase in Eu^{3+} removal during the complexation until about 30 min, when the removal starts to become steady. As a result, 30 min was considered as the system equilibrium time. About 57% of Eu^{3+} was removed within 120 min. The results of batch experiments in Figure 4.2b reveals a steady increase in the amount of metal bound to a unit of BPI in mol/g (q) as the initial concentration of Eu^{3+} solution (C_i) increases. q became steady at around 2 mol/L C_i. Nevertheless, the BPI-COOEu film could be produced at 1 mol/L C_i. A lower C_i led to particles formation, which BPI-COOK was observed to break apart and particles of BPI-COOEu was formed during the complexation.

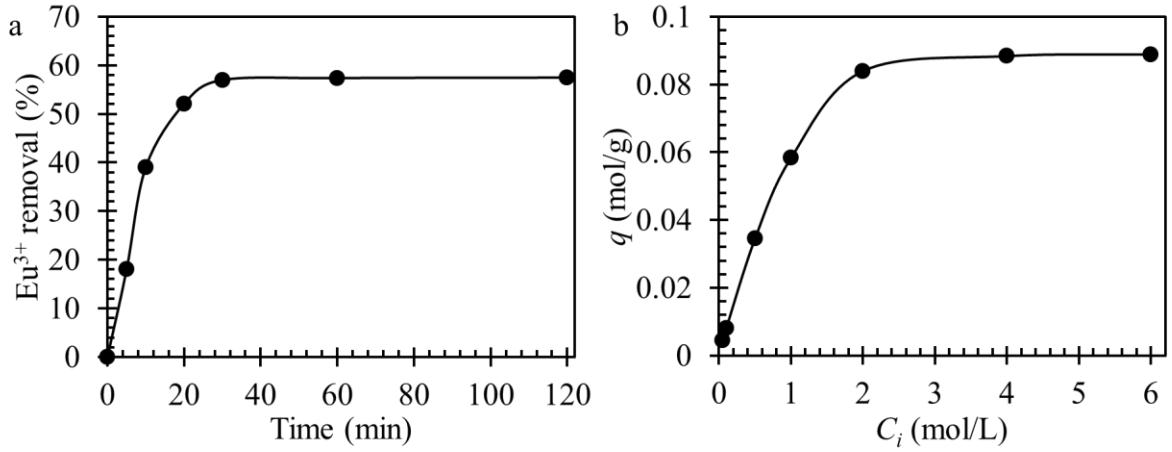

Figure 4.2 BPI-COOEu complexation kinetic study. (a) Eu^{3+} (1 mol/L) removed by the complexation over time (Eu^{3+} removal calculated from Equation 4-1), (b) batch experiment of BPI-COOK submerged in 0.5 – 6 mol/L Eu^{3+} solution for 30 min. q is the amount of metal bound to a unit of BPI (mol/g), and C_i is the initial metal ion concentration (mol/L).

4.3.2 Photoluminescent property of biopolyimide-europium complex

The BPI-COOEu particles and film viewed under a xenon lamp equipped with 320 nm bandpass filter is displayed in Figure 4.3 and Figure 4.4, respectively. The luminating light could be observed by naked eyes. According to Figure 4.5, the emission bands appeared at 579, 592, 616, 650 and 692 nm are ascribed to the $^5D_0 \rightarrow {}^7F_J$ (J = 0 – 4) transition of Eu^{3+}.[140,142,145] The prominent emission at 616 nm is responsible for the red emission. In Figure 4.6, the control experiment shows that BPI-COOH and BPI-COOK has no emission wavelength at 500 – 800 nm. According to Figure 4.6, $EuCl_3$ solution (0.1 mol/L) displayed the intensity bands ascribed to $^5D_0 \rightarrow {}^7F_J$ (J = 1 – 3), and the $EuCl_3$ reference in Figure 4.4 has an orange emission. $^5D_0 \rightarrow {}^7F_1$ transition is a magnetic dipole transition, which the resulted intensity depends on the symmetry of crystal structure.[146] It is prominent in $EuCl_3$ solution as the ion contains inversion center in the water environment.[147] On the other hand, BPI-COOEu was observed with an intensified $^5D_0 \rightarrow {}^7F_2$ transition. This electric dipole (ED) transition is dubbed as the hypersensitive transition, which its resultant intensity may depend on several factors. ED transition is more intense with a distorted center of symmetry, and the distortion usually occurred in a complexed lanthanide like BPI-COOEu.[146] The same phenomenon was previously observed in the europium-alginate/polyacrylamide complex.[148] $^5D_0 \rightarrow {}^7F_2$ transition obeyed selection rule of quadrupole transitions ($|\Delta S| = 0$, $|\Delta L| \leq 2$, $|\Delta J| \leq 2$), which were affected by the inhomogeneity dielectric surrounding Eu^{3+}.[149] The presence of BPI may increase the inhomogeneity and intensify the $^5D_0 \rightarrow {}^7F_2$ transition. The metal-ligand covalency via charge transfer was also observed to affect the hypersensitive transition.[150]

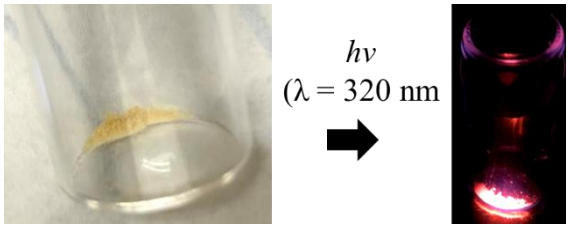

Figure 4.3 BPI-COOEu particles produced from 0.1 mol/L Eu^{3+} viewed under xenon lamp equipped with 320 nm bandpass filter

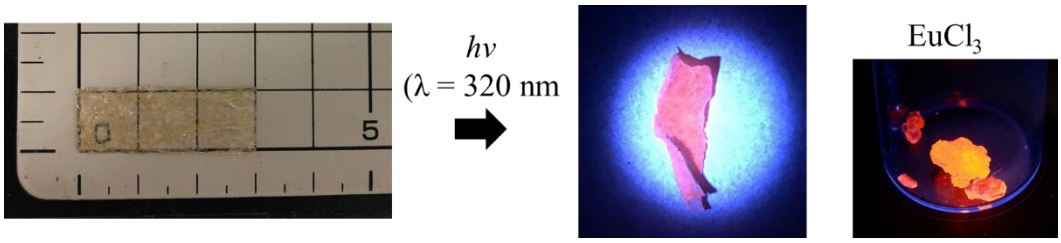

Figure 4.4 BPI-COOEu films (100 x 300 mm) produced from 1 mol/L Eu^{3+} viewed under xenon lamp equipped with 320 nm bandpass filter (the side of the film is flexible enough to be bent by hands). $EuCl_3$ was used as a reference.

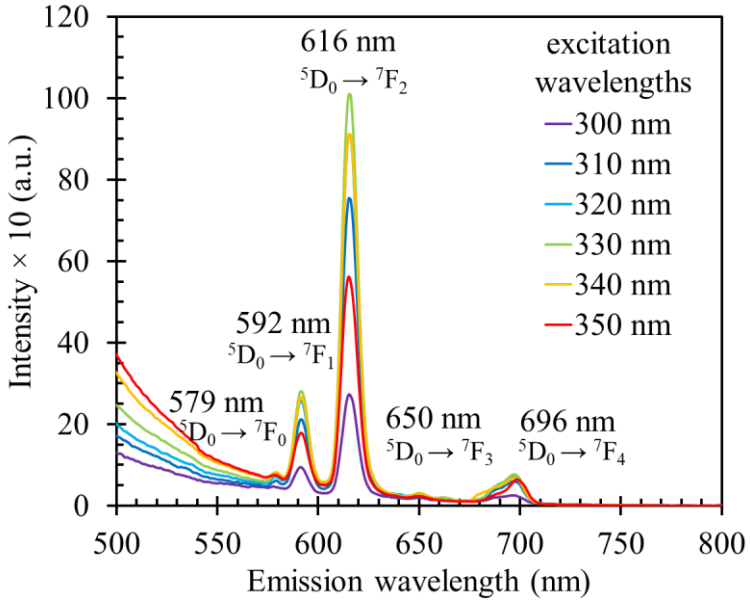

Figure 4.5 Emission spectra of the BPI-COOEu particles at different excitation wavelengths

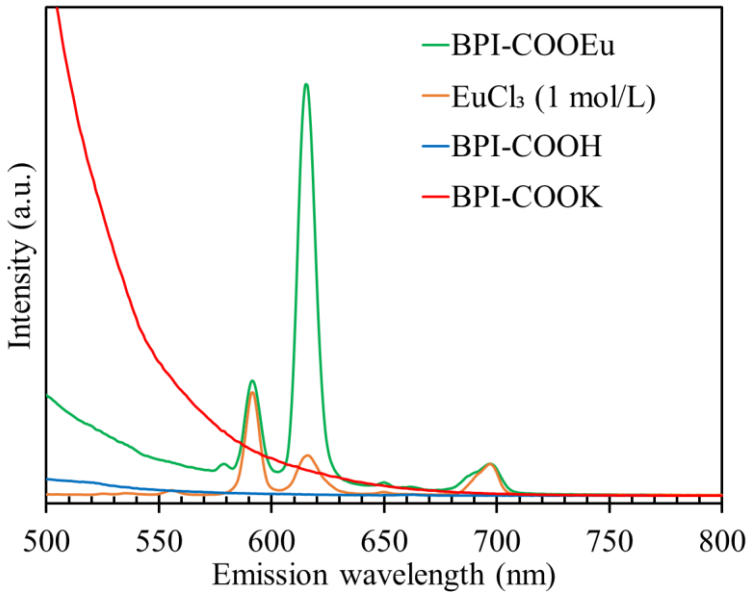

Figure 4.6 Emissions of the control experiment with excitation wavelength of 330 nm

The Jablonski diagram in Figure 4.7a illustrates the mechanism of BPI-COOEu photoluminescent under 330 nm excitation. The energy was first adsorbed by BPI, which had its fluorescent observed in the emission range of 350 – 500 nm (Figure 4.7b). This is mostly due to the presence of benzene rings in the BPI structure (Figure 4.7c). As the singlet state (S_1) was short-lived, the energy was first transferred to the triplet state (T_1) before passed on to the Eu^{3+} through the intramolecular energy transfer (Figure 4.7c-d).[146] The intramolecular energy transfer may involve the intramolecular energy transfer or/and Förster mechanism.[151]

4.3.3 Biopolyimide-europium complex as volatile organic compounds sensor

In Figure 4.8, the emission spectra of the BPI-COOEu films after solvent contact are tabulated. It was observed that the methanol and ethanol caused enhancement effects on the emissions. The enhancement could occur when LUMO of the solvents possess higher energy than that of the sensor, facilitating the energy transfer to the state above $^5D_0$, widening the energy gap, and enhancing the emission.[152] On the other hand, the contacts with acetone resulted in quenching effects. Acetone promoted the strongest quenching effect in the

photoluminescent of BPI-COOEu. Such quenching effects by acetone were previously observed in the europium-polymer composites.[143,145] The film of ethyl acetate and hexane test displayed similar emission spectra to that of free BPI-COOEu.

The circulatory test results are shown in Figure 4.9. In all 5 cycles, the peak intensities of 616 nm emission were observed at around 1400 for the BPI-COOEu film exposed to acetone. However, after DI water washes, the intensities increased to 2800. The experiment depict the reusability of the BPI-COOEu film as a VOCs sensor.

With higher acetone concentration, a stronger quenching effect was observed (Figure 4.10). BPI-COOEu was observed to be able to sense 0.05% acetone through the quenching effect. At this concentration, the emission band at 616 nm was observed to be quenched to a small extent.

The phenomenon of quenched emission by acetone could be explained by the solvent having the region of UV adsorption range (300 – 360 nm) similar to BPI-COOEu as well as the intermolecular interactions that caused the transferred of energy to acetone molecules.[143,153] A mechanism that involved lone pair-π interaction is proposed in Figure 4.11. The lone pair-π interaction was described as a non-covalent bond between a neutral electron-rich molecule and π ring.[154] Such an interaction could occur between a lone pair from the O atom (sp^2 orbital) of acetone and a π bond of an aromatic ring in BPI-COOEu. The adsorption of UV and transfer of energy by an aromatic ring in BPI-COOEu was dependent on the excitation (HUMO → LUMO) of π bonds. The lone pair-π interaction may prevent the excitation and result in the quenching effect. A similar mechanism was previously proposed in the bipyridyl moiety system.[155]

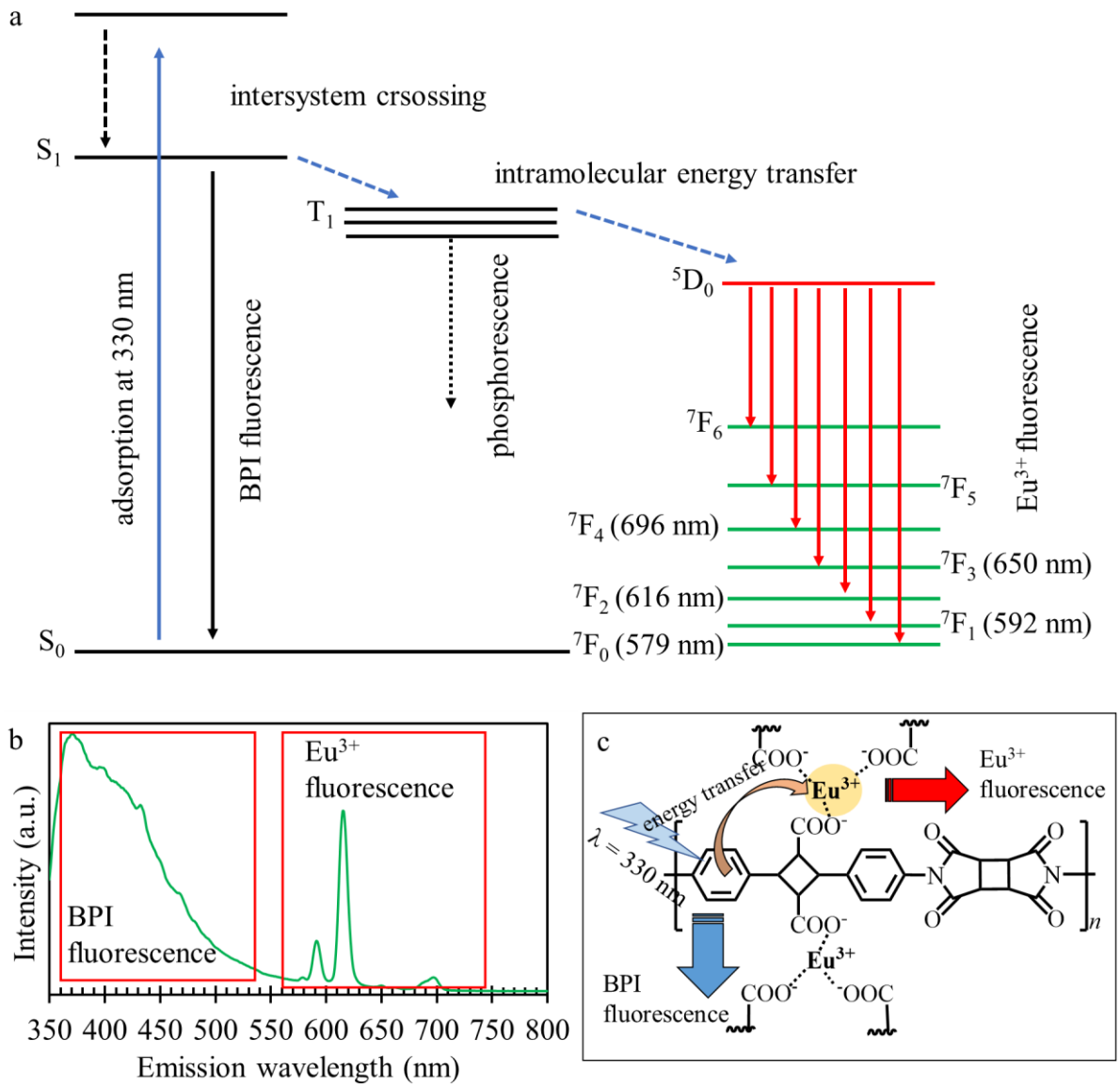

Figure 4.7. Fluorescence emission mechanism in BPI-COOEu. (a) Simplified Jablonski diagram illustrating the transfer of energy from BPI to Eu^{3+} under 330 nm excitation (S_0 – ground state, S_1 – excited state, T_1 – lowest triplet state, ^7F_J – ground state of $4f^6$ with less than half-filled shells, creating 6 possible lowest *J* values denoted as 0 to 6), (b) Emission bands showing BPI and Eu^{3+} fluorescence, (c) illustration of mechanism in BPI-COOEu

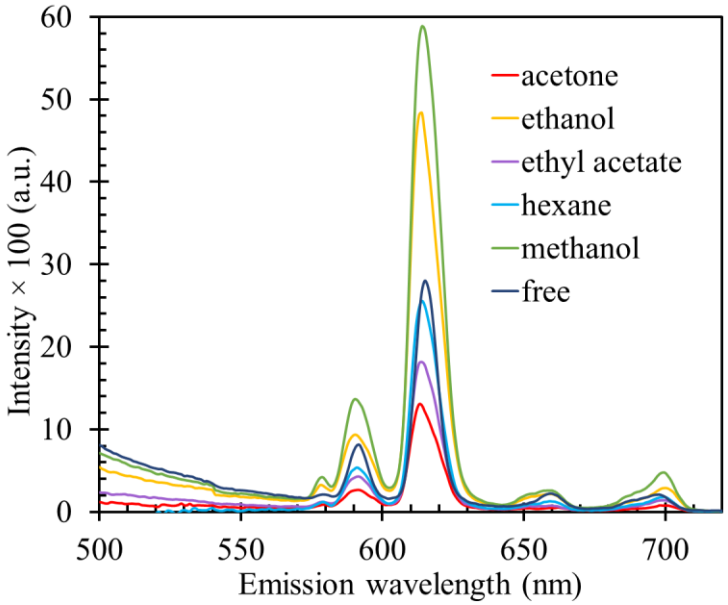

Figure 4.8 Emission spectra for BPI-COOEu film at excitation wavelength of 320 nm after solvent contact for 10 min

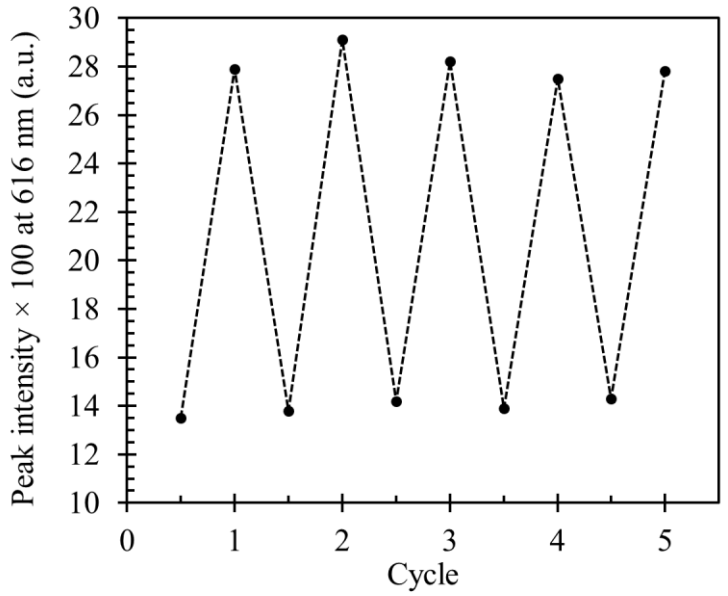

Figure 4.9 BPI-COOEu film and acetone quenching circulatory tests for 5 cycles. DI water was used to wash the film after each acetone test

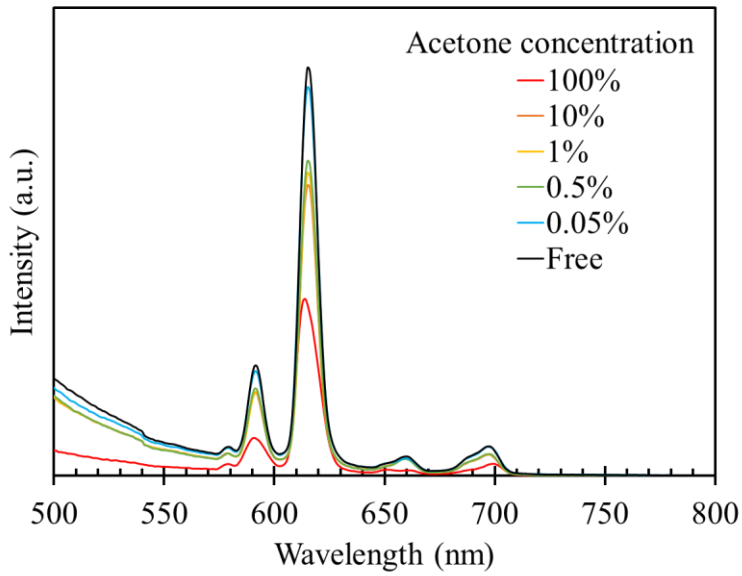

Figure 4.10. Acetone concentration variation for the quenching of PI-COOEu photoluminescent

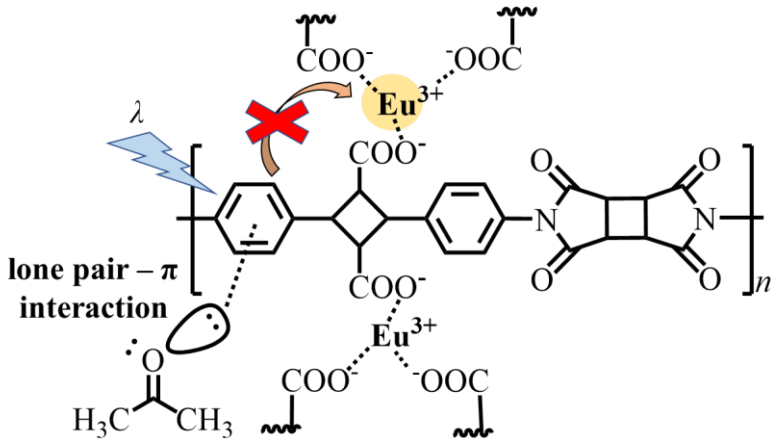

Figure 4.11. Proposed mechanisms for the quenching of BPI-COOEu photoluminescent due to the interaction between a lone pair from acetone and a π bond of an aromatic ring

4.4 Conclusion

A bio-based organic/inorganic complex containing Eu^{3+} (BPI-COOEu) was successfully produced. In particles and film form, BPI-COOEu had red emission under 320 nm excitation. The emission at 616 nm predominantly caused the color. The study showed enhancement and quenching effects in emission bands after the contact between BPI-COOEu film and solvents. The exposure to acetone caused strong quenching effects on the film, and this was observed to be neutralized when the film was washed with DI water in the 5-cycle circulatory experiment. The study uncovered a novel bio-based sensor suitable for a more sustainable society.

CHAPTER 5

General conclusion

In this study, the organic/inorganic composites of biopolyamides (BPA) and biopolyimide (BPI) were synthesized by the 4-aminocinnamic acid (4ACA). These polymers bearing novel functional groups and structures were tested for their performances according to the desired applications.

The quaternized derivative of 4,4'-diaminotruxillic acid (Q-4ATA) was developed to contain quaternary amines. The monomer was polymerized with diamines into several cationic BPA. One of the BPA in the series, PA-R4 contained 99% renewable source according to the sustainability metric as it was a product of Q-4ATA and 4,4′-diamino-α-truxillic acid dimethyl ester. With cationic side chain, all BPA displayed an anion-exchange ability with PA-R4 possessing 30.0 mg/g of maximum experimental I^- removal from solution. The temperature at 5% of PA-R4 composition was 300 °C. Together with the ability for the BPA to retain water, such value of thermal stability led to an I^- adsorption under near boiling point temperature which surpassed the performance of commercial polystyrene resin.

BPI bound by the carboxylic acid side chain (BPI-COOH) was modified in KOH to obtain a polymer containing carboxylate-potassium salt (BPI-COOK). BPI-COOAl, BPI-COOCu, and BPI-COOEu salts were obtained from a simple complexation process where BPI-COOK films were left in contact with the metal ion solutions. The exchange of K^+ into the targeted multivalent metal ions such as Al^{3+}, Cu^{2+} and Eu^{3+} on the carboxylate side change was determined to be an exothermic reaction. With the formation of metal carboxylate complexes, BPI-COOAl and BPI-COOCu became flame retardant. For both complexes, the second burn during the Underwriters Laboratories standard 94 for vertical burning test was distinguished within 10 s. BPI-COOAl yielded favorable microscale calorie combustion results with ignition

time at 427 s and total heat release of 4.5 W/g. Moreover, it exhibited an improved thermo-mechanical property and retained its optical transparency when compared to those of its precursors. With an addition of a rare earth metal, the BPI-COOEu displayed photoluminescent property. Its enhanced and quenched emissions due to solvents contact served as the underly mechanism of the material to be developed into VOCs sensor.

The developments of bio-based organic/inorganic composites of BPI and BPA depicted creative and practical ways of producing efficient bio-based functional materials in green society.

References

(1) Hammer, J.; Kraak, M. H. S.; Parsons, J. R. Plastics in the Marine Environment: The Dark Side of a Modern Gift. In *Reviews of Environmental Contamination and Toxicology*; Whitacre, D. M., Ed.; Springer Science: New York, 2012; Vol. 220, pp 1–44. https://doi.org/10.1007/978-1-4614-3414-6.

(2) Parrenin, F.; Masson-Delmotte, V.; Köhler, P.; Raynaud, D.; Paillard, D.; Schwander, J.; Barbante, C.; Landais, A.; Wegner, A.; Jouzel, J. Synchronous Change of Atmospheric CO2 and Antarctic Temperature During the Last Deglacial Warming. *Science* **2013**, *339* (6123), 1060–1063. https://doi.org/10.1126/science.1226368.

(3) Jambeck, J.; Geyer, R.; Wilcox, C.; Siegler, T. R.; Perryman, M.; Andrady, A.; Narayan, R.; Law, K. L. Plastic Waste Inputs from Land into the Ocean. *Science* **2015**, *347* (6223), 768–771. https://doi.org/10.1126/science.1260352.

(4) Babu, R. P.; O'Connor, K.; Seeram, R. Current Progress on Bio-Based Polymers and Their Future Trends. *Prog. Biomater.* **2013**, *2* (1), 8. https://doi.org/10.1186/2194-0517-2-8.

(5) Sharma, S. K.; Mudhoo, A. *A Handbook of Applied Biopolymer Technology Synthesis, Degradation and Applications*; The Royal Society of Chemistry: Cambridge, 2011. https://doi.org/10.1039/9781849733458.

(6) Audic, J. L.; Lemiègre, L.; Corre, Y. M. Thermal and Mechanical Properties of a Polyhydroxyalkanoate Plasticized with Biobased Epoxidized Broccoli Oil. *J. Appl. Polym. Sci.* **2014**, *131* (6), 1–7. https://doi.org/10.1002/app.39983.

(7) Yang, S. lin; Wu, Z. H.; Yang, W.; Yang, M. B. Thermal and Mechanical Properties of Chemical Crosslinked Polylactide (PLA). *Polym. Test.* **2008**, *27* (8), 957–963.

https://doi.org/10.1016/j.polymertesting.2008.08.009.

(8) Xu, J.; Guo, B. H. Poly(Butylene Succinate) and Its Copolymers: Research, Development and Industrialization. *Biotechnol. J.* **2010**, *5* (11), 1149–1163. https://doi.org/10.1002/biot.201000136.

(9) Burgess, S. K.; Leisen, J. E.; Kraftschik, B. E.; Mubarak, C. R.; Kriegel, R. M.; Koros, W. J. Chain Mobility, Thermal, and Mechanical Properties of Poly(Ethylene Furanoate) Compared to Poly(Ethylene Terephthalate). *Macromolecules* **2014**, *47* (4), 1383–1391. https://doi.org/10.1021/ma5000199.

(10) Shamsipur, M.; Pourmortazavi, S. M.; Hajimirsadeghi, S. S.; Atifeh, S. M. Effect of Functional Group on Thermal Stability of Cellulose Derivative Energetic Polymers. *Fuel* **2012**, *95*, 394–399. https://doi.org/10.1016/j.fuel.2011.09.036.

(11) Mali, S.; Grossmann, M. V. E.; García, M. A.; Martino, M. N.; Zaritzky, N. E. Effects of Controlled Storage on Thermal, Mechanical and Barrier Properties of Plasticized Films from Different Starch Sources. *J. Food Eng.* **2006**, *75* (4), 453–460. https://doi.org/10.1016/j.jfoodeng.2005.04.031.

(12) Bensabeh, N.; Moreno, A.; Roig, A.; Monaghan, O. R.; Ronda, J. C.; Cádiz, V.; Galià, M.; Howdle, S. M.; Lligadas, G.; Percec, V. Polyacrylates Derived from Biobased Ethyl Lactate Solvent via SET-LRP. *Biomacromolecules* **2019**, *20* (5), 2135–2147. https://doi.org/10.1021/acs.biomac.9b00435.

(13) Schulz, D. N.; Patil, A. O. Functional Polymers: An Overview. In *Functional Polymers: Modern Synthetic Methods and Novel Structures*; Washington, D.C., 1998; pp 1–14. https://doi.org/10.1021/bk-1998-0704.

(14) Arkin, A. H.; Hazer, B.; Borcakli, M. Chlorination of Poly(3-Hydroxy Alkanoates)

Containing Unsaturated Side Chains. *Macromolecules* **2000**, *33* (9), 3219–3223. https://doi.org/10.1021/ma991535j.

(15) Arkin, A. H.; Hazer, B. Chemical Modification of Chlorinated Microbial Polyesters. *Biomacromolecules* **2002**, *3* (6), 1327–1335. https://doi.org/10.1021/bm020079v.

(16) Boonyawan, D.; Sarapirom, S.; Tunma, S.; Chaiwong, C.; Rachtanapun, P.; Auras, R. Characterization and Antimicrobial Properties of Fluorine-Rich Carbon Films Deposited on Poly(Lactic Acid). *Surf. Coatings Technol.* **2011**, *205* (SUPPL. 2), S552–S557. https://doi.org/10.1016/j.surfcoat.2011.03.095.

(17) Mahmood, S. F.; Lund, B. R.; Yagneswaran, S.; Aghyarian, S.; Smith, D. W. Direct Fluorination of Poly(3-Hydroxybutyrate-Co)-Hydroxyhexanoate. In *Green Polymer Chemistry: Biocatalysis and Materials II*; American Chemical Society: Washington, 2013; Vol. 1144, pp 291–301. https://doi.org/10.1021/bk-2013-1144.ch020.

(18) Thuronyi, B. W.; Privalsky, T. M.; Chang, M. C. Y. Engineered Fluorine Metabolism and Fluoropolymer Production in Living Cells. *Angew. Chemie* **2017**, *129* (44), 13825–13828. https://doi.org/10.1002/ange.201706696.

(19) Choudhari, S. K.; Kariduraganavar, M. Y. Development of Novel Composite Membranes Using Quaternized Chitosan and Na^{+}-MMT Clay for the Pervaporation Dehydration of Isopropanol. *J. Colloid Interface Sci.* **2009**, *338* (1), 111–120. https://doi.org/10.1016/j.jcis.2009.05.071.

(20) Seong, H. S.; Whang, H. S.; Ko, S. W. Synthesis of a Quaternary Ammonium Derivative of Chito-Oligosaccharide as Antimicrobial Agent for Cellulosic Fibers. *J. Appl. Polym. Sci.* **2000**, *76* (14), 2009–2015. https://doi.org/10.1002/(SICI)1097-4628(20000628)76:14<2009::AID-APP3<3.0.CO;2-W.

(21) Tan, H.; Ma, R.; Lin, C.; Liu, Z.; Tang, T. Quaternized Chitosan as an Antimicrobial Agent: Antimicrobial Activity, Mechanism of Action and Biomedical Applications in Orthopedics. *Int. J. Mol. Sci.* **2013**, *14* (1), 1854–1869. https://doi.org/10.3390/ijms14011854.

(22) Zou, X.; Zhao, X.; Ye, L. Synthesis of Cationic Chitosan Hydrogel with Long Chain Alkyl and Its Controlled Glucose-Responsive Drug Delivery Behavior. *RSC Adv.* **2015**, *5* (116), 96230–96241. https://doi.org/10.1039/c5ra16328e.

(23) Papageorgiou, S. K.; Kouvelos, E. P.; Favvas, E. P.; Sapalidis, A. A.; Romanos, G. E.; Katsaros, F. K. Metal-Carboxylate Interactions in Metal-Alginate Complexes Studied with FTIR Spectroscopy. *Carbohydr. Res.* **2010**, *345* (4), 469–473. https://doi.org/10.1016/j.carres.2009.12.010.

(24) Liu, Y.; Wang, J.; Zhao, J.; Zhang, C.; Ran, J.; Zhu, P. The Flame Retardancy and Thermal Degradation Behaviors of Trivalent Metal-Alginate Films. *Nanomater. Energy* **2014**, *3* (1), 3–10. https://doi.org/10.1680/nme.13.00030.

(25) Liu, Y.; Zhang, C. J.; Zhao, J. C.; Guo, Y.; Zhu, P.; Wang, D. Y. Bio-Based Barium Alginate Film: Preparation, Flame Retardancy and Thermal Degradation Behavior. *Carbohydr. Polym.* **2016**, *139*, 106–114. https://doi.org/10.1016/j.carbpol.2015.12.044.

(26) Liu, Y.; Zhao, X. R.; Peng, Y. L.; Wang, D.; Yang, L.; Peng, H.; Zhu, P.; Wang, D. Y. Effect of Reactive Time on Flame Retardancy and Thermal Degradation Behavior of Bio-Based Zinc Alginate Film. *Polym. Degrad. Stab.* **2016**, *127*, 20–31. https://doi.org/10.1016/j.polymdegradstab.2015.12.024.

(27) Banerjee, A.; Nayak, D.; Lahiri, S. Speciation-Dependent Studies on Removal of Arsenic by Iron-Doped Calcium Alginate Beads. *Appl. Radiat. Isot.* **2007**, *65* (7), 769–775. https://doi.org/10.1016/j.apradiso.2007.02.007.

(28) Liu, H.; Chen, F.; Liu, B.; Estep, G.; Zhang, J. Super Toughened Poly(Lactic Acid) Ternary Blends by Simultaneous Dynamic Vulcanization and Interfacial Compatibilization. *Macromolecules* **2010**, *43* (14), 6058–6066. https://doi.org/10.1021/ma101108g.

(29) Liu, H.; Guo, X.; Song, W.; Zhang, J. Effects of Metal Ion Type on Ionomer-Assisted Reactive Toughening of Poly(Lactic Acid). *Ind. Eng. Chem. Res.* **2013**, *52* (13), 4787–4793. https://doi.org/10.1021/ie303317k.

(30) Yu, L. P.; Zhang, X.; Wei, D. X.; Wu, Q.; Jiang, X. R.; Chen, G. Q. Highly Efficient Fluorescent Material Based on Rare-Earth-Modified Polyhydroxyalkanoates. *Biomacromolecules* **2019**, *20* (9), 3233–3241. https://doi.org/10.1021/acs.biomac.8b01722.

(31) Schlichting, G. J.; Horan, J. L.; Jessop, J. D.; Nelson, S. E.; Seifert, S.; Yang, Y.; Herring, A. M. A Hybrid Organic/Inorganic Ionomer from the Copolymerization of Vinylphosphonic Acid and Zirconium Vinylphosphonate. *Macromolecules* **2012**, *45* (9), 3874–3882. https://doi.org/10.1021/ma300196y.

(32) Lam, J. Y.; Shih, C. C.; Lee, W. Y.; Chueh, C. C.; Jang, G. W.; Huang, C. J.; Tung, S. H.; Chen, W. C. Bio-Based Transparent Conductive Film Consisting of Polyethylene Furanoate and Silver Nanowires for Flexible Optoelectronic Devices. *Macromol. Rapid Commun.* **2018**, *39* (13), 1–5. https://doi.org/10.1002/marc.201800271.

(33) Mo, Z. J.; Hao, Z. H.; Yang, Q.; Zhao, L.; Xu, J. P.; Li, L. Controllable Synthesis of the Al4B2O9 Nanowhisker and Their Applications in Reinforced Polyhydroxyalkanoate Composites. *RSC Adv.* **2016**, *6* (48), 42627–42632. https://doi.org/10.1039/c6ra04655j.

(34) Tang, G.; Wang, X.; Xing, W.; Zhang, P.; Wang, B.; Hong, N.; Yang, W.; Hu, Y.; Song, L. Thermal Degradation and Flame Retardance of Biobased Polylactide Composites

Based on Aluminum Hypophosphite. *Ind. Eng. Chem. Res.* **2012**, *51* (37), 12009–12016. https://doi.org/10.1021/ie3008133.

(35) Arphavasin, S.; Singhatanadgit, W.; Ngamviriyavong, P.; Janvikul, W.; Meesap, P.; Patntirapong, S. Enhanced Osteogenic Activity of a Poly(Butylene Succinate)/Calcium Phosphate Composite by Simple Alkaline Hydrolysis. *Biomed. Mater.* **2013**, *8* (5). https://doi.org/10.1088/1748-6041/8/5/055008.

(36) Hwang, S. Y.; Yoo, E. S.; Im, S. S. Effects of TS-1 Zeolite Structures on Physical Properties and Enzymatic Degradation of Poly (Butylene Succinate) (PBS)/TS-1 Zeolite Hybrid Composites. *Polymer (Guildf).* **2011**, *52* (4), 965–975. https://doi.org/10.1016/j.polymer.2011.01.010.

(37) Suvannasara, P.; Tateyama, S.; Miyasato, A.; Matsumura, K.; Shimoda, T.; Ito, T.; Yamagata, Y.; Fujita, T.; Takaya, N.; Kaneko, T. Biobased Polyimides from 4-Aminocinnamic Acid Photodimer. *Macromolecules* **2014**, *47* (5), 1586–1593. https://doi.org/10.1021/ma402499m.

(38) Tateyama, S.; Masuo, S.; Suvannasara, P.; Oka, Y.; Miyazato, A.; Yasaki, K.; Teerawatananond, T.; Muangsin, N.; Zhou, S.; Kawasaki, Y.; Zhu, L.; Zhou, Z.; Takaya, N.; Kaneko, T. Ultrastrong, Transparent Polytruxillamides Derived from Microbial Photodimers. *Macromolecules* **2016**, *49* (9), 3336–3342. https://doi.org/10.1021/acs.macromol.6b00220.

(39) Dwivedi, S.; Kaneko, T. Robustification of ITO Nanolayer by Surface-Functionalization of Transparent Biopolyimide Substrates. *J. Appl. Polym. Sci.* **2018**, *135* (40), 1–9. https://doi.org/10.1002/app.46709.

(40) Ding, P.; Kang, B.; Zhang, J.; Yang, J.; Song, N.; Tang, S.; Shi, L. Phosphorus-Containing Flame Retardant Modified Layered Double Hydroxides and Their

Applications on Polylactide Film with Good Transparency. *J. Colloid Interface Sci.* **2015**, *440*, 46–52. https://doi.org/10.1016/j.jcis.2014.10.048.

(41) Liu, Y.; Wang, J. S.; Zhu, P.; Zhao, J. C.; Zhang, C. J.; Guo, Y.; Cui, L. Thermal Degradation Properties of Biobased Iron Alginate Film. *J. Anal. Appl. Pyrolysis* **2016**, *119*, 87–96. https://doi.org/10.1016/j.jaap.2016.03.014.

(42) Xiao, P.; Zhang, J. J.; Wang, Z. Q.; Lin, H. Photon Conversion and Radiation Synergism in Eu/Tb Complexes Incorporated Poly Methyl Methacrylate. *Adv. Mater. Sci. Eng.* **2016**, *2016*, 1–11. https://doi.org/10.1155/2016/2618253.

(43) Abrams, I. M. High Porosity Polystyrene Cation Exchange Resins. *Ind. Eng. Chem. Res.* **1956**, *48* (9), 1469–1472. https://doi.org/10.1021/ie51400a030.

(44) Reichenberg, D. Properties of Ion-Exchange Resins in Relation to Their Structure. III. Kinetics of Exchange. *J. Am. Chem. Soc.* **1953**, *75* (3), 589–597. https://doi.org/10.1021/ja01099a022.

(45) Massoud, A.; Waly, S. A. Preparation and Characterization of Poly (Acrylic Acid-Dimethylaminoethylmethacrylate) as Amphoteric Exchange Resin and Its Adsorption Properties. *Colloid Polym. Sci.* **2014**, *292* (12), 3077–3083. https://doi.org/10.1007/s00396-014-3335-4.

(46) Pathak, P. D.; Mandavgane, S. A.; Kulkarni, B. D. Fruit Peel Waste as a Novel Low-Cost Bio Adsorbent. *Rev. Chem. Eng.* **2015**, *31* (4), 361–381. https://doi.org/10.1515/revce-2014-0041.

(47) Fomina, M.; Gadd, G. M. Biosorption: Current Perspectives on Concept, Definition and Application. *Bioresour. Technol.* **2014**, *160*, 3–14. https://doi.org/10.1016/j.biortech.2013.12.102.

(48) Hall, P.; Berg, G.; Bjelkengren, G.; Boice, J. D.; Ericsson, U.-B.; Hallquist, A.; Lidberg, M.; Lundell, Gör.; Tennvall, J.; Wiklund, K.; Holm, L.-E. Cancer Mortality after Iodine-131 Therapy for Hyperthyroidism. *Int. J. Cancer* **1992**, *50* (6), 886–890. https://doi.org/10.1002/ijc.2910500611.

(49) Hieu, T. T.; Russell, A. W.; Cuneo, R.; Clark, J.; Kron, T.; Hall, P.; Doi, S. A. R. Cancer Risk after Medical Exposure to Radioactive Iodine in Benign Thyroid Diseases: A Meta-Analysis. *Endocr. Relat. Cancer* **2012**, *19* (5), 645–655. https://doi.org/10.1530/ERC-12-0176.

(50) Ye, Z.; Chen, L.; Liu, C.; Ning, S.; Wang, X.; Wei, Y. The Rapid Removal of Iodide from Aqueous Solutions Using a Silica-Based Ion-Exchange Resin. *React. Funct. Polym.* **2019**, *135*, 52–57. https://doi.org/10.1016/j.reactfunctpolym.2018.12.002.

(51) Ezzeldin, H. A.; Apblett, A.; Foutch, G. L. Synthesis and Properties of Anion Exchangers Derived from Chloromethyl Styrene Codivinylbenzene and Their Use in Water Treatment. *Int. J. Polym. Sci.* **2010**, 1–9. https://doi.org/10.1155/2010/684051.

(52) Choung, S.; Kim, M.; Yang, J. S.; Kim, M. G.; Um, W. Effects of Radiation and Temperature on Iodide Sorption by Surfactant-Modified Bentonite. *Environ. Sci. Technol.* **2014**, *48* (16), 9684–9691. https://doi.org/10.1021/es501661z.

(53) Morita, T.; Niwa, K.; Fujimoto, K.; Kasai, H.; Yamada, H.; Nishiutch, K.; Sakamoto, T.; Godo, W.; Taino, S.; Hayashi, Y.; Takeno, K.; Nishigaki, T.; Fujiwara, K.; Aratake, H.; Kamonoshita, S.; Hashimoto, H.; Kobayashi, T.; Otosaka, S.; Imanaka, T. Detection and Activity of Iodine-131 in Brown Algae Collected in the Japanese Coastal Areas. *Sci. Total Environ.* **2010**, *408* (16), 3443–3447. https://doi.org/10.1016/j.scitotenv.2010.04.001.

(54) Hu, Q. H.; Weng, J. Q.; Wang, J. S. Sources of Anthropogenic Radionuclides in the

Environment: A Review. *J. Environ. Radioact.* **2010**, *101* (6), 426–437. https://doi.org/10.1016/j.jenvrad.2008.08.004.

(55) Konings, R. J. M.; Wiss, T.; Beneš, O. Predicting Material Release during a Nuclear Reactor Accident. *Nat. Mater.* **2015**, *14* (March), 247–252. https://doi.org/10.1038/nmat4224.

(56) Lemma, F. G. Di; Colle, J. Y.; Bene, O.; Konings, R. J. M. A Separate Effect Study of the Influence of Metallic Fission Products on CsI Radioactive Release from Nuclear Fuel. *J. Nucl. Mater.* **2015**, *465*, 499–508. https://doi.org/10.1016/j.jnucmat.2015.05.037.

(57) Kosaka, K.; Asami, M.; Kobashigawa, N.; Ohkubo, K.; Terada, H.; Kishida, N.; Akiba, M. Removal of Radioactive Iodine and Cesium in Water Purification Processes after an Explosion at a Nuclear Power Plant Due to the Great East Japan Earthquake. *Water Res.* **2012**, *46* (14), 4397–4404. https://doi.org/10.1016/j.watres.2012.05.055.

(58) Kitada, S.; Oikawa, T.; Watanabe, S.; Nagai, K.; Kobayashi, Y.; Matsuki, M.; Tsuchiya, K.; Nakamura, K.; Sasaki, M.; Shinoda, Y.; Iwamoto, T. Removal of Radioactive Iodine and Cesium in Water Purification. *Desalin. Water Treat.* **2015**, *54* (13), 3494–3501. https://doi.org/10.1080/19443994.2014.923205.

(59) Van Der Bruggen, B.; Vandecasteele, C.; Van Gestel, T.; Doyen, W.; Leysen, R. A Review of Pressure-Driven Membrane Processes in Wastewater Treatment and Drinking Water Production. *Environ. Prog.* **2003**, *22* (1), 46–56. https://doi.org/10.1002/ep.670220116.

(60) Chae, S.; Kin, C. Removal of Cesium (137 Cs) and Iodide (127 I) by Microfiltration Nanofiltration Reverse Osmosis Membranes. *J. Korean Soc. Water Wastewater* **2014**, *28* (5), 549–554. https://doi.org/10.11001/jksww.2014.28.5.549.

(61) Sato, I.; Kudo, H.; Tsuda, S. Removal Efficiency of Water Purifier and Adsorbent for Iodine, Cesium, Strontium, Barium and Zirconium in Drinking Water. *J. Toxicol. Sci.* **2011**, *36* (6), 829–834. https://doi.org/10.2131/jts.36.829.

(62) Yang, O. B.; Kim, J. C.; Lee, J. S.; Kim, Y. G. Use of Activated Carbon Fiber for Direct Removal of Iodine from Acetic Acid Solution. *Ind. Eng. Chem. Res.* **1993**, *32* (8), 1692–1697. https://doi.org/10.1021/ie00020a023.

(63) Hoskins, J. S.; Karafil, T. Removal and Sequestration of Iodide Using Silver-Impregnated Activated Carbon. *Environ. Sci. Technol.* **2002**, *36* (4), 784–789. https://doi.org/10.1021/es010972m.

(64) Sánchez-Polo, M.; Rivera-Utrilla, J.; Salhi, E.; Gunten, U. Removal of Bromide and Iodide Anions from Drinking Water by Silver-Activated Carbon Aerogels. *J. Colloid Interface Sci.* **2006**, *300* (1), 437–441. https://doi.org/10.1016/j.jcis.2006.03.037.

(65) Zhang, X.; Gu, P.; Li, X.; Zhang, G. Efficient Adsorption of Radioactive Iodide Ion from Simulated Wastewater by Nano Cu_2O/Cu Modified Activated Carbon. *Chem. Eng. J.* **2017**, *322*, 129–139. https://doi.org/10.1016/j.cej.2017.03.102.

(66) Choi, B. S.; Park, G. Il; Kim, J. H.; Lee, J. W.; Ryu, S. K. Adsorption Equilibrium and Dynamics of Methyl Iodide in a Silver Ion-Exchanged Zeolite Column at High Temperatures. *Adsorption* **2001**, *7*, 91–103. https://doi.org/10.1023/A:1011660121182.

(67) Fabrega, J.; Luoma, S. N.; Tyler, C. R.; Galloway, T. S.; Lead, J. R. Silver Nanoparticles: Behaviour And Effects in the Aquatic Environment. *Environ. Int.* **2011**, *37* (2), 517–531. https://doi.org/10.1016/j.envint.2010.10.012.

(68) Rajaganapathy, V.; Xavier, F.; Sreekumar, D.; Mandal, P. K. Heavy Metal Contamination in Soil, Water and Fodder and Their Presence in Livestock and Products:

A Review. *J. Environ. Sci. Technol.* **2011**, *4* (3), 234–249. https://doi.org/10.3923/jest.2011.234.249.

(69) Parker, K. E.; Golovich, E. C.; Wellman, D. M. *Iodine Adsorption on Ion-Exchange Resins and Activated Carbons – Batch Testing*; Alexandria, VA, 2014. https://doi.org/10.2172/1163822.

(70) Tachibana, Y.; Nogami, M.; Nomura, M.; Suzuki, T. Simultaneous Removal of Various Iodine Species in Aqueous Solutions of High Salt Concentrations Using Novel Functional Adsorbents. *J. Radioanal. Nucl. Chem.* **2015**, *307* (3), 1911–1918. https://doi.org/10.1007/s10967-015-4441-6.

(71) Shadmon, H.; Basu, A.; Eckhard, L. H.; Domb, A. J.; Beyth, N. Synthesis, Characterization and Antibacterial Activity of Heterocyclic Quaternary Ammonium Polymers. *New J. Chem.* **2018**, *42* (18), 15427–15435. https://doi.org/10.1039/c8nj03392g.

(72) Dekel, D. R.; Amar, M.; Willdorf, S.; Kosa, M.; Dhara, S.; Diesendruck, C. E. Effect of Water on the Stability of Quaternary Ammonium Groups for Anion Exchange Membrane Fuel Cell Applications. *Chem. Mater.* **2017**, *29* (10), 4425–4431. https://doi.org/10.1021/acs.chemmater.7b00958.

(73) El-hoshoudy, A. N. Quaternary Ammonium Based Surfmer-Co-Acrylamide Polymers for Altering Carbonate Rock Wettability during Water Flooding. *J. Mol. Liq.* **2018**, *250*, 35–43. https://doi.org/10.1016/j.molliq.2017.11.119.

(74) Hugues, C.; Bressy, C.; Bartolomeo, P.; Margaillan, A. Complexation of an Acrylic Resin by Tertiary Amines: Synthesis and Characterisation of New Binders for Antifouling Paints. *Eur. Polym. J.* **2003**, *39* (2), 319–326. https://doi.org/10.1016/S0014-3057(02)00222-7.

(75) Tsvetkov, V. N. The Structure of the Monomer Unit and the Flexibility of Rigid Chain Polymer Molecules. Review. *Polym. Sci. U.S.S.R.* **1977**, *19* (10), 2485–2508. https://doi.org/10.1016/0032-3950(77)90329-X.

(76) Sudo, A.; Sugita, S. A Highly Rigid Diamine Monomer Derived from Naturally Occurring Myo-inositol and Its Use for Polyamide Synthesis. *J. Polym. Sci.* **2016**, *54*, 3436–3443. https://doi.org/10.1002/pola.28231.

(77) Tabone, M. D.; Cregg, J. J.; Beckman, E. J.; Landis, A. E. Sustainability Metrics: Life Cycle Assessment and Green Design in Polymers. *Environ. Sci. Technol.* **2010**, *44* (21), 8264–8269. https://doi.org/10.1021/es101640n.

(78) Jheng, L. C.; Hsu, S. L. C.; Lin, B. Y.; Hsu, Y. L. Quaternized Polybenzimidazoles with Imidazolium Cation Moieties for Anion Exchange Membrane Fuel Cells. *J. Memb. Sci.* **2014**, *460*, 160–170. https://doi.org/10.1016/j.memsci.2014.02.043.

(79) Clesceri, L. S. Iodine. In *Standard Methods for the Examination of Water and Wastewater*; American Public Health Association, American Water Works Association, Water Environment Federation, 1999; pp 4500–I.

(80) International Atomic Energy Agency. Iodine in Fuel Reprocessing Plants. In *Radioiodine Removal in Nuclear Facilities Methods and Techniques for Normal and Emergency Situations*; Vienna, Austria, 1980; Vol. 201, pp 1–3.

(81) Kester, D. R.; Deudall, I. W.; Connors, D. N.; Pytkowicz, R. M. Preparation of Artificial Seawater. *Limnol. Oceanogr.* **1967**, *12* (1), 176–179. https://doi.org/10.4319/lo.1967.12.1.0176.

(82) Kéki, S.; Zsuga, M.; Kuki, Á. Theoretical Size Distribution in Linear Step-Growth Polymerization for a Small Number of Reacting Species. *J. Phys. Chem. B* **2013**, *117*

(15), 4151–4155. https://doi.org/10.1021/jp401238m.

(83) Reichardt, C.; Welton, T. *Solvents and Solvent Effects in Organic Chemistry, Fourth Edition*; Wiley-VCH Verlag GmbH & Co. KGaA: Weinheim, 2010. https://doi.org/10.1002/9783527632220.ch7.

(84) Janardhan, R.; Gedam, P. H.; Sampathkumaran, P. S. The Effect of Polymer Molecular Weight in the Adsorption Process. *J. Colloid Interface Sci.* **1990**, *140* (2), 391–400. https://doi.org/10.1016/0021-9797(90)90359-V.

(85) Teixeira-Dias, J. J. C. Chemical Kinetics. In *Molecular Physical Chemistry*; 2017; pp 83–122. https://doi.org/10.1007/978-3-319-41093-7.

(86) Majidnia, Z.; Idris, A. Photocatalytic Reduction of Iodine in Radioactive Waste Water Using Maghemite and Titania Nanoparticles in PVA-Alginate Beads. *J. Taiwan Inst. Chem. Eng.* **2015**, *54*, 137–144. https://doi.org/10.1016/j.jtice.2015.03.005.

(87) Schwarzenbach, R. P.; Gschwend, P. M.; Imboden, D. M. Sorption I: General Introduction and Sorption Processes Involving Organic Matter. In *Environmental Organic Chemistry*; John Wiley & Sons, Inc.: Hoboken, NJ, 2002; pp 275–330. https://doi.org/10.1002/0471649643.

(88) Monson, L.; Braunwarth, M.; Extrand, C. W. Moisture Absorption by Various Polyamides and Their Associated Dimensional Changes. *J. Appl. Polym. Sci.* **2008**, *107*, 355–363. https://doi.org/10.1002/app.27057.

(89) Cai, S.; Zhang, B.; Cremaschi, L. Review of Moisture Behavior and Thermal Performance of Polystyrene Insulation in Building Applications. *Build. Environ.* **2017**, *123*, 50–65. https://doi.org/10.1016/j.buildenv.2017.06.034.

(90) Dai, J. L.; Zhang, M.; Hu, Q. H.; Huang, Y. Z.; Wang, R. Q.; Zhu, Y. G. Adsorption and

Desorption of Iodine by Various Chinese Soils: II Iodide and Iodate. *Geoderma* **2009**, *153* (1–2), 130–135. https://doi.org/10.1016/j.geoderma.2009.07.020.

(91) Wang, X.; Zhan, J.; Xing, W.; Wang, X.; Song, L.; Qian, X.; Yu, B.; Hu, Y. Flame Retardancy and Thermal Properties of Novel UV-Curable Epoxy Acrylate Coatings Modified by a Silicon-Bearing Hyperbranched Polyphosphonate Acrylate. *Ind. Eng. Chem. Res.* **2013**, *52* (16), 5548–5555. https://doi.org/10.1021/ie3033813.

(92) Wang, M.; Han, X. W.; Liu, L.; Zeng, X. F.; Zou, H. K.; Wang, J. X.; Chen, J. F. Transparent Aqueous $Mg(OH)_2$ Nanodispersion for Transparent and Flexible Polymer Film with Enhanced Flame-Retardant Property. *Ind. Eng. Chem. Res.* **2015**, *54* (51), 12805–12812. https://doi.org/10.1021/acs.iecr.5b03172.

(93) Laachachi, A.; Ball, V.; Apaydin, K.; Toniazzo, V.; Ruch, D. Diffusion of Polyphosphates into (Poly(Allylamine)-Montmorillonite) Multilayer Films: Flame Retardant-Intumescent Films with Improved Oxygen Barrier. *Langmuir* **2011**, *27* (22), 13879–13887. https://doi.org/10.1021/la203252q.

(94) Li, Y.-C.; Schulz, J.; Mannen, S.; Delhom, C.; Condon, B.; Chang, S.; Zammarano, M.; Grunlan, J. C. Flame Retardant Behavior of Polyelectrolyte−Clay Thin Film Assemblies on Cotton Fabric. *ACS Nano* **2010**, *4* (6), 3325–3337. https://doi.org/10.1021/nn100467e.

(95) Priolo, M. A.; Gamboa, D.; Grunlan, J. C. Transparent Clay−Polymer Nano Brick Wall Assemblies with Tailorable Oxygen Barrier. *Appl. Mater. Interfaces* **2010**, *2* (1), 312–320. https://doi.org/10.1021/am900820k.

(96) Wang, H.; Zhou, X.; Abro, M.; Gao, M.; Deng, M.; Qin, Z.; Sun, Y.; Yue, L.; Zhang, X. Mussel-Inspired General Interface Modification Method and Its Application in Polymer Reinforcement and as a Flame Retardant. *ACS Omega* **2018**, *3* (5), 4891–4898.

https://doi.org/10.1021/acsomega.8b00182.

(97) Wojtal, P.; Luo, D.; Chen, S.; Zhitomirsky, I. Composite Polymer-Metal Hydroxide Coatings with Flame-Retardant Properties. *Mater. Manuf. Process.* **2016**, *31* (9), 1201–1205. https://doi.org/10.1080/10426914.2015.1037909.

(98) Wang, D. Y.; Liu, Y.; Wang, Y. Z.; Artiles, C. P.; Hull, T. R.; Price, D. Fire Retardancy of a Reactively Extruded Intumescent Flame Retardant Polyethylene System Enhanced by Metal Chelates. *Polym. Degrad. Stab.* **2007**, *92* (8), 1592–1598. https://doi.org/10.1016/j.polymdegradstab.2007.04.015.

(99) Huang, N. H.; Chen, Z. J.; Wang, J. Q.; Wei, P. Synergistic Effects of Sepiolite on Intumescent Flame Retardant Polypropylene. *Express Polym. Lett.* **2010**, *4* (12), 743–752. https://doi.org/10.3144/expresspolymlett.2010.90.

(100) Nińã, I.; Iorgulescu, M.; Spiroiu, M. F. The Adsorption of Heavy Metal Ions on Porous Calcium Alginate Microparticles. *Anal. Chem.* **2007**, *I*, 4–12.

(101) Wang, F.; Lu, X.; Li, X. Y. Selective Removals of Heavy Metals (Pb^{2+}, Cu^{2+}, and Cd^{2+}) from Wastewater by Gelation with Alginate for Effective Metal Recovery. *J. Hazard. Mater.* **2016**, *308*, 75–83. https://doi.org/10.1016/j.jhazmat.2016.01.021.

(102) Nestle, N.; Kimmich, R. Heavy Metal Uptake of Alginate Gels Studied by NMR Microscopy. *Colloids Surfaces A Physicochem. Eng. Asp.* **1996**, *115*, 141–147. https://doi.org/10.1016/0927-7757(96)03608-4.

(103) Mallakpour, S. E.; Hajipour, A.; Mahdavian, A.; Khoee, S. Synthesis and Characterization of Novel Optically Active and Flame-Retardant Heterocyclic Polyimides. *J. Appl. Polym. Sci.* **2000**, *76*, 240–248. https://doi.org/10.1002/(SICI)1097-4628(20000411)76:2<240::AID-APP13>3.0.CO;2-

A.

(104) Zuo, L.; Fan, W.; Zhang, Y.; Zhang, L.; Gao, W.; Huang, Y.; Liu, T. Graphene/Montmorillonite Hybrid Synergistically Reinforced Polyimide Composite Aerogels with Enhanced Flame-Retardant Performance. *Compos. Sci. Technol.* **2017**, *139*, 57–63. https://doi.org/10.1016/j.compscitech.2016.12.008.

(105) Liu, Y.-L.; Hsiue, G.-H.; Lan, C.-W.; Kuo, J.-K.; Jeng, R.-J.; Chiu, Y.-S. Synthesis, Thermal Properties, and Flame Retardancy of Phosphorus Containing Polyimides. *J. Appl. Polym. Sci.* **1997**, *63* (7), 875–882. https://doi.org/10.1002/(sici)1097-4628(19970214)63:7<875::aid-app7>3.0.co;2-n.

(106) Çakmakçi, E.; Güngör, A. Preparation and Characterization of Flame Retardant and Proton Conducting Boron Phosphate/Polyimide Composites. *Polym. Degrad. Stab.* **2013**, *98* (5), 927–933. https://doi.org/10.1016/j.polymdegradstab.2013.03.003.

(107) Suzuki, H.; Abe, T.; Takaishi, K.; Narita, M.; Hamada, F. 2000 The Synthesis and X-ray Structure of 1,2,3,4-cyclobutane Tetracarboxylic Dianhydride and the Preparation of a New Type of Polyimide Showing Excellent Transparency and Heat Resistance.Pdf. *J. Polym. Sci. Part A* **2000**, *38* (1), 108–166. https://doi.org/10.1002/(SICI)1099-0518(20000101)38:1<108::AID-POLA14>3.0.CO;2-G.

(108) Wojcieszak, R.; Santarelli, F.; Paul, S.; Dumeignil, F.; Cavani, F.; Gonçalves, R. V. Recent Developments in Maleic Acid Synthesis from Bio-Based Chemicals. *Sustain. Chem. Process.* **2015**, *3* (9), 1–11. https://doi.org/10.1186/s40508-015-0034-5.

(109) Liu, Y. Is the Free Energy Change of Adsorption Correctly Calculated? *J. Chem. Eng. Data* **2009**, *54* (7), 1981–1985. https://doi.org/10.1021/je800661q.

(110) Okamoto, Y.; Kubota, T.; Gotoh, H.; Ohto, Y.; Aritani, H.; Tanaka, T.; Yoshida, S.

XAFS Study of Zirconia-Supported Copper Catalysts for the NO-CO Reaction: Deactivation, Rejuvenation and Stabilization of Cu Species. *J. Chem. Soc. - Faraday Trans.* **1998**, *94* (24), 3743–3752. https://doi.org/10.1039/a807152g.

(111) Plazinski, W.; Drachb, M. Binding of Bivalent Metal Cations by α-l-Guluronate: Insights from the DFT-MD Simulations. *New J. Chem.* **2015**, *39* (5), 3987–3994. https://doi.org/10.1039/C4NJ02206H.

(112) Motekait is, R. J.; Martell, A. E. Complexes of Aluminum(III) with Hydroxy Carboxylic Acids. *Inorg. Chem.* **1984**, *23* (1), 18–23. https://doi.org/10.1021/ic00169a006.

(113) Zaafarany, I. Non-Isothermal Decomposition of Al, Cr and Fe Cross-Linked Trivalent Metal-Alginate Complexes. *J. King Abdulaziz Univ.* **2010**, *22* (1), 193–202. https://doi.org/10.4197/sci.22-1.13.

(114) Cheong, J. Y.; Ahn, J.; Seo, M.; Nam, Y. S. Flame-Retardant, Flexible Vermiculite-Polymer Hybrid Film. *RSC Adv.* **2015**, *5* (76), 61768–61774. https://doi.org/10.1039/c5ra08382f.

(115) Li, S.; Deng, L.; Xu, C.; Wu, Q.; Wang, Z. Making a Supertough Flame-Retardant Polylactide Composite through Reactive Blending with Ethylene-Acrylic Ester-Glycidyl Methacrylate Terpolymer and Addition of Aluminum Hypophosphite. *ACS Omega* **2017**, *2* (5), 1886–1895. https://doi.org/10.1021/acsomega.7b00162.

(116) Cao, K.; Guo, Y.; Zhang, M.; Arrington, C. B.; Long, T. E.; Odle, R. R.; Liu, G. Mechanically Strong, Thermally Stable, and Flame Retardant Poly(Ether Imide) Terminated with Phosphonium Bromide. *Macromolecules* **2019**, *52* (19), 7361–7368. https://doi.org/10.1021/acs.macromol.9b01465.

(117) Lu, S.; Panchapakesan, B. All-Optical Micromirrors From Nanotube MOMS With

Wavelength Selectivity. *J. Microelectromechanical Syst.* **2007**, *16* (6), 1515–1523. https://doi.org/10.1557/proc-1015-bb07-05.

(118) Tuinstra, F.; Koenig, J. L. Raman Spectrum of Graphite. *J. Chem. Phys.* **1970**, *53* (3), 1126–1130. https://doi.org/10.1063/1.1674108.

(119) Caṇado, L. G.; Takai, K.; Enoki, T.; Endo, M.; Kim, Y. A.; Mizusaki, H.; Jorio, A.; Coelho, L. N.; Magalhães-Paniago, R.; Pimenta, M. A. General Equation for the Determination of the Crystallite Size La of Nanographite by Raman Spectroscopy. *Appl. Phys. Lett.* **2006**, *88* (16), 1–4. https://doi.org/10.1063/1.2196057.

(120) Rosenburg, F.; Ionescu, E.; Nicoloso, N.; Riedel, R. High-Temperature Raman Spectroscopy of Nano-Crystalline Carbon in Silicon Oxycarbide. *Materials (Basel).* **2018**, *11* (1). https://doi.org/10.3390/ma11010093.

(121) Hu, S.; Song, L.; Pan, H.; Hu, Y. Thermal Properties and Combustion Behaviors of Chitosan Based Flame Retardant Combining Phosphorus and Nickel. *Ind. Eng. Chem. Res.* **2012**, *51* (9), 3663–3669. https://doi.org/10.1021/ie2022527.

(122) Hajibeygi, M.; Maleki, M.; Shabanian, M. The Effects of Poly(Amide-Imide) Coating on the Thermal, Combustion and Mechanical Properties of Polyvinyl Chloride ZnO Nanocomposites. *Prog. Org. Coatings* **2018**, *122* (April), 96–106. https://doi.org/10.1016/j.porgcoat.2018.05.013.

(123) Feng, X.; Wang, X.; Xing, W.; Yu, B.; Song, L.; Hu, Y. Simultaneous Reduction and Surface Functionalization of Graphene Oxide by Chitosan and Their Synergistic Reinforcing Effects in PVA Films. *Ind. Eng. Chem. Res.* **2013**, *52* (36), 12906–12914. https://doi.org/10.1021/ie402073x.

(124) Wang, X. L.; Chen, L.; Wu, J. N.; Fu, T.; Wang, Y. Z. Flame-Retardant Pressure-

Sensitive Adhesives Derived from Epoxidized Soybean Oil and Phosphorus-Containing Dicarboxylic Acids. *ACS Sustain. Chem. Eng.* **2017**, *5* (4), 3353–3361. https://doi.org/10.1021/acssuschemeng.6b03201.

(125) Corsi, J. S.; Fu, J.; Wang, Z.; Lee, T.; Ng, A. K.; Detsi, E. Hierarchical Bulk Nanoporous Aluminum for On-Site Generation of Hydrogen by Hydrolysis in Pure Water and Combustion of Solid Fuels. *ACS Sustain. Chem. Eng.* **2019**, *7* (13), 11194–11204. https://doi.org/10.1021/acssuschemeng.9b00481.

(126) Hu, W.; Donat, F.; Scott, S. A.; Dennis, J. S. The Interaction between CuO and Al_2O_3 and the Reactivity of Copper Aluminates below 1000 °C and Their Implication on the Use of the Cu-Al-O System for Oxygen Storage and Production. *RSC Adv.* **2016**, *6* (114), 113016–113024. https://doi.org/10.1039/c6ra22712k.

(127) Yu, C. W. F.; Kim, J. T. Building Pathology, Investigation of Sick Buildings - VOC Emissions. *Indoor Built Environ.* **2010**, *19* (1), 30–39. https://doi.org/10.1177/1420326X09358799.

(128) Chin, J. Y.; Godwin, C.; Parker, E.; Robins, T.; Lewis, T.; Harbin, P.; Batterman, S. Levels and Sources of Volatile Organic Compounds in Homes of Children with Asthma. *Indoor Air* **2014**, *24* (4), 403–415. https://doi.org/10.1111/ina.12086.

(129) Benner, B. A.; Gordon, G. E.; Wise, S. A. Mobile Sources of Atmospheric Polycyclic Aromatic Hydrocarbons: A Roadway Tunnel Study. *Environ. Sci. Technol.* **1989**, *23* (10), 1269–1278. https://doi.org/10.1021/es00068a014.

(130) Guieysse, B.; Hort, C.; Platel, V.; Munoz, R.; Ondarts, M.; Revah, S. Biological Treatment of Indoor Air for VOC Removal: Potential and Challenges. *Biotechnol. Adv.* **2008**, *26* (5), 398–410. https://doi.org/10.1016/j.biotechadv.2008.03.005.

(131) Son, Y. S.; Kim, K. J.; Kim, J. C. A Review on VOCs Control Technology Using Electron Beam. *Asian J. Atmos. Environ.* **2010**, *4* (2), 63–71. https://doi.org/10.5572/ajae.2010.4.2.063.

(132) Zhang, X.; Gao, B.; Creamer, A. E.; Cao, C.; Li, Y. Adsorption of VOCs onto Engineered Carbon Materials: A Review. *J. Hazard. Mater.* **2017**, *338*, 102–123. https://doi.org/10.1016/j.jhazmat.2017.05.013.

(133) Fujio, Y.; Plashnitsa, V. V.; Elumalai, P.; Miura, N. Stabilization of Sensing Performance for Mixed-Potential-Type Zirconia-Based Hydrocarbon Sensor. *Talanta* **2011**, *85* (1), 575–581. https://doi.org/10.1016/j.talanta.2011.04.024.

(134) Sato, T.; Plashnitsa, V. V.; Utiyama, M.; Miura, N. Potentiometric YSZ-Based Sensor Using NiO Sensing Electrode Aiming at Detection of Volatile Organic Compounds (VOCs) in Air Environment. *Electrochem. commun.* **2010**, *12* (4), 524–526. https://doi.org/10.1016/j.elecom.2010.01.034.

(135) Ho, C. K.; Lindgren, E. R.; Rawlinson, K. S.; McGrath, L. K.; Wright, J. L. Development of a Surface Acoustic Wave Sensor for In-Situ Monitoring of Volatile Organic Compounds. *Sensors* **2003**, *3* (7), 236–247. https://doi.org/10.3390/s30700236.

(136) Yoon, J.; Chae, S. K.; Kim, J. M. Colorimetric Sensors for Volatile Organic Compounds (VOCs) Based on Conjugated Polymer-Embedded Electrospun Fibers. *J. Am. Chem. Soc.* **2007**, *129* (11), 3038–3039. https://doi.org/10.1021/ja067856+.

(137) Lin, H.; Jang, M.; Suslick, K. S. Preoxidation for Colorimetric Sensor Array Detection of VOCs. *J. Am. Chem. Soc.* **2011**, *133* (42), 16786–16789. https://doi.org/10.1021/ja207718t.

(138) Mirzaei, A.; Leonardi, S. G.; Neri, G. Detection of Hazardous Volatile Organic

Compounds (VOCs) by Metal Oxide Nanostructures-Based Gas Sensors: A Review. *Ceram. Int.* **2016**, *42* (14), 15119–15141. https://doi.org/10.1016/j.ceramint.2016.06.145.

(139) Ji, H.; Zeng, W.; Li, Y. Gas Sensing Mechanisms of Metal Oxide Semiconductors: A Focus Review. *Nanoscale* **2019**, *11* (47), 22664–22684. https://doi.org/10.1039/c9nr07699a.

(140) Bünzli, J. C. G.; Piguet, C. Taking Advantage of Luminescent Lanthanide Ions. *Chem. Soc. Rev.* **2005**, *34* (12), 1048–1077. https://doi.org/10.1039/b406082m.

(141) Truillet, C.; Lux, F.; Brichart, T.; Lu, G. W.; Gong, Q. H.; Perriat, P.; Martini, M.; Tillement, O. Energy Transfer from Pyridine Molecules towards Europium Cations Contained in Sub 5-Nm Eu_2O_3 Nanoparticles: Can a Particle Be an Efficient Multiple Donor-Acceptor System? *J. Appl. Phys.* **2013**, *114* (11). https://doi.org/10.1063/1.4821428.

(142) Zhou, Y.; Yan, B. A Responsive MOF Nanocomposite for Decoding Volatile Organic Compounds. *Chem. Commun.* **2016**, *52* (11), 2265–2268. https://doi.org/10.1039/c5cc09029f.

(143) Wang, K.; Ma, Y.; Tang, H. Lanthanide Coordination Polymers as Luminescent Sensors for the Selective and Recyclable Detection of Acetone. *Crystals* **2017**, *7* (7), 1–10. https://doi.org/10.3390/cryst7070199.

(144) Yan, B. Lanthanide-Functionalized Metal-Organic Framework Hybrid Systems to Create Multiple Luminescent Centers for Chemical Sensing. *Acc. Chem. Res.* **2017**, *50* (11), 2789–2798. https://doi.org/10.1021/acs.accounts.7b00387.

(145) Zhang, Z. Y.; Zhu, H.; Xu, Q. Q.; Liu, F. Y.; Zhu, A. X.; Kou, J. F. Hybrid Luminescent

Alginate Hydrogels Containing Lanthanide with Potential for Acetone Sensing. *New J. Chem.* **2019**, *43* (33), 13205–13211. https://doi.org/10.1039/c9nj01522a.

(146) Binnemans, K. Interpretation of Europium(III) Spectra. *Coord. Chem. Rev.* **2015**, *295*, 1–45. https://doi.org/10.1016/j.ccr.2015.02.015.

(147) Bünzli, J.-C. G.; Yersin, J.-R. Fluorescence Spectra and Lifetime Measurements of Aqueous Solutions of Europium Nitrate and Perchlorate. *Inorg. Chem.* **1979**, *18* (3), 605–607. https://doi.org/10.1021/ic50193a017.

(148) Wang, M. X.; Yang, C. H.; Liu, Z. Q.; Zhou, J.; Xu, F.; Suo, Z.; Yang, J. H.; Chen, Y. M. Tough Photoluminescent Hydrogels Doped with Lanthanide. *Macromol. Rapid Commun.* **2015**, *36* (5), 465–471. https://doi.org/10.1002/marc.201400630.

(149) Jørgensen, C. K.; Judd, B. R. Hypersensitive Pseudoquadrupole Transitions in Lanthanides. *Mol. Phys.* **1964**, *8* (3), 281–290. https://doi.org/10.1080/00268976400100321.

(150) Henrie, D. E.; Fellows, R. L.; Choppin, G. R. Hypersensitivity in the Electronic Transitions of Lanthanide and Actinide Complexes. *Coord. Chem. Rev.* **1976**, *18*, 199–224. https://doi.org/10.1016/S0010-8545(00)82044-5.

(151) Vuojola, J. Luminescent Lanthanide Reporters: New Concepts for Use in Bioanalytical Applications, 2013. https://doi.org/10.1088/2050-6120/2/1/012001.

(152) Shanmugaraju, S.; Umadevi, D.; González-Barcia, L. M.; Delente, J. M.; Byrne, K.; Schmitt, W.; Watson, G. W.; Gunnlaugsson, T. "Turn-on" Fluorescence Sensing of Volatile Organic Compounds Using a 4-Amino-1,8-Naphthalimide Tröger's Base Functionalised Triazine Organic Polymer. *Chem. Commun.* **2019**, *55* (81), 12140–12143. https://doi.org/10.1039/c9cc05585a.

(153) Liu, X. J.; Zhang, Y. H.; Chang, Z.; Li, A. L.; Tian, D.; Yao, Z. Q.; Jia, Y. Y.; Bu, X. H. A Water-Stable Metal-Organic Framework with a Double-Helical Structure for Fluorescent Sensing. *Inorg. Chem.* **2016**, *55* (15), 7326–7328. https://doi.org/10.1021/acs.inorgchem.6b00935.

(154) Mooibroek, T. J.; Gamez, P.; Reedijk, J. Lone Pair-π Interactions: A New Supramolecular Bond? *CrystEngComm* **2008**, *10* (11), 1501–1515. https://doi.org/10.1039/b812026a.

(155) Muddassir, M.; Usman, M.; Alarifi, A.; Afzal, M.; Alshali, K. A.; Beagan, A.; Kumar, A.; Abduhd, N. A. Y.; Ahmad, M. Experimental Sensing and DFT Mechanism of Zn(II) Complex for Highly Sensitive and Selective Detection of Acetone. *Crystals* **2020**, *10* (4). https://doi.org/10.3390/cryst10040324.

List of Publications

Journal

1. Phanthuwongpakdee, J.; Babel, S.; Dwivedi, S.; Takada, K.; Hirayama, T.; Kaneko, T. Anion-Scavenging Biopolyamides from Quaternized 4-Aminocinnamic Acid Photodimers. ACS Sustain. Chem. Eng. **2020**. https://doi.org/10.1021/acssuschemeng.9b07003.

2. Phanthuwongpakdee, J.; Babel, S.; Laohhasurayotin, K.; Sattayaporn, S.; Kaneko, T. Anthocyanin Based Agricultural Wastes as Bio-Adsorbents for Scavenging Radioactive Iodide from Aqueous Environment. J. Environ. Chem. Eng. **2020**, 104147. https://doi.org/10.1016/j.jece.2020.104147. *(Work from minor research)*

Book Chapter

1. Phanthuwongpakdee, J.; Babel, S.; Kaneko, T. Natural Adsorbents for Removal of Different Iodine Species from Aqueous Environment: A Review. In Recent Trends in Waste Water Treatment and Water Resource Management; Springer Singapore: Singapore, **2020**; pp 171–198. https://doi.org/10.1007/978-981-15-0706-9_17.

Patent

1. Kaneko, T.; Takada, K.; Dwivedi, S.; Phanthuwongpakdee, J. 第４級アンモニウム基含有ポリアミド. P200016674, 2020.

Conferences

1. Phanthuwongpakdee, J.; Dwivedi, S.; Takada, K.; Babel, S.; Kaneko, T. Syntheses of Ionized Bio-Based Polyimide Derived from 4-Aminocinnamic Acid. In The 10th International

Conference of Modification, Degradation and Stabilization of Polymers (Modest 2018); Tokyo, 2018; p 43.

2. Phanthuwongpakdee, J.; Dwivedi, S.; Takada, K.; Kaneko, T. Design and Syntheses of Cationic Biopolyamide Dervied from Exotic Amino Acid. In 67th Symposium on Macromolecules; Hokkaido, 2018.

3. Phanthuwongpakdee, J.; Dwivedi, S.; Takada, K.; Babel, S.; Kaneko, T. Syntheses of Cationic Bio-Based Resin from Exotic Amino Acid. In The 3rd International Workshop on Corrosion and Protection of Materials; Hanoi, 2018.

4. Phanthuwongpakdee, J.; Babel, S.; Kaneko, T. Adsorption of Iodide in the Water by Natural Products and Waste Biomass for the Application of Radioactive Iodide Remediation. In 8th International Conference on Sustainable Waste Management (8th IconSWM 2018); Vijayawada, 2018; pp 1006–1013.

Potential Publication

1. “Flame retardant organic glass of thermostable biopolyimide metal hybrids” by Jakkapon Phanthuwongpakdee, Toyohiro Haritmoto, Sandhya Babel, Kenji Takada, Tatsuo Kaneko (About to submit)

Appendix

Table A1. Elemental composition of PA-R4

element	elemental composition (%)		
	before KOH treatment	after KOH treatment	after washing with DI water
C	60.59	55.22	62.98
N	11.58	9.07	12.26
O	6.18	7.72	5.23
K	ND	11.62	0.358
I	5.77	ND	0.034
Cl	ND	ND	2.03
Au	15.90	16.36	17.11
Total	100	100	100

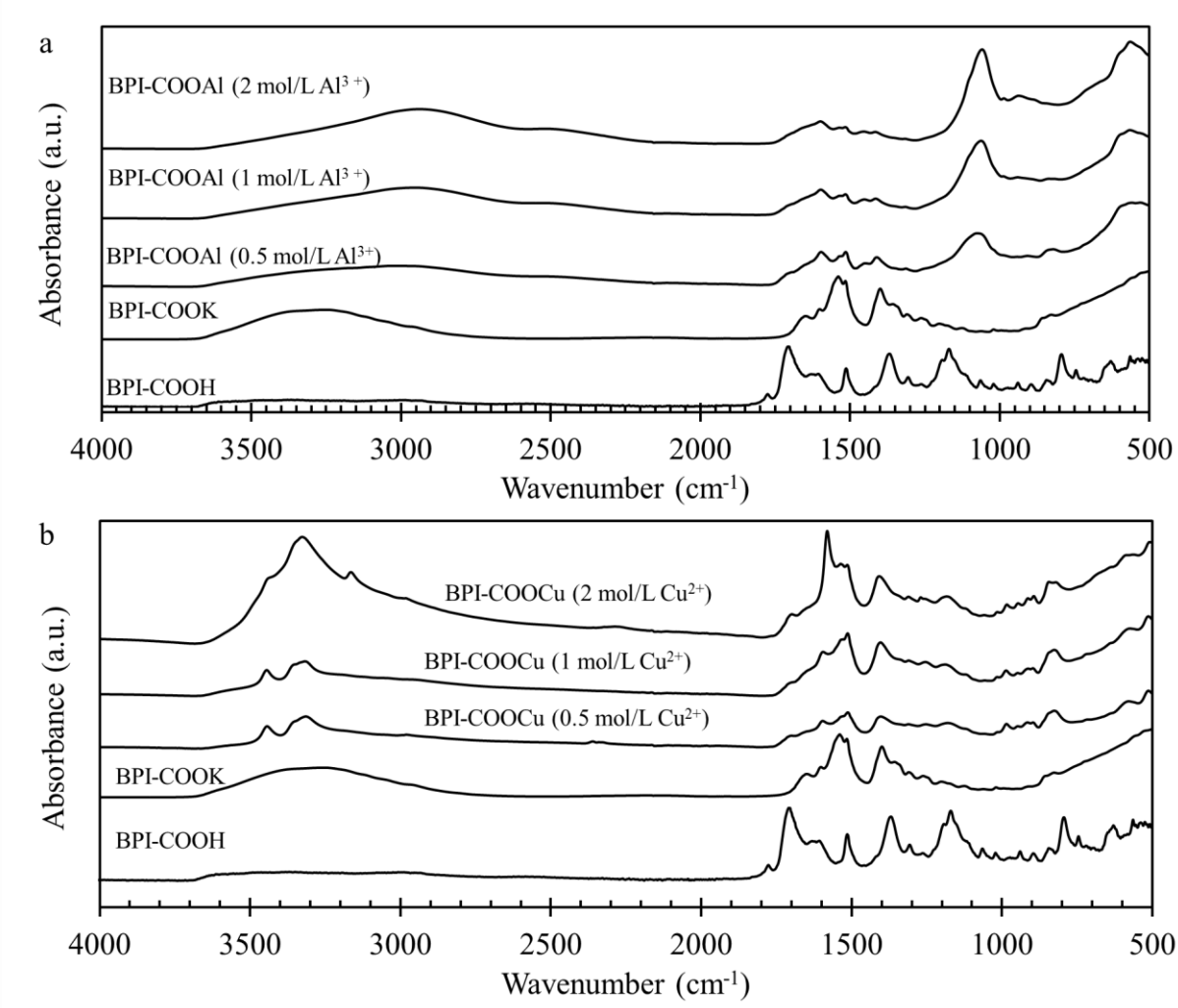

Figure A1. Full FTIR spectra. (a) BPI-COOAl, (b) BPI-COOCu